EMERGENT PROPERTIES IN EXACTLY SOLVABLE DISCRETE MODELS FOR TWO-DIMENSIONAL TOPOLOGICAL PHASES

by

Yu-Ting Hu

A dissertation submitted to the faculty of
The University of Utah
in partial fulfillment of the requirements for the degree of

Doctor of Philosophy

in

Physics

Department of Physics and Astronomy

The University of Utah

December 2013

The University of Utah Graduate School

STATEMENT OF DISSERTATION APPROVAL

The dissertation of   **Yu-Ting Hu**

has been approved by the following supervisory committee members:

Yong-Shi Wu	, Chair	**8/22/2013**
		Date Approved
Oleg Starykh	, Member	**8/22/2013**
		Date Approved
Paolo Gondolo	, Member	**8/22/2013**
		Date Approved
Z. Valy Vardeny	, Member	**8/22/2013**
		Date Approved
Feng Liu	, Member	**8/22/2013**
		Date Approved

and by   **Carleton DeTar**   , Chair/Dean of

the Department/College/School of   **Physics and Astronomy**

and by David B. Kieda, Dean of The Graduate School.

ABSTRACT

Topological phases are new kind of quantum phases of matter with properties robust against weak disorders and interactions. They occur in two-dimensional electron liquids with quantized Hall conductance and in topological insulators etc. The description of these phases goes beyond Landau's theory of symmetry breaking. They are (partially) characterized by exotic properties, such as topology-dependent ground state degeneracy(GSD), fractional quantum numbers of anyonic excitations and topology-protected bulk-edge duality etc.

In this dissertation, we systematically examine exactly solvable discrete models, particularly the so-called Levin-Wen models, for two-dimensional topological phases. They were expected to describe a large class of nonchiral (or, time reversal invariant) two-dimensional topological phases and to provide a Hamiltonian approach to some topological quantum field theories, which are related to topological invariants defined in the mathematical literature. We first show how to construct concrete models of the Levin-Wen type on a two-dimensional graph (generalized lattice), associated with the data from representation theory (the 3j- and 6j-symbols) of finite groups or quantum groups. Then an operator approach is developed to deal with the properties of the models, such as topology-dependent GSD and fractional quantum numbers for quasiparticle excitations. In this approach we are able to demonstrate the topological invariance/symmetry of the models under the mutation transformations of the graph on which the system lives, and explore this invariance to compute the topology-dependent GSD on a torus. Moreover, we use the operator approach to study the fluxon excitations, i.e., quasiparticles living on plaquettes, and to exhibit their fractional exchange (braiding) and exclusion statistics. Also, we explicitly show the correspondence between the degenerate ground states and the quasiparticle excitations: (1) the GSD on a torus is equal to the number of quasiparticle species; and (2) the modular matrices S and T obtained from the modular transformation of the torus for the ground states coincide with those obtained from the fractional exchange statistics of quasiparticles. In this way the present study reveals the first time in the literature the Hilbert space structure for the degenerate ground states as well as that for the excited states, and the interconnection between them in the Levin-Wen models.

CONTENTS

APPENDICES

LIST OF FIGURES

LIST OF TABLES

ACKNOWLEDGMENTS

CHAPTER 1

INTRODUCTION

In recent years topological phases of matter have received growing attention from the science community. They represent a novel class of quantum matter, with some important properties discrete and robust against weak disorders and interactions. Experimental examples include two-dimensional electron liquids with quantum Hall effect [1, 2, 3], certain phases in quantum spin liquids [4, 5, 6, 7, 8], and topological insulators [9, 10, 11, 12, 13]. Topological phases have potential applications: some of them may be used for fault-tolerant quantum computation [14, 15, 16, 17].

1.1 Topological phases

Before the discovery of quantum Hall effect, the standard paradigm for phase transition was Laudau's theory [18] of symmetry breaking. In Laudau's theory, the continuous phase transitions are driven by thermal fluctuations. Typically energy dominates at low temperature while entropy dominates at high temperature. The phase transitions are associated with a symmetry breaking, and characterized by one or sevaral local order parameters that measure the order in the degrees of freedom (d.o.f.) of the system in the low-temperature phase. Successful examples include crystals, ferromagnetism, superfulids, superconductivity, etc. For many years, it was thought that Laudau's theory described essentially all ordered phases in phase transitions.

The fractional quantum Hall effect (FQHE) phases, however, are new kind of quantum phases beyond the Landau paradigm. First, purely quantum effects, particularly quantum entanglement at large distances, play a significant role in the formation of new topological orders. Thus topological phase transitions can occur at zero temperature. Second, it may happen that two different topological phases have the same symmetry and no local order parameters can distinguish between them. Topologically ordered states are known to be the ground states of a gapful spectrum of certain many-body Hamiltonians, and the ground states are degenerate on a torus with robust degeneracy. Hence the topological phases

are believed to be governed by a novel interplay between energy and information at the quantum level [19].

In many cases, including the FQHE and certain phases in quantum spin liquids, topological phases can be characterized by the following topological properties that are stable to local perturbations.

First, ground states are gapped with a robust ground state degeneracy (GSD) on a torus [20, 21, 22]. But the ground state is nondegenerate on a sphere [23], implying that the degeneracy is only sensitive to the spatial topology (for a given Hamiltonian). The topological degeneracy are necessary for explaining the fractional physical quantities. In FQHE for example, though the degenerate ground states look alike with each other, the topological degeneracy is needed [20, 21] for the correct Hall conductivity. The topology dependence goes beyond our conventional intuition and experience with symmetry breaking.

Second, the topological phases support unusual quasiparticles with fractional quantum numbers [24, 25, 26]. For example, Laughlin's wavefunction [3] for FQHE at filling factors $\nu = \frac{1}{2n+1}$ hosts vortex-like quasiparticle excitations, carrying fractional charges compared to those of the constituent particles of the system. Moreover, these quasiparticles have fractional statistics [27, 28, 29, 30]. In general, we expect that quasiaprticles in topological phases exhibit two types of fractional statistics. One is the fractional exchange statistics: the wavefunction acquires a $U(1)$ phase under the exchange of abelian anyons, or is transformed by a unitary matrix under the exchange of nonabelian anyons. They also exhibit the fractional (mutual) exclusion statistics: the effective number of available single-particle states, when adding one more quasiparticle into the system, linearly depends on the number of existing quasiparticles. A typical new feature of the generalized Pauli exclusion principle is mutual exclusion between different species, resulting in a matrix of statistical parameters, as well as unusual thermodynamics for ideal gases with only statistical interactions. These unusual statistics indicate that the d.o.f. in the system are highly entangled with one another over long range. Experimentally, the nonabelian Ising anyons are believed to be realized by half quantum vortex in $p+ip$ superfuids [31], and by the charge $e/4$ quasiparticles in $\nu = 5/2$ FQH liquids [32, 33].

Third, they have gapless boundary excitations near the edge of the system. The excitations in the bulk of FQHE have an energy gap, but the gapless "edge waves" appears [34] on (or near) the boundary. These edge modes are connected [35] to one-dimensional chiral Luttinger liquids.

These properties are closely related to each other. The GSD is closely related to

fractionization of quasiparticle quantum numbers, including fractional (braiding) statistics. The topological degeneracy also occurs in systems with nonabelian anyonic quasiparticles (the meaning of "nonabelian" will be explained later) on the plane (or, on the sphere). These robust properties may be summarized by the concept of the so-called "topological orders" [36] happening in topological phases. These properties may be systematically studied using effective field theories.

Effective theories for topological phases are Chern-Simons theories or (more generally) topological quantum field theories [37]. Landau-Ginsburg-Chern-Simons theory [38, 39] for the FQHE used the Chern-Simons coupling to attach an odd number of flux quanta to electrons, making them effectively bosons and able to "Bose condensate," resulting in an effective scalar field theory plus a Chern-Simons term that takes care of statistical transmutation. Other effective theories [22, 40, 41, 42] include pure Chern-Simons fields in an external electromagnetic field.

To see why the FQHE can be effectively described by topological phases, we note that in TQFT observables (or correlation functions) are invariant under smooth deformation of space-time. It is this deformation symmetry that relates the fractional quantum numbers (e.g., GSD) to the topological invariants.

The Chern-Simons theories, which are known to be chiral breaking time reversal and parity symmetry, are formulated in continuum spacetime and have no lattice counterpart. Doubled topological phases, which respect these symmetries, on the other hand, do admit a discrete description. Examples include Kitaev's toric code model [14].

More recently, Levin and Wen (LW) [43] constructed a discrete model to describe a large class of doubled phases. Their original motivation was to generate ground states that exhibit the phenomenon of string-net condensation [44, 45] as a physical mechanism for topological phases. The LW model is defined on a trivalent lattice (or graph) with an exactly soluble Hamiltonian. The ground states in this model can be viewed as the fixed-point states of some renormalization group flow [46]. These fixed-point states look the same at all length scales and have no local degrees of freedom. Like Kitaev's toric code model [14], we expect that the subspace of degenerate ground states in the LW model can be used as a fault-tolerant code for quantum computation.

The LW model can be viewed as a Hamiltonian version of the Turaev-Viro topological quantum field theory (TQFT) in three-dimensional spacetime [47, 48, 17] and, in particular cases, discretized version of *doubled* Chern-Simons theory [49, 50]. In discrete TQFT, the topological observables are invariant under topology-preserving mutations of the space-

time graph. The study of these topological observables provides a systematic approach to understand those robust properties in topological phases. The mutation symmetry is important. First, it implies that all local operators have trivial correlation functions in the ground-state subspace. (The only local operator which has nonvarnishing correlation functions is the identity transformation.) Hence, we have the superselection rule for any local operator $\mathcal{O}$: $\langle \Phi_a | \mathcal{O} | \Phi_b \rangle = 0$ for any two different degenerate ground states Φ_i and Φ_b. This properties gives rise to the GSD as a topological observable.

For the elementary excitations, the mutation symmetry implies that all nontrivial local operators only depend on the topology of (evolution of) configuration space of all quasiparticles. This properties gives rise to further topological observables: the fractional exchange statistics and the fractional exclusion statistics. In the continuum TQFT, quasiparticles can be understood as punctures in the space manifold. Under deformation symmetry, the only dynamics in the bulk are the braiding of punctures that transforms between the degenerate states (with the configuration of the remaining punctures fixed). This braiding gives rise to braid group representations [29]; and thus quasiparticles obey the fractional statistics. In the discrete models, the observables are invariant under the mutation of space-time graph. The quasiparticles can be viewed as the topological defects on the spatial graph, and the above argument is valid in the discrete case too.

In this dissertation, we consider these exactly solvable models, particularly focusing on Levin-Wen models, and study the robust emergent properties in the operator approach: the GSD, and anyonic quasiparticle excitations.

1.2   Levin-Wen models

Let us briefly review the Levin-Wen models. The model is defined on a trivalent graph embedded to a closed oriented surface. The Hilbert space is spanned by the degrees of freedom on edges. See Fig. 1.1. For each edge, we assign a label j (called string type), which runs over a finite set of integers $j = 0, 1, ..., N$. The Hilbert space is spanned by all configurations of the labels on edges. Each label j has a "conjugate" j^*, which is also an integer and satisfies $j^{**} = j$. If we reverse the direction of one edge and replace the label j by j^* on this edge, we require the state to be the same. See Fig. 1.1. There is unique "trivial" label $j = 0$ satisfying $0^* = 0$.

There are two types of local operators, Q_v defined at vertices v and B_p^s (indexed by the label $s = 0, 1, ..., N$) at plaquettes p. Let us first define the operator Q_v. On a trivalent graph, Q_v acts on the labels of three edges incoming to the vertex v. We define the action of Q_v on the basis vector with j_1, j_2, j_3 by
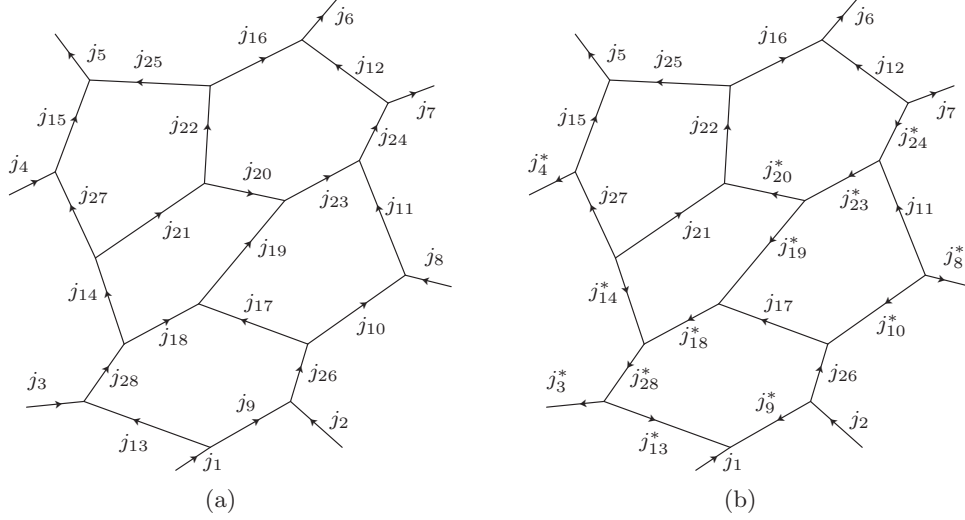
Figure 1.1. A configuration of string types on a directed trivalent graph. The configuration (b) is treated the same as (a), with some of the directions of some edges reversed and the corresponding labels j conjugated j^*.

$$Q_v \left| \begin{array}{c} j_3 \\ j_1 \end{array} \begin{array}{c} j_2 \end{array} \right\rangle = \delta_{j_1 j_2 j_3} \left| \begin{array}{c} j_3 \\ j_1 \end{array} \begin{array}{c} j_2 \end{array} \right\rangle \tag{1.1}$$

where the tensor $\delta_{j_1 j_2 j_3}$ equals either 1 or 0, which determines whether the triple $\{j_1, j_2, j_3\}$ is "allowed" to meet at the vertex. Since there is no special ordering in this triple $\{j_1, j_2, j_3\}$, we require $\delta_{j_1 j_2 j_3}$ is symmetric under permutations of the three labels: $\delta_{j_1 j_2 j_3} = \delta_{j_2 j_3 j_1} = \delta_{j_1 j_3 j_2}$. To be compatible with the conjugation structure of labels, the branching rule satisfy $\delta_{0jj^*} = \delta_{0j^*j} = 1$, $\delta_{0ij^*} = 0$ if $i \neq j$, and $\delta_{j_1 j_2 j_3} = \delta_{j_3^* j_2^* j_1^*}$.

In the representation language, the label set $\{0, 1, \ldots, N\}$ can be thought as (the representatives of) all irreducible representations of a finite group or more generally a quantum group. The trivial label 0 is the trivial representation. The branching rule tells whether the tensor product $j_1 \otimes j_2 \otimes j_3$ contains the trivial representation or not.

To define the operator B_p^s, we need more data. We associate to each label j a real nonzero number d_j, called the quantum dimension. They are compatible with the branching rule by the condition:

$$\sum_k d_k \delta_{ijk^*} = d_i d_j. \tag{1.2}$$

Let $\alpha_i = \text{sgn}(d_i)$, and require the *trimodality condition*:

$$\alpha_i \alpha_j \alpha_k = 1, \quad \text{if } \delta_{ijk} = 1. \tag{1.3}$$

We also need a tensor G_{kln}^{ijm} called the (symmetrized) $6j$ symbol. They consist of complex numbers and satisfy

$$
\begin{aligned}
\text{tetrahedral symmetry:} \quad & G_{kln}^{ijm} = G_{nk^*l^*}^{mij} = G_{ijn^*}^{klm^*} = \alpha_m \alpha_n \overline{G_{l^*k^*n}^{j^*i^*m^*}}, \\
\text{pentagon id:} \quad & \sum_n \mathrm{d}_n G_{kp^*n}^{mlq} G_{mns^*}^{jip} G_{lkr^*}^{js^*n} = G_{q^*kr^*}^{jip} G_{mls^*}^{riq^*}, \\
\text{orthogonality:} \quad & \sum_n \mathrm{d}_n G_{kp^*n}^{mlq} G_{pk^*n}^{l^*m^*i^*} = \frac{\delta_{iq}}{\mathrm{d}_i} \delta_{mlq} \delta_{k^*ip},
\end{aligned}
\tag{1.4}
$$

where the bar means the complex conjugate.

The data $\{\mathrm{d}_j, \delta_{ijk}, G_{klm}^{ijm}\}$ is the basic ingredient of the representation theory of a group, or more generally a quantum group. For instance, these conditions are satisfied if we take the labels j to be the irreducible representations of a finite group, α_j is the Frobenius-Schur indicator telling if the representation j is real or pseudoreal, $\mathrm{d}_j = \alpha_j \dim(j)$ the dimension $\dim(j)$ of the corresponding representation space multiplied by the Frobenius-Schur indicator α_j, and G_{kln}^{ijm} the symmetrized Racah $6j$ symbol for the group. See Chapter 2. In this example, the LW model is mapped to the Kitaev's qauntum double model.

The operator B_p^s acts on the boundary edges of the plaquette p, and has the matrix elements on a triangle plaquette,

$$
\left\langle
\begin{array}{c} j_5 \; j_3' \; j_6 \\ j_1' \, j_2' \\ j_4 \end{array}
\middle| B_p^s \middle|
\begin{array}{c} j_5 \; j_3 \; j_6 \\ j_1 \, j_2 \\ j_4 \end{array}
\right\rangle
= v_{j_1} v_{j_2} v_{j_3} v_{j_1'} v_{j_2'} v_{j_3'} G_{sj_3'j_1'}^{j_5 j_1^* j_3} G_{sj_1'j_2'^*}^{j_4 j_2^* j_1} G_{sj_2'j_3'^*}^{j_6 j_3^* j_2}
\tag{1.5}
$$

where $v_j \equiv \sqrt{\mathrm{d}_j}$, where the square root is randomly taken but once for all. The same rule applies when the plaquette p is a quadrangle, a pentagon, or a hexagon and so on. Note that the matrix is nondiagonal only on the labels of the boundary edges (i.e., j_1, j_2, and j_3 on the above graph).

The operators B_p^s have the properties

$$
B_p^{s\dagger} = B_p^{s^*}
\tag{1.6}
$$

$$
B_p^r B_p^s = \sum_t \delta_{rst^*} B_p^t
\tag{1.7}
$$

The first one can be verified by the symmetry condition in (1.4), and the second one can be verified by the three conditions in (1.4).

The Hamiltonian of the model is (here $D = \sum_j \mathrm{d}_j^2$)

$$
H = -\sum_v Q_v - \sum_p B_p, \quad B_p = \frac{1}{D} \sum_s \mathrm{d}_s B_p^s
\tag{1.8}
$$

where the sum run over vertices v and plaquettes p of the trivalent graph.

The main property of Q_v and B_p is that they are mutually-commuting projection operators: (1) $[Q_v, Q_{v'}] = 0 = [B_p, B_{p'}], [Q_v, B_p] = 0$; (2) and $Q_v Q_{v'} = \delta_{vv'} Q_v$ and

$B_p B_{p'} = \delta_{pp'} B_p$. Thus the Hamiltonian is exactly soluble. The elementary energy eigenstates are given by common eigenvectors of all these projections. The ground states satisfies $Q_v = B_p = 1$ for all v, p, while the excited states violate these constraints for some plaquettes or vertices.

In particular, in most cases the data $\{d, \delta, G\}$ are derived from representations of groups or quantum groups (quasitriangular Hopf algebra), we have $\delta_{rst^*} = \delta_{srt^*}$. Then B_p^s's commute with each other,

$$[B_{p_1}^r, B_{p_2}^s] = 0 \tag{1.9}$$

which can be verified by the conditions in (1.4) when p_1 and p_2 are the two nearest neighboring plaquettes, and by eq (1.7) together with $\delta_{rst^*} = \delta_{srt^*}$ when $p_1 = p_2$.

1.3   Outline of dissertation

This dissertation mainly focuses on three parts.

The first part includes Chapters 2 and 3, presenting the concrete construction of Levin-Wen models associated with finite groups and quantum groups. In Chapter 2, we start with irreducible representations of a finite group, and construct the $3j$-symbols. By imposing the proper symmetry on the $3j$-symbols, we derive the *symmetrized $6j$-symbols* that are used to define the Levin-Wen Hamiltonian. The algorithm and examples are discussed. The construction reveals how Levin-Wen models are treated as topological gauge theories with finite gauge group, or more generally, a generalized version with "quantum gauge group." Gauge filed theories are usually formulated by Lie algebras for Lie groups, or group elements for finite groups. Levin-Wen models can be viewed as topological gauge field theories in the dual formulations, using representations of the gauge group. The former formulation emphasize the role of gauge transformations, while the latter the observables under the gauge symmetry, which is convenient to systematically study the topological observables we are interested in. In Chapter 3, we derive the symmetrized $6j$-symbols from more general algebraic structure (unitary spherical fusion categories), and discuss the example of semion data and Fibonacci data, both of which are related to the quantum group $\mathcal{U}_q(\mathfrak{su}(2))$.

In the second part, we study the topological properties of the degenerate ground states. There are two types of topological observables in the ground states: GSD, and modular matrices S and T, as discussed in Chapters 4 and 5, respectively. In Chapter 4, we introduce the mutation symmetry and discuss the topological observables invariant under mutations. The mutation symmetry implies that degenerate ground states look the same everywhere locally, and we cannot distinguish between them by any local measurement. We show that

the GSD only depends on the spatial topology of the system. In Chapter 5, we derive the modular matrices S and T that characterize how different ground states on a torus are transformed into each other. By these transformations, we prove that the topological charges of the ground states are classified by the quantum double structure. The topological numbers, i.e., the GSD, S and T are the characteristics of these topological charges.

In the third part, we study the fractional quantum numbers in elementary excitations. In Chapter 6, we develop an operator approach to deal with the topological properties in the fluxon excitations. We explicitly formulate the operators to crate, annihilate and hop the fluxons. In this operator approach, we show that the topological charges of the fluxon excitations include two parts: the particle species of the fluxons and the relative d.o.f among these fluxons. We show that these topological charges are classified by the quantum double structure.

In Chapters 7 and 8, we discuss the two types of fractional exchange statistics and fractional exclusion statistics. In Chapter 7, we derive the modular S and T matrices from the exchange statistics, where T gives the topological spins of quasiparticles while S the amplitude of exchanging two quasiparticles twice.

S and T can be obtained in two ways, namely from modular transformations of torus on the degenerate ground states as in Chapter 5, and from fractional statistics of quasiparticles as in Chapter 7. We show that these two sets of S and T are identical, and hence confirm the correspondence between the degenerate ground states on a torus and the particle species of quasiparticles in the bulk.

In Chapter 9, we briefly introduce other discrete exactly solvable models for two-dimensional topological phases. Kitaev models can be mapped to Levin-Wen models with finite groups by a Fourier transformation in the ground states and fluxon excitations. Dijkgraaf-Witten models are discussed by introducing local ordering of the discrete space graph. The analysis in this dissertation can be adapted in these models. Finally, in the last chapter, we briefly summarize the above emergent topological properties and future directions.

CHAPTER 2

CONCRETE CONSTRUCTION OF
LEVIN-WEN MODELS WITH
FINITE GROUPS

In this chapter, we shall [51] concretely construct the Levin-Wen models from finite group representations.

Many examples of the Levin-Wen model come from representation theory, e.g., of a finite group, of a quantum double of a finite group, and of the q-deformed Lie groups at a complex root q of unity. In mathematics, the $6j$-symbols used to define Levin-Wen models can be derived from (unitary spherical) fusion categories, and these fusion categories are known to be equivalent to category of representations of some weak Hopf algebras (of which the dual representations and the tensor product representations make sense), see [52] for instance. Examples include Wigner's $6j$-symbols (or Racah's coefficients) in group representation theories. As a consequence, Levin-Wen models are equivalent to generalized discrete topological gauge theories, where the gauge groups are generalized to weak Hopf algebras as the gauge algebras. In particular, with the symmetrized $6j$-symbols for a finite group $\mathbb{G}$, the Levin-Wen model is equivalent to a discrete gauge theory with $\mathbb{G}$ the gauge group. However, this interpretation is hidden implicitly in the definition of the model. By investigating the representation theories, we can better understand this equivalence.

The tensor category theory is a powerful mathematical tool in the study of the Levin-Wen models. The Levin-Wen models are believed to be the discrete Hamiltonian version of some TQFTS, which in turn are known to be described by category theories. For example, the fractional quantum Hall liquids are described by Chern-Simons theories. Chern-Simons theories satisfy a property called *holography*, which means that the bulk theory in a finite region is equivalent to a conformal field theory (CFT) on the boundary (in this case, a Wess-Zumino-Witten theory (WZW)). The latter is known to be related to a modular tensor category (MTC).

However, it is not straightforward to use the concept of tensor categories in the study of Levin-Wen models. By filling in the necessary mathematical tricks, e.g., expressing a tensor category in terms of matrices and tensors, we intend to provide more computational tools, so that physicists can study the Levin-Wen model numerically. We also hope to provide a more convenient language that would be useful to study the excited states in the Levin-Wen models.

In this chapter, we shall construct Levin-Wen models from finite group representation theories. Given any finite group $\mathbb{G}$, the input data $\{d, \delta, G\}$ can be derived. The Levin-Wen models with these data become the discrete topological gauge field theory, with the finite gauge group $\mathbb{G}$.

Levin-Wen Hilbert space is spanned by the string types. These string types are the irreducible representations of $\mathbb{G}$. By a Fourier transformation, i.e., between the irreducible representations and group elements, the language of string types is mapped to the traditional language of gauge fields using group elements.

2.1 Symmetrized $6j$-symbols from group representation theory

The physical significance of group representations lies in the conjugate representations and the tensor product representations. They are the basic ingredients of the mathematical structure of the Hilbert space of a many-body quantum system with antiparticles. The $6j$-symbols provide a tensor description of the group representation theories that conveniently deal with the conjugate representations and the tensor product representations. An important example is the Wigner's $6j$-symbols (or, Racah's coefficients) in the angular momentum theory.

Unfortunately, the $6j$-symbols are not uniquely defined — they are defined up to some nontrivial phases. These phases can be fixed by imposing some "simple" symmetry properties on the $6j$-symbols. In this chapter we will impose the tetrahedral symmetry conditions (1.4) on the $6j$-symbols. The $6j$-symbols satisfying Eq. (1.4) are *symmetrized*. In this section, we start by introducing the intertwining operators (or, $\mathbb{G}$-morphisms, will be defined later), and construct the symmetrized $3j$-symbols and then the symmetrized $6j$-symbols.

Let $\mathbb{G}$ be a group. A *unitary representation* of the group $\mathbb{G}$ is a pair (ρ, V), where a vector space V is equipped with unitary operators

$$\rho(g) : V \to V; e_m \mapsto \sum_n [\rho(g)]_{nm} e_n, \tag{2.1}$$

one for each $g \in \mathbb{G}$, such that

$$\rho(\mathbb{1}) = \mathbb{1}_V \tag{2.2}$$

is the identity map on V for the identity element $\mathbb{1} \in \mathbb{G}$, and

$$\rho(g)\rho(h) = \rho(gh). \tag{2.3}$$

Here $[\rho(g)]_{nm}$ is the representation matrix, and e_n the basis vectors in V.

Given two representations (ρ, V) and (ρ', V') of $\mathbb{G}$, an *intertwining operator* is a linear operator

$$f : V \to V'; e_m \mapsto \sum_{m'} f_{m'm} e_{m'} \tag{2.4}$$

that commutes with the group action, i.e.,

$$\sum_n [\rho'(g)]_{n'm'} f_{m'm} = \sum_n f_{n'n}[\rho(g)]_{nm}, \tag{2.5}$$

for all $g \in \mathbb{G}$, where m, n runs in basis of V and m', n' of V'.

It is convenient to introduce the *graphical presentation* of the equations of intertwining operators. This technique would help us to read the tensor equations more intuitively. We draw Eq. (2.5) like

$$\tag{2.6}$$

where the lines denote the vector spaces V and V', the coupon denotes the intertwining operator f between them, and the circle labeled by g denotes the group action on the corresponding representation space. The upward direction is the "metaphorical" time arrow to indicate the order of composition of linear maps between vector spaces. We present the composition of f and $\rho(g)$ by putting the coupon of f on top of $\rho(g)$, with an internal line to indicate the contraction that them. The identity map on V will be presented by a vertical arrow $\uparrow_V$ directed upward.

Now consider the tensor product representations. Given any two representations (ρ, V) and (ρ', V'), the *tensor product representation* of them is the pair $(\rho \otimes \rho', V \otimes V')$ where

$V \otimes V'$ is the tensor product of vector spaces and the representation operator $(\rho \otimes \rho')(g)$ is defined by

$$(\rho \otimes \rho')(g) : V \otimes V' \to V \otimes V';$$
$$(\rho \otimes \rho')(g)(v \otimes v') = \rho(g)v \otimes \rho'(g)v', \tag{2.7}$$

for all elements $v \in V$ and $v' \in V$. The $\rho \otimes \rho'$ is well-defined on $V \otimes V'$ because all elements in $V \otimes V'$ are linear combinations of $v \otimes v'$, and $(\rho \otimes \rho')(g)$ is a linear operator.

The tensor product $f_1 \otimes f_2$ of two intertwining operators $f_1 : V_1 \to V_1'$ and $f_2 : V_2 \to V_2'$ is defined by $(f_1 \otimes f_2)(v_1 \otimes v_2) = (f_1 v_1) \otimes (f_2 v_2)$ for all $v_1 \in V_1$ and $v_2 \in V_2$. This defining equation is presented by

$$\tag{2.8}$$

where on the RHS the two parallel vertical lines labeled by V_1 and V_2 presents $V_1 \otimes V_2$.

The diagrams satisfy the *sliding principle*, namely, sliding up or down the coupons does not affect the final results,e.g.,

$$\tag{2.9}$$

which reads $(f_1 \otimes \mathrm{id}_{W_2})(\mathrm{id}_{V_1} \otimes f_2) = (\mathrm{id}_{W_1} \otimes f_2)(f_1 \otimes \mathrm{id}_{V_2}) = f_1 \otimes f_2$, with the identity maps inserted at appropriate positions in the composition.

2.1.1   Dual representations

Let I be a complete set of the inequivalent unitary irreducible representations of a group $\mathbb{G}$, usually labeled by some numbers. In particular, we label 0 the trivial representation $(\rho_0, \mathbb{C})$ in which $\rho_0(g) = 1$ for all $g \in \mathbb{G}$. Though irreducible representations in the set I are chose quite arbitrarily, we fix one set I once and for all. Different choices differ by a similarity transformation of each representation. For example, the group $SU(2)$ has irreducible representations $j = 0, \frac{1}{2}, 1, \frac{3}{2}, \ldots$. Take the $j = 1/2$ representation of the form $\exp(i\theta \cdot \mathbf{s})$, where we can choose $\mathbf{s} = \{\sigma^x/2, \sigma^y/2, \sigma^z/2\}$, or $\mathbf{s}' = \{-\sigma^x/2, \sigma^y/2, -\sigma^z/2\}$ with σ the pauli matrices.

Each (unitary) irreducible representation (ρ_j, V_j) for $j \in I$ comes with a conjugate representation (ρ_j^*, V_j^*), such that $\rho_j^*(g)$ is the complex conjugate of $\rho_j(g)$ for all $g \in \mathbb{G}$.

The conjugate representation of j in I is also irreducible. In general it does not match any representation in I, but it must be equivalent to one in I, called the dual of j^* and denoted by j^*. If (ρ_j, V_j) is equivalent to its complex conjugate, we say it is self-dual and have $j = j^*$.

For example, each irreducible representation of $SU(2)$ is equivalent to its conjugate. Take $j = 1/2$ representation of the form $\exp(i\theta \cdot \mathbf{s})$ with $\mathbf{s} = \{\sigma^x/2, \sigma^y/2, \sigma^z/2\}$. Its conjugate form is $\overline{\exp(i\theta \cdot \mathbf{s})} = \exp(i\theta \cdot \mathbf{s}')$ with $\mathbf{s}' = \{-\sigma^x/2, \sigma^y/2, -\sigma^z/2\}$, where the bar means the complex conjugate.

These two representations are not the same, but equivalent up to a similarity transformation as follows. There is an intertwining operator called the duality map for $j = 1/2$ representation,

$$\omega_{1/2}: \quad 1 \mapsto \sum_{m,n=\pm 1/2} \Omega^{1/2}_{m_1 m_2} |m,n\rangle$$

$$\Omega^{1/2} = \eta \sigma^y \tag{2.10}$$

where $m_1, m_2 = -1/2, 1/2$, and η is an arbitrary complex number. The condition for $\omega_{1/2}$ to be an intertwining operator is given by

$$\sum_{m'n'} [\rho_{1/2}(g)]_{mm'} [\rho_{1/2}(g)]_{nn'} (\Omega^{1/2})_{m'n'} = (\Omega^{1/2})_{mn}. \tag{2.11}$$

which has only one solution as given by Eq. (2.10). Since the representation is unitary, we see that the duality map takes the $j = 1/2$ representation to its complex conjugate, by

$$\Omega^{1/2} \rho_{1/2}(g) (\Omega^{1/2})^{-1} = \overline{\rho_{1/2}(g)} \tag{2.12}$$

for all $g \in SU(2)$. In quantum theory, the duality map $\omega^{1/2}$ is related to the time reversal symmetry transformation on a spin-1/2 system.

In general, each irreducible representation $j \in I$ comes with a *dual* $j^* \in I$ such that there exists an invertible intertwining operator called the *duality map*

$$\omega_j: \quad \mathbb{C} \mapsto V_j \otimes V_{j^*}; \, 1 \mapsto \sum_{m,n} \Omega^j_{mn} e_m \otimes e_n, \tag{2.13}$$

where e_m runs in the basis of V_j and e_n of V_{j^*}, and Ω^j_{mn} is a complex matrix that satisfies the *normalization condition*

$$(\Omega^j)^\dagger \Omega^j = \mathbb{1}. \tag{2.14}$$

The ω_j maps the representation j (or j^*) to its complex conjugate by

$$(\Omega^j)^{-1} \rho_j(g) \Omega^j = \overline{\rho_{j^*}(g)} \equiv \rho^*_{j^*}(g),$$

$$\Omega^j \rho_{j^*}(g) (\Omega^j)^{-1} = \overline{\rho_j(g)} \equiv \rho^*_j(g) \tag{2.15}$$

for all $g \in \mathbb{G}$, which can be directly verified by the defining property of the intertwining operator that $\rho_j(g)\Omega^j(\rho_{j*}(g))^T = \Omega^j$ for all $g \in \mathbb{G}$.

Unless specified, we suppress the coupon to a dot in the graphical presentation by

$$
\begin{array}{c}
\end{array}
\equiv
\begin{array}{c}
\end{array}
,
\tag{2.16}
$$

where on the LHS the dashed line denotes $V_0 = \mathbb{C}$, and on the RHS we abbreviated V_j by j, and suppressed the dashed line. The representation j is *self-dual* iff $j^* = j$. For example, the trivial representation 0 is always self-dual.

The duality map is unique up to a complex factor. In fact, if there are two matrices Ω^j and Λ^j satisfying the intertwining operator condition, then the matrix $\Omega^j(\Lambda^j)^{-1}$ commutes with $\rho_j(g)$ for all $g \in \mathbb{G}$. Schur's lemma implies that Ω^j must be a multiple of Λ^j.

From the uniqueness of the duality map it follows that Ω^j for any self-dual $j \in I$ must be symmetric or antisymmetric. In fact, since $(\Omega^j)^T$ is also an intertwining operator, hence we have $(\Omega^j)^T = \alpha_j \Omega^j$ for some complex number α_j. Taking the transpose again yields $\alpha_j^2 = 1$.

The $\alpha_j = \pm 1$ is an intrinsic property of the representation j and is called the *Frobenius–Schur (FS) indicator*. For a self-dual $j \in I$, α_j is invariant under any rescaling of ω^j. In fact, α_j is explicitly determined by $\sum_{g \in \mathbb{G}} \mathrm{tr}_j(g^2) = \alpha_j \sum_{g \in \mathbb{G}} (\mathrm{tr}(g))^2$ (the summation occurs for a finite group $\mathbb{G}$, and is replaced by the haar measure $\int dg$ in a Lie group situation).

For example, all representations $j = 0, \frac{1}{2}, 1, \frac{3}{2}, \ldots$ of $SU(2)$ group are self-dual with $\alpha_j = (-1)^{2j}$. If $j^* \neq j$, we define $\alpha_j = 1$ by setting $\Omega^j = (\Omega^{j^*})^T$.

The inverse duality map $\omega_j^{-1} : V_{j^*} \otimes V_j \to \mathbb{C}$ is presented by

$$
\begin{array}{c}
\end{array}
\equiv
\begin{array}{c}
\end{array}
.
\tag{2.17}
$$

and satisfies

$$
\begin{array}{c}
\end{array}
=
\begin{array}{c}
\end{array}
,
\begin{array}{c}
\end{array}
=
\begin{array}{c}
\end{array}
\tag{2.18}
$$

where the bare straight lines on both RHS denote the identity maps. Again, ω_j^{-1} is abbreviated to a dot unless specified.

According to the normalization condition (2.14), we see that under the complex conjugation, the duality map transforms according to the FS indicator

$$\overline{\Omega^j_{mn}} = \alpha_j \left[(\Omega^{j^*})^{-1} \right]_{mn}$$

$$\overline{\Omega^{j^*}_{nm}} = \alpha_j \left[(\Omega^j)^{-1} \right]_{nm} \tag{2.19}$$

In our convention (2.14), one allows the freedom of a pure phase to determine the duality map. For example, for $j = 1/2$ representation of $SU(2)$, the η in Eq. (2.10) could be an arbitrary pure phase. In the next subsection, similar phases are dealt with to determine the $3j$-symbols. As we will see in Eq. (2.25) and (2.26), these two kinds of phases are actually dependent of each other. We have already observed the dependence between them in quantum theory, where the former is related to the time reversal transformation and the latter is related to the Clebsch-Gordan coefficient (will be defined in Eq. (2.31)).

2.1.2 $3j$-symbols

The tensor product $i \otimes j$ of any two (unitary) irreducible representations $i, j \in I$ can be decomposed into a direct sum of irreducible representations. The decomposition properties are specified by the $3j$-symbols. In this following we will discuss decomposition properties in a more symmetric way, i.e., consider the decomposition of three irreducible representations instead of two.

In general, in the decomposition of the tensor product $j_1 \otimes j_2 \otimes j_3$ of any three irreducible representations j_1, j_2, and j_3 of $\mathbb{G}$, the trivial representation 0 may appear more than once. Throughout this chapter, we assume that the group is multiplicity free, namely, the trivial representation 0 appears at most once in the decomposition of $j_1 \otimes j_2 \otimes j_3$ for all $j_1, j_2, j_3 \in I$. However, the generalization of the results in this chapter is straightforward.

A $3j$-symbol for any triple (j_1, j_2, j_3) is an intertwining operator

$$C_{j_1 j_2 j_3} : V_{j_1} \otimes V_{j_2} \otimes V_{j_3} \to \mathbb{C}$$

$$|j_1 m_1; j_2 m_2; j_3 m_3\rangle \mapsto C_{j_1 j_2 j_3; m_1 m_2 m_3}, \tag{2.20}$$

that satisfies the *normalization condition*

$$\sum_{m_1 m_2 m_3} C_{j_1 j_2 j_3; m_1 m_2 m_3} \overline{C_{j_1 j_2 j_3; m_1 m_2 m_3}} = 1. \tag{2.21}$$

Presented graphically, the normalization condition is

$$\tag{2.22}$$

for all $j_1, j_2, j_3 \in I$, where the $\overline{C_{j_1 j_2 j_3}}$ denotes the conjugate $3j$-symbol as defined by

$$\overline{C_{j_1 j_2 j_3}} : \mathbb{C} \to V_{j_1} \otimes V_{j_2} \otimes V_{j_3},$$

$$1 \mapsto \sum_{m_1 m_2 m_3} \overline{C_{j_1 j_2 j_3; m_1 m_2 m_3}} \, |j_1 m_1; j_2 m_2; j_3 m_3\rangle, \tag{2.23}$$

The triple (j_1, j_2, j_3) is called admissible if there exists nonzero $3j$-symbol $C_{j_1 j_2 j_3}$. It means that the trivial representation 0 appears in the decomposition of the tensor product $j_1 \otimes j_2 \otimes j_3$. We assign the fusion rules $\delta_{j_1 j_2 j_3} = 1$ if (j_1, j_2, j_3) is admissible and $\delta_{j_1 j_2 j_3} = 0$ otherwise.

Similar to the duality map, the phase of the $3j$-symbol is not determined by the defining equation. The undetermined phase may be a function of of j_1, j_2, and j_3 but is independent of m_1, m_2, and m_3. The phase may also depend on the order in which j_1, j_2, and j_3 appear in the $3j$-symbol. Thus the $3j$-symbols are defined only up to some phases and this freedom can be exploited to impose some symmetry properties on the $3j$-symbols. For example, by an appropriate choice of these phases, we can make the $3j$-symbol symmetric or antisymmetric under permutations of the j's and the corresponding m's.

In this chapter, we will not consider the usual permutations directly applied on the triple, but those that take any triple $(j_1 j_2 j_3)$ to

$$(j_1 j_2 j_3), (j_2 j_3 j_1), (j_3 j_1 j_2), (j_3{}^* j_2{}^* j_1{}^*), (j_2{}^* j_1{}^* j_3{}^*), (j_1{}^* j_3{}^* j_2{}^*). \tag{2.24}$$

For odd permutations, we take all representations to their dual in additional to the permutation on the order. Then we will require symmetry conditions under such permutations. The reason for such permutations is the following. The dual representation of $j_1 \otimes j_2 \otimes j_3$ is $(j_3{}^* j_2{}^* j_1{}^*)$, and thus we have certain symmetry property induced by this duality map. We think that this symmetry property (if exists) under our above permutations is more fundamental, because in the representation theory of more general algebra, the symmetry induced by the usual odd permutation does not hold, while the symmetry induced by the above duality map still holds.

We require the *cyclic conditions* on the $3j$-symbols by

$$C_{j_1 j_2 j_3; m_1 m_2 m_3} = \alpha_{j_3} C_{j_3 j_1 j_2; m_3 m_1 m_2}, \tag{2.25}$$

and the *dagger condition*

$$\overline{C_{j_1 j_2 j_3; m_1 m_2 m_3}} = \sum_{n_1 n_2 n_3} C_{j_3{}^* j_2{}^* j_1{}^*; n_3 n_2 n_1} \Omega^{j_3{}^*}_{n_3 m_3} \Omega^{j_2{}^*}_{n_2 m_2} \Omega^{j_1{}^*}_{n_1 m_1}, \tag{2.26}$$

for all $j_1, j_2, j_3 \in I$, $m_1 = 1, 2, \ldots, d_{j_1}$, $m_2 = 1, 2, \ldots, d_{j_2}$ and $m_3 = 1, 2, \ldots, d_{j_3}$. Graphically they are presented by

$$\text{(2.27)}$$

and

$$\text{(2.28)}$$

where Eq. (2.27) is obtained by using the relation (2.19), which has a slightly different form from Eq. (2.25), which can be adapted to quantum group case in the next chapter.

By the condition (2.28), the normalization condition (2.22) can be expressed by

$$= 1, \qquad \text{(2.29)}$$

for all admissible (j_1, j_2, j_3).

In some literatures (for example, see [53]), $3j$-symbols are defined of similar form as the Clebsch-Gordan coefficient in the angular momentum theory that specifies the rule to decompose the tensor product of any two irreducible representations of the group $SU(2)$. Let us define Clebsch-Gordan coefficient in terms of the $3j$-symbols as follows. A Clebsch-Gordan coefficient is $\mathbb{G}$ –morphism

$$C^{j_3^*}_{j_1 j_2} : V_{j_1} \otimes V_{j_2} \to V_{j_3^*}$$
$$|j_1 m_1; j_2 m_2\rangle \mapsto \sum_{m_3^*} C^{j_3^* m_3^*}_{j_1 m_1; j_2 m_2} |j_3^* m_3^*\rangle \qquad \text{(2.30)}$$

defined by

$$\text{(2.31)}$$

where the second equality is due to the symmetry condition (2.25).

Under these the symmetry conditions, it is safe to suppress the coupons of the $3j$-symbols, the duality maps, the inverse duality maps, and their compositions, into a trivalent

or two-valent vertex. We also suppress the arrows without introducing any confusion. We enumerate the suppression rules for two-valent vertices as follows

$$(2.32)$$

and for three-valent vertices

$$(2.33)$$

For example, an important property of the Clebsch-Gordan coefficient (2.31) is

$$(2.34)$$

for any $g \in \mathbb{G}$, where $d_{j_3} = \alpha_{j_3} \dim_{j_3}$. The conditions (2.25),(2.26) and the normalization condition (2.21) are used to derive the coefficients d_{j_3}. More details about d_{j_3} will be discussed in the next subsection.

Before ending this subsection, we check the self-consistency of the cyclic condition, the dagger condition, and the normalization condition.

First, applying the cyclic condition (2.25) three times on $C_{j_1 j_2 j_3}$ yields $C_{j_1 j_2 j_3} = \alpha_{j_1} \alpha_{j_2} \times \alpha_{j_3} C_{j_1 j_2 j_3}$. But the extra phase is eliminated by the property that

$$\alpha_{j_1} \alpha_{j_2} \alpha_{j_3} = 1, \qquad (2.35)$$

for all $j_1, j_2, j_3 \in I$ if $\delta_{j_1 j_2 j_3} = 1$.

Second, we need to verify $C_{jjj;m_1m_2m_3} = C_{jjj;m_3m_1m_2}$ for any admissible triple (j, j, j). Assume $C_{jjj;m_1m_2m_3} = \beta C_{jjj;m_3m_1m_2}$ with $\beta = 1$ or $\exp(\pm 2\pi i/3)$. Since the $3j$-symbol $C_{jjj;m_1m_2m_3}$ is proportional to $\sum_{g \in \mathbb{G}} \rho_{m_1'm_1}(g)\rho_{m_2'm_2}(g)\rho_{m_3'm_3}(g)T_{m_1'm_2'm_3'}$ for arbitrary tensor T (the summation occurs for a finite group $\mathbb{G}$, and is replaced by the haar measure $\int dg$ in a Lie group situation), the symmetry condition (2.25) amounts to $\sum_g \rho_{m_1'm_1}(g)\rho_{m_2'm_2}(g) \times \rho_{m_3'm_3}(g) = \beta \sum_g \rho_{m_1'm_3}(g)\rho_{m_2'm_1}(g)\rho_{m_3'm_2}(g)$. With the identification $m_1 = m_2', m_2 = m_1'$ and $m_3' = m_3$, the contraction yields $\sum_g \operatorname{tr}(g^2)\operatorname{tr}(g) = \beta \sum_g \operatorname{tr}(g^2)\operatorname{tr}(g)$. This verifies $\beta = 1$.

In the following we show that the symmetry conditions (2.25) and (2.26) can be achieved by a rescaling of the $3j$-symbols. The rescaling is taken as follows.

For each admissible (j_1, j_2, j_3), we start with a set (2.24) of $3j$-symbols generated by the permutations on $(j_1 j_2 j_3)$. Suppose they satisfy the first symmetry condition (2.25).

We consider two situations. The first situation is when the admissible triple (j_1, j_2, j_3) satisfies $j_1 = j_1^*, j_2 = j_3^*$ (or similarly, $j_2 = j_2^*, j_1 = j_3^*$ or $j_3 = j_3^*, j_1 = j_2^*$).

By Schur's lemma, we have

$$
\begin{array}{ccc}
\includegraphics{fig} & = & \beta_{j_1 j_2 j_3} \times \includegraphics{fig}
\end{array}
\tag{2.36}
$$

for some complex number $\beta_{j_1 j_2 j_3}$. The $\beta \equiv \beta_{j_1 j_2 j_3} = \beta_{j_3 j_1 j_2} = \beta_{j_2 j_3 j_1}$ does not depend on the order of $j_1 j_2 j_3$ as required by the first symmetry condition (2.25). Apply the conjugate transformation (2.58) on both sides of Eq. (2.36), we obtain $\beta\bar{\beta} = 1$. On the other hand, the normalization condition (2.22) implies

$$
\includegraphics{fig} = \beta \times \includegraphics{fig} = \beta \operatorname{id}_{\mathbb{C}}.
\tag{2.37}
$$

Since the LHS is evaluated to $\left(\sum_{m_1m_2m_3} |C_{j_1j_2j_3;m_1m_2m_3}|^2\right) \operatorname{id}_{\mathbb{C}}$ and thus β must be positive. Together with the above result $|\beta| = 1$ it implies $\beta = 1$. Hence the first symmetry condition (2.25) automatically implies the second symmetry condition (2.26).

The second situation is when the triple (j_1, j_2, j_3) does not match any cyclic permutation of (j_3^*, j_2^*, j_1^*), $C_{j_1j_2j_3}$ and $C_{j_3^*j_2^*j_1^*}$. We assume Eq. (2.36) with $\beta \equiv \beta_{j_1j_2j_3}$ to be determined. Notice that β must be positive according to Eq. (2.37). The following rescaling cancels β in Eq. (2.36).

$$
C_{j_1j_2j_3} \mapsto \frac{1}{\sqrt{\beta}}C_{j_1j_2j_3}, \quad C_{j_1^*j_2^*j_3^*} \mapsto \sqrt{\beta}C_{j_1^*j_2^*j_3^*}.
\tag{2.38}
$$

2.1.3   Normalized $6j$-symbols

There are two equivalent ways to decompose any tensor product $i \otimes j \otimes k$ for $i, j, k \in I$ through the $3j$-symbols, which are related by some global factors. Each way is specified by an intertwining operator between the tensor product representation and any irreducible representation. A $6j$-symbol F is a complex tensor defined by

$$
\begin{array}{c}
{}^{j^*}\diagdown\,{}^{i^*}\diagup\,{}^{l^*} \\
m \diagdown\diagup \\
\Big|\,k
\end{array}
= \sum_n F^{ijm}_{kln} \;
\begin{array}{c}
{}^{i^*}\diagdown\,{}^{l^*} \\
{}^{j^*}\diagdown\, n \\
\Big|\,k
\end{array}
\,. \tag{2.39}
$$

Here the order of the indices in the tensor F is taken to fit the convention as in (1.4). The F only depends on the representation labels, which has the origin that all unitary representations are decomposable.

There are two important identities. The first one is the pentagon identity (Biedenharn-Elliot identity)

$$
\sum_n F^{mlq}_{kp^*n} F^{jip}_{mns^*} F^{js^*n}_{lkr^*} = F^{jip}_{q^*kr^*} F^{riq^*}_{mls^*}. \tag{2.40}
$$

which comes from two equivalent ways to express the one of the following morphism as a linear combination of the other

$$
\begin{array}{ccc}
\diagup\!\diagdown\!\diagup & & \diagup\!\diagdown \\
\diagdown\!\diagup & \Rightarrow & \diagdown\!\diagup \\
\Big| & & \Big|
\end{array}
\tag{2.41}
$$

Assume the F tensor is defined using the $3j$-symbols under the conditions (2.22), (2.25) and (2.26), then we have the second identity called the orthogonality condition,

$$
\sum_n F^{ijm}_{kln} Fjkn^*{}_{lip} = \delta_{pm}\delta_{m^*kl}\delta_{jmi} \tag{2.42}
$$

To prove it, we start with the RHS of Eq. (2.39) and apply the identity

$$
\begin{array}{c}
\diagup\!\diagdown \\ \bullet \\ \Big|
\end{array}
=
\begin{array}{c}
\diagup\,\bullet\!\diagdown\!\diagup \\ \bullet
\end{array}
, \tag{2.43}
$$

on both trivalent vertices. Applying the identity (2.39) and (2.43) again takes back the diagram to the LHS of Eq. (2.39), and proves the orthogonality condition. Notice that the orthogonality condition depends on the particular symmetry conditions, whereas the pentagon identity holds in any convention of the $6j$.

The tensor F can be explicitly expressed in terms of the $3j$-symbols and the duality maps. Compose the both sides of Eq. (2.39) by the duality maps and the $3j$-symbols in

an appropriate way and use the Schur's lemma to eliminate the summation over n on the RHS to a particular n, we obtain

$$\text{(diagram)} = F^{ijm}_{kln} \text{(diagram)}. \tag{2.44}$$

The RHS diagram can be reduced. The bubbles can be removed by the relation

$$\text{(diagram)} = \frac{1}{\text{(diagram)}} \times \text{(diagram)}. \tag{2.45}$$

The RHS is an intertwining operator from the irreducible representations space i to itself, and thus must be a multiple of the identity map by Schur's lemma. The coefficient d_i is determined by the normalization condition (2.22). Apply this relation to the RHS and use the normalization condition (2.22), and we have

$$F^{ijm}_{kln} = \text{(diagram)} \times \text{(diagram)} \tag{2.46}$$

In the evaluation we eliminate all $\oslash$–like diagrams, which evaluate to 1 according to the normalization condition (2.22).

In the last line above, the diagram $\oslash$ evaluates to

$$\text{d}_n \equiv \text{(diagram)} = \alpha_n \text{tr}(\Omega^{n\dagger}\Omega^n) = \alpha_n \text{dim}_n, \tag{2.47}$$

where $\text{dim}_n = \text{dim}(V_n)$ is the dimension of the representation space V_n. The d_j may be positive or negative, but it has some similar properties as the dimension d_j. For example, the property $d_i d_j = \sum_k \delta_{ijk^*} d_k$ implies $\text{d}_i \text{d}_j = \sum_k \delta_{ijk^*} \text{d}_k$, because $\alpha_i \alpha_j = \alpha_k$ for any admissible (i, j, k^*).

We define the *symmetrized* $6j$-*symbol* in terms of $3j$-symbols and duality maps by

$$G^{ijm}_{kln} \equiv \sum_{a_i,b_i,a_j,b_j,\ldots,a_n,b_n} \Omega^i_{a_i b_i} \Omega^j_{a_j b_j} \Omega^m_{a_m b_m} \Omega^k_{a_k b_k} \Omega^l_{a_l b_l} \times$$
$$\Omega^n_{a_n b_n} C_{lm^*k;a_l b_m a_k} C_{k^*j^*n;b_k b_j a_n} C_{n^*i^*l^*;b_n b_i b_l} C_{ijm;a_i a_j a_m}, \tag{2.48}$$

where $a_i, b_i = 1, 2, \ldots, d_i$. Its diagram presentation is

$$G^{ijm}_{kln} \equiv \text{(diagram)} \tag{2.49}$$

Or equivalently, by the relation (2.31), it can be expressed in terms of Clebsch-Gordan coefficient by

$$G^{ijm}_{kln} = \qquad \qquad \qquad (2.50)$$

The tensor G differs from F by

$$G^{ijm}_{kln} = F^{ijm}_{kln}/\mathrm{d}_n \qquad (2.51)$$

We emphasize that the definition has good symmetry properties only under the conditions (2.22), (2.25) and (2.26). If the $3j$-symbols follow other conventions, the relationship (2.51) may need to be modified for G to be symmetrized.

The diagram in (2.50) has the shape of a tetrahedron,

$$ \qquad \qquad \qquad (2.52)$$

and has the corresponding tetrahedral symmetry. The geometric symmetry of a tetrahedron consists of 24 transformations generated by two rotation generators and one reflection generator. Correspondingly, we will show that the symmetrized $6j$ symbols have the tetrahedral symmetry in (1.4). The two rotation generators correspond to the conditions (2.25) and (2.26), and the reflection generator corresponds to unitarity of the representations, as explained in the following.

First, the diagram in (2.52) allows a rotation by $2\pi/3$. We can apply a corresponding rotation to the diagram and obtain

$$ \qquad = \qquad = \qquad , \qquad (2.53)$$

where we used the properties (2.18) in the first equality, and the first symmetry condition (2.25) in the second equality. Hence we obtain the first equality in the tetrahedral symmetry in Eq. (1.4)

$$G^{ijm}_{kln} = G^{mij}_{nk^*l^*}. \qquad (2.54)$$

Second, we can "drag" the line l^* to the right,

$$ \qquad = \qquad \qquad (2.55)$$

where $\Omega^n = \alpha_n(\Omega^{n^*})^T$ is used at the bottom and the top tips. Using again the first symmetry condition (2.25) to transform the diagram to the shape as in the definition (2.50), we obtain the second equality of tetrahedral symmetry in (1.4)

$$G^{mij}_{nk^*l^*} = G^{klm^*}_{ijn^*}. \tag{2.56}$$

The last equality of tetrahedral symmetry corresponds to the upsidedown "reflection" of the diagram. It is related to taking the complex conjugate of the duality map and the $3j$-symbols. Let us define the conjugate transformation by

$$\omega_j : 0 \to j \otimes j^*; \; 1 \mapsto \sum_{m_1, m_2} \Omega^j_{m_1 m_2} |m_1, m_2\rangle$$

$$\Downarrow$$

$$\overline{\omega_j} : j \otimes j^* \to 0; \; |m_1, m_2\rangle \mapsto \overline{\Omega^j_{m_1 m_2}} \tag{2.57}$$

and

$$C_{j_1 j_2 j_3} : V_{j_1} \otimes V_{j_2} \otimes V_{j_3} \to \mathbb{C},$$

$$|j_1 m_1; j_2 m_2; j_3 m_3\rangle \mapsto C_{j_1 j_2 j_3; m_1 m_2 m_3},$$

$$\Downarrow$$

$$\overline{C_{j_1 j_2 j_3}} : \mathbb{C} \to V_{j_1} \otimes V_{j_2} \otimes V_{j_3},$$

$$1 \mapsto \sum_{m_1 m_2 m_3} \overline{C_{j_1 j_2 j_3; m_1 m_2 m_3}} |j_1 m_1; j_2 m_2; j_3 m_3\rangle, \tag{2.58}$$

and require $\overline{c\,\omega_j} = \overline{c}\,\overline{\omega_j}$ and $\overline{\overline{\omega_j}} = \omega_j$ for any complex number c (and the same rule applies to $C_{j_1 j_2 j_3}$). By $c\,\omega_j$ we mean

$$c\,\omega_j : 0 \to j \otimes j^*; \; 1 \mapsto \sum_{m_1, m_2} c\Omega^j_{m_1 m_2} |m_1, m_2\rangle. \tag{2.59}$$

We show the *transformation rule* under such transformations in the following.

By the relationship (2.19) we have

$$\Leftrightarrow \quad \alpha_j \times \tag{2.60}$$

The dagger condition (2.26) on the $3j$-symbols implies

$$\Leftrightarrow \tag{2.61}$$
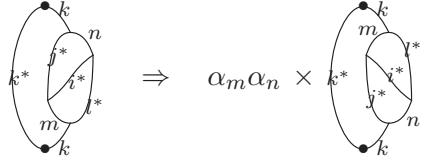
For the compositions of the duality map and the $3j$ symbols, we have

$$\Leftrightarrow \quad \alpha_k \times \tag{2.62}$$

Now let us apply these complex conjugate transformation rules to the RHS of Eq. (2.50). One one hand, the transformation takes any complex number to its complex conjugate, i.e.,

$$G_{kln}^{ijm} \quad \Rightarrow \quad \overline{G_{kln}^{ijm}}. \tag{2.63}$$

One the other hand, we apply the above transformation rules to all trivalent and two vertices in the diagram, and have

$$\Rightarrow \quad \alpha_m \alpha_n \times$$ (2.64)

Using the first symmetry condition (2.25) to transform the diagram on the RHS to the standard shape in the definition (2.50), we obtain the last equality of tetrahedral symmetry in Eq. (1.4):

$$\overline{G_{kln}^{ijm}} = \alpha_m \alpha_n G_{l^*k^*n}^{j^*i^*m^*}. \tag{2.65}$$

Therefore we obtain the *tetrahedral symmetry*

$$G_{kln}^{ijm} = G_{nk^*l^*}^{mij} = G_{ijn^*}^{klm^*} = \alpha_m \alpha_n \overline{G_{l^*k^*n}^{j^*i^*m^*}}, \tag{2.66}$$

From the relationship (2.51), we also have the *pentagon identity*

$$\sum_n \mathrm{d}_n G_{kp^*n}^{mlq} G_{mns^*}^{jip} G_{lkr^*}^{js^*n} = G_{q^*kr^*}^{jip} G_{mls^*}^{riq^*}, \tag{2.67}$$

and the *orthogonality condition*

$$\sum_n \mathrm{d}_n \mathrm{d}_n G_{kln}^{ijm} G_{lip}^{jkn^*} = \delta_{pm} \delta_{m^*kl} \delta_{jmi}. \tag{2.68}$$

The last two identities are directly derived from two identities (2.40).

2.2   Algorithm and examples

The $3j$-symbols and $6j$-symbols are intertwining operators. The intertwining operator can be obtained by taking the average of any initial map over all group actions.

Suppose (ρ, V) and (ρ', V') are irreducible representations of $\mathbb{G}$, and $T : V \to V'$ is any linear operator. Then $\tilde{T} : V \to V'$ is an intertwining operator (an intertwining operator) where $\tilde{T}$ is an average of T over all group actions given by

$$\tilde{T} = \frac{1}{|\mathbb{G}|} \sum_{g \in \mathbb{G}} \rho'(g) T \rho(g^{-1}). \tag{2.69}$$

if $\mathbb{G}$ is a finite group, with $|\mathbb{G}|$ the order of the group $\mathbb{G}$. The summation is replaced by the haar measure $\int dg$ for a Lie group.

The duality maps and the $3j$-symbols for an arbitrary group can be constructed in this way. By Schur's lemma, all duality maps and the $3j$-symbols are unique up to some constant factors. (We assumed that 0 appears at most once in the decomposition of $i \otimes k \otimes k$ for all $i, j, k \in I$.) These factors will be fixed by the conditions (2.14), (2.22), (2.25) and (2.26). The symmetrized $6j$-symbols are constructed based on these duality maps and $3j$-symbols.

Starting with a set I of irreducible representations $[\rho_j(g)]_{mn}$ of a finite group $\mathbb{G}$, we detail the search for the duality maps, the $3j$-symbols, and the $6j$-symbols by the following algorithm.

1. Find the dual pairs (j, j^*) for all $j \in I$, such that there exists nonzero matrix

$$\Omega^j_{mn} = \frac{1}{|\mathbb{G}|} \sum_{g \in G} [\rho_j(g)]_{mm'} [\rho_{j^*}(g)]_{nn'} T_{m'n'} \qquad (2.70)$$

   where $m, n = 1, \ldots, d_j$ and $T_{m'n'}$ is a nonzero random matrix. (It is possible that Ω^j happens to be zero for some special matrices T while in fact there exists a nonzero Ω^j. Therefore T should be random enough to avoid this possibility.) If $j \neq j^*$, we set $\Omega^{j^*} = (\Omega^j)^T$.

2. Renormalize the matrices ω^j such that $(\Omega^j)^\dagger \Omega^j = \mathbb{1}$.

3. Determine the FS indicator α_j for each $j \in I$ according to $\Omega^j_{mn} = \alpha_j \Omega^{j^*}_{nm}$.

4. We collect together triples by the cyclic permutations $(j_1 j_2 j_3) \mapsto (j_2 j_3 j_1)$ and $(j_1 j_2 j_3) \mapsto (j_3{}^* j_2{}^* j_1{}^*)$. For each set of $(j_1 j_2 j_3)$, $(j_2 j_3 j_1)$, $(j_3 j_1 j_2)$, $(j_3{}^* j_2{}^* j_1{}^*)$, $(j_2{}^* j_1{}^* j_3{}^*)$, and $(j_1{}^* j_3{}^* j_2{}^*)$ generated from one triple $(j_1 j_2 j_3)$, we pick up an arbitrary representative, say $(j_1 j_2 j_3)$, and find the $3j$-symbol for $(j_1 j_2 j_3)$ by

$$C_{j_1 j_2 j_3; m_1 m_2 m_3} = \frac{1}{|\mathbb{G}|} \sum_{g \in G} [\rho_{j_1}(g)]_{m'_1 m_1} \times$$

$$[\rho_{j_2}(g)]_{m'_2 m_2} [\rho_{j_3}(g)]_{m'_3 m_3} T_{m'_1 m'_2 m'_3}, \qquad (2.71)$$

   with $m_1 = 1, \ldots, d_{j_1}$, $m_2 = 1, \ldots, d_{j_2}$, and $m_3 = 1, \ldots, d_{j_3}$, and T a nonzero random tensor. We set the $3j$-symbols for other triples by

$$C_{j_3 j_1 j_2; m_3 m_1 m_2} = \alpha_{j_3} C_{j_1 j_2 j_3; m_1 m_2 m_3}, \qquad (2.72)$$

if $(j_3 j_2 j_1) \neq (j_1 j_2 j_3)$, and

$$C_{j_3{}^* j_2{}^* j_1{}^*; n_3 n_2 n_1} =$$

$$\sum_{m_1 m_2 m_3} \overline{C_{j_1 j_2 j_3; m_1 m_2 m_3} \Omega^{j_1}_{m_1 n_1} \Omega^{j_2}_{m_2 n_2} \Omega^{j_3}_{m_3 n_3}}, \qquad (2.73)$$

if $(j_3{}^*j_2{}^*j_1{}^*)$ differs from any cyclic permutation of $(j_1j_2j_3)$. The other triples are obtained by the same rule (2.72) under cyclic permutation.

5. Determine the fusion rule $\delta_{j_1j_2j_3}$. We set $\delta_{j_1j_2j_3} = 1$ and say (j_1, j_2, j_3) is admissible, if the tensor $C_{j_1j_2j_3;m_1m_2m_3}$ is nonzero. Otherwise we set $\delta_{j_1j_2j_3} = 0$. (In step 4 and 5 we assume that the fusion rule is multiplicity free, i.e., $C_{j_1j_2j_3;m_1m_2m_3}$ is unique up to a constant factor no matter what the random tensor T is. In a general case, we may need to find more than one independent tensor $C_{j_1j_2j_3;m_1m_2m_3}$ by trying various random tensors T, which we will not detail in this chapter.)

6. Renormalize the $3j$-symbols such that

$$\sum_{m_1m_2m_3n_1n_2n_3} \Omega^{j_1}_{m_1n_1}\Omega^{j_2}_{m_2n_2}\Omega^{j_3}_{m_3n_3} \times$$
$$C_{j_1j_2j_3;m_1m_2m_3}C_{j_3{}^*j_2{}^*j_1{}^*;n_3n_2n_1} = 1. \tag{2.74}$$

7. The symmetrized $6j$-symbol is

$$G^{ijm}_{kln} = \sum_{a_i,b_i,a_j,b_j,\ldots,a_n,b_n} \Omega^i_{a_ib_i}\Omega^j_{a_jb_j}\Omega^m_{a_mb_m}\Omega^k_{a_kb_k}\Omega^l_{a_lb_l} \times$$
$$\Omega^n_{a_nb_n}C_{lm{}^*k;a_lb_ma_k}C_{k{}^*j{}^*n;b_kb_ja_n}C_{n{}^*i{}^*l{}^*;b_nb_ib_l}C_{ijm;a_ia_ja_m}. \tag{2.75}$$

where $a_i, b_i = 1, 2, \ldots, d_i$.

2.2.1 Abelian groups

It is known that any abelian group is dual to its representations by a Fourier transformation.

Consider the abelian group $\mathbb{G} = \mathbb{Z}_{M_1} \times \mathbb{Z}_{M_2} \times \ldots$. The set of complete irreducible representations is $I = \{(m_1, n_2, \ldots), m_1 = 1, 2, \ldots, M_1; m_2 = 1, 2, \ldots, M_2; \ldots\}$. All of them are one-dimensional. Let us denote each representation by $m = (m_1, m_2, \ldots)$.

The fusion rules are given by $\delta_{ijk} = 1$ iff $i_l + j_l + k_l = 0 \bmod M_l$ for all l, and i is dual to j if $i_l + j_l = 0 \bmod M_l$ for all l.

The intertwining operators are trivial:

$$\Omega^j = 1, \text{ for all } j,$$
$$C_{ijk} = \delta_{ijk}, \tag{2.76}$$

and the $6j$-symbol is given by

$$G^{ijm}_{kln} = \delta_{ijm}\delta_{klm{}^*}\delta_{jkn{}^*}\delta_{inl}. \tag{2.77}$$

2.2.2 $\mathbb{G} = D_3$

The Dihedral group D_3 (also known as the symmetry or permutation group S_3) is the simplest nonabelian group. The multiplication table is presented in Table 2.1, where 1 denotes the identity element.

All group elements are generated by S and R, where S is a rotation by π radians about an axis passing the center of a triangle and one of its vertices and R is a rotation by $2\pi/3$ about the center of the triangle. The multiplication table above corresponds to $1 = S^0 R^0$, $2 = S^0 R^1$, $3 = S^0 R^2$, $4 = S^1 r^1$, $5 = S^1 R^0$, and $6 = S^1 R^2$.

There are three inequivalent classes of irreducible representations, with the dimensions $\dim_0 = \dim_1 = 1$ and $\dim_2 = 2$. One set $I = \{0, 1, 2\}$ of irreducible representations is presented in Table 2.2.

All representations $j = 0, 1, 2$ are self-dual, with the duality maps being

$$\Omega^0 = 1, \quad \Omega^1 = 1, \quad \Omega^2 = \begin{pmatrix} 1 & 0 \\ 0 & 1 \end{pmatrix}. \tag{2.78}$$

All of them are symmetric matrices, and hence we have $\alpha_j = 1$ and thus $d_j = \dim_j$ for all $j = 0, 1, 2$.

The independent nonzero $3j$-symbols are

$$C_{000} = C_{011} = 1,$$
$$C_{022;1m_1m_2} = \begin{pmatrix} \frac{1}{2} & 0 \\ 0 & \frac{1}{2} \end{pmatrix}_{m_1 m_2},$$
$$C_{122;1m_1m_2} = \begin{pmatrix} 0 & \frac{i}{\sqrt{2}} \\ \frac{-i}{\sqrt{2}} & 0 \end{pmatrix}_{m_1 m_2},$$
$$C_{222;m_1m_2m_3} = \begin{pmatrix} \{0, \frac{1}{2}\} & \{\frac{1}{2}, 0\} \\ \{\frac{1}{2}, 0\} & \{0, -\frac{1}{2}\} \end{pmatrix}_{m_1 m_2 m_3}, \tag{2.79}$$

where $m_1, m_2, m_3 = 1, 2$. The representation 0 and 1 are one-dimensional so that the corresponding m takes on exactly one value denoted by $_1$. The normalization factors are

Table 2.1. Multiplication table of $\mathbb{G} = D_3$ (or S_3).

	1	2	3	4	5	6
1	1	2	3	4	5	6
2	2	3	1	5	6	4
3	3	1	2	6	4	5
4	4	6	5	1	3	2
5	5	4	6	2	1	3
6	6	5	4	3	2	1

Table 2.2. Irreducible representations of $\mathbb{G} = D_3$ (or S_3).

	ρ_0	ρ_1	ρ_2
1	1	1	$\begin{pmatrix} 1 & 0 \\ 0 & 1 \end{pmatrix}$
2	1	1	$\begin{pmatrix} -\frac{1}{2} & -\frac{\sqrt{3}}{2} \\ \frac{\sqrt{3}}{2} & -\frac{1}{2} \end{pmatrix}$
3	1	1	$\begin{pmatrix} -\frac{1}{2} & \frac{\sqrt{3}}{2} \\ -\frac{\sqrt{3}}{2} & -\frac{1}{2} \end{pmatrix}$
4	1	-1	$\begin{pmatrix} \frac{1}{2} & \frac{\sqrt{3}}{2} \\ \frac{\sqrt{3}}{2} & -\frac{1}{2} \end{pmatrix}$
5	1	-1	$\begin{pmatrix} -1 & 0 \\ 0 & 1 \end{pmatrix}$
6	1	-1	$\begin{pmatrix} \frac{1}{2} & -\frac{\sqrt{3}}{2} \\ -\frac{\sqrt{3}}{2} & -\frac{1}{2} \end{pmatrix}$

determined by the conditions (2.22), (2.25) and (2.26). All other nonzero $3j$-symbols are determined through the first symmetry condition $C_{ijj;m_1m_2m_3} = C_{jij;m_3m_1m_2} = C_{jji;m_2m_3m_1}$ for triples $(i,j,j) = (011), (022)$ and (122).

The fusion rules are given by $\delta_{000} = \delta_{011} = \delta_{022} = \delta_{122} = \delta_{222} = 1$, corresponding to the nonzero $3j$-symbols.

The independent nonzero symmetrized $6j$-symbols (2.50) are

$$G_{000}^{000} = 1, G_{111}^{000} = 1, G_{222}^{000} = \frac{1}{\sqrt{2}}, G_{011}^{011} = 1, G_{222}^{011} = \frac{1}{\sqrt{2}},$$

$$G_{022}^{022} = \frac{1}{2}, G_{122}^{022} = \frac{1}{2}, G_{222}^{022} = \frac{1}{2}, G_{122}^{122} = \frac{1}{2}, G_{222}^{122} = -\frac{1}{2}. \tag{2.80}$$

All other nonzero $6j$-symbols are obtained through the tetrahedral symmetry (1.4). One verifies that they do satisfy all three identities (2.66), (2.67) and (2.68).

2.2.3 $\quad \mathbb{G} = D_4$

Consider the Dihedral group D_4 of order 8. The multiplication table is presented in Table 2.3, where 1 denotes the identity element.

All group elements are generated by S and R, where S is a rotation by π radians about an axis passing the center of a triangle and one of its vertices and R is a rotation by $\pi/2$

Table 2.3. Multiplication table of $\mathbb{G} = D_4$.

	1	2	3	4	5	6	7	8
1	1	2	3	4	5	6	7	8
2	2	3	4	1	8	5	6	7
3	3	4	1	2	7	8	5	6
4	4	1	2	3	6	7	8	5
5	5	6	7	8	1	2	3	4
6	6	7	8	5	4	1	2	3
7	7	8	5	6	3	4	1	2
8	8	5	6	7	2	3	4	1

about the center of the triangle. The multiplication table above corresponds to $1 = S^0 R^0$, $2 = S^0 R^1$, $3 = S^0 R^2$, $4 = S^0 R^3$, $5 = S^1 R^0$, $6 = S^1 R^1$, $7 = S^1 R^2$, and $8 = S^1 R^3$.

There are five inequivalent classes of irreducible representations. One set $I = \{0, 1, 2, 3, 4\}$ of irreducible representations is presented in Table 2.4.

All representations $j = 0, 1, 2, 3, 4$ are self-dual with the duality maps being

$$\Omega^0 = 1, \quad \Omega^1 = 1, \quad \Omega^2 = 1, \Omega^3 = 1, \quad \Omega^4 = \begin{pmatrix} 1 & 0 \\ 0 & 1 \end{pmatrix}. \tag{2.81}$$

which implies $\alpha_j = 1$ and thus $d_j = \dim_j$ for all $j = 0, 1, 2, 3, 4$.

Table 2.4. Irreducible representations of D_4.

	ρ_0	ρ_1	ρ_2	ρ_3	ρ_4
1	1	1	1	1	$\begin{pmatrix} 1 & 0 \\ 0 & 1 \end{pmatrix}$
2	1	1	-1	-1	$\begin{pmatrix} 0 & -1 \\ 1 & 0 \end{pmatrix}$
3	1	1	1	1	$\begin{pmatrix} -1 & 0 \\ 0 & -1 \end{pmatrix}$
4	1	1	-1	-1	$\begin{pmatrix} 0 & 1 \\ -1 & 0 \end{pmatrix}$
5	1	-1	1	-1	$\begin{pmatrix} 1 & 0 \\ 0 & -1 \end{pmatrix}$
6	1	-1	-1	1	$\begin{pmatrix} 0 & -1 \\ -1 & 0 \end{pmatrix}$
7	1	-1	1	-1	$\begin{pmatrix} -1 & 0 \\ 0 & 1 \end{pmatrix}$
8	1	-1	-1	1	$\begin{pmatrix} 0 & 1 \\ 1 & 0 \end{pmatrix}$

The independent nonzero $3j$-symbols are

$$C_{000} = C_{011} = C_{022} = C_{033} = C_{044} = C_{234} = 1,$$

$$C_{044} = \begin{pmatrix} \frac{1}{\sqrt{2}} & 0 \\ 0 & \frac{1}{\sqrt{2}} \end{pmatrix}, \qquad C_{144} = \begin{pmatrix} 0 & \frac{i}{\sqrt{2}} \\ -\frac{i}{\sqrt{2}} & 0 \end{pmatrix},$$

$$C_{244} = \begin{pmatrix} \frac{1}{\sqrt{2}} & 0 \\ 0 & -\frac{1}{\sqrt{2}} \end{pmatrix}, \quad C_{344} = \begin{pmatrix} 0 & \frac{1}{\sqrt{2}} \\ \frac{1}{\sqrt{2}} & 0 \end{pmatrix}. \tag{2.82}$$

The fusion rules are thus obtained by $\delta_{111} = \delta_{122} = \delta_{133} = \delta_{144} = \delta_{155} = \delta_{234} = \delta_{255} = \delta_{355} = \delta_{455} = 1$.

The independent nonzero symmetrized $6j$-symbols (2.50) are

$$G_{000}^{000} = 1, G_{111}^{000} = 1, G_{222}^{000} = 1, G_{333}^{000} = 1, G_{444}^{000} = \frac{1}{\sqrt{2}},$$

$$G_{011}^{011} = 1, G_{233}^{011} = 1, G_{322}^{011} = 1, G_{444}^{011} = \frac{1}{\sqrt{2}}, G_{022}^{022} = 1,$$

$$G_{133}^{022} = 1, G_{444}^{022} = \frac{1}{\sqrt{2}}, G_{033}^{033} = 1, G_{444}^{033} = \frac{1}{\sqrt{2}}, G_{044}^{044} = \frac{1}{2},$$

$$G_{144}^{044} = \frac{1}{2}, G_{244}^{044} = \frac{1}{2}, G_{344}^{044} = \frac{1}{2}, G_{123}^{123} = 1, G_{444}^{123} = -\frac{i}{\sqrt{2}},$$

$$G_{144}^{144} = \frac{1}{2}, G_{244}^{144} = -\frac{1}{2}, G_{344}^{144} = -\frac{1}{2}, G_{244}^{244} = \frac{1}{2},$$

$$G_{344}^{244} = -\frac{1}{2}, G_{344}^{344} = \frac{1}{2}. \tag{2.83}$$

All other nonzero $6j$-symbols are obtained through the tetrahedral symmetry in Eq. (1.4).

2.2.4 $\mathbb{G} = Q_8$

It is interesting to compare the Dihedral group D_4 and the quaternion group Q_8. Both have the same order of 8, and share the same character table and thus the same fusion rules. In fact, their corresponding group algebra $\mathbb{C}[D_4]$ and $\mathbb{C}[Q_8]$, which in general contain more information than the character tables, are isomorphic to each other. To encode the full information of their representations, we need the intertwining operators. The two groups can be distinguished by the intertwining operators, or more explicitly, by the complete set of $3j$-symbols.

The multiplication table is presented in Table 2.5, where 1 denotes the identity element.

The group elements are identified with the quaternion numbers by $\{1, \mathbf{i}, \mathbf{j}, \mathbf{k}, -1, -\mathbf{i}, -\mathbf{j}, -\mathbf{k}\}$, where $\mathbf{i}^2 = \mathbf{j}^2 = 1$ and $\mathbf{k} = \mathbf{ij} = -\mathbf{ji}$.

There are five inequivalent classes of irreducible representations. One set $I = \{0, 1, 2, 3, 4\}$ of irreducible representations is presented in Table 2.6.

Table 2.5. Multiplication table of $\mathbb{G} = Q_8$.

	1	2	3	4	5	6	7	8
1	1	2	3	4	5	6	7	8
2	2	5	4	7	6	1	8	3
3	3	8	5	2	7	4	1	6
4	4	3	6	5	8	7	2	1
5	5	6	7	8	1	2	3	4
6	6	1	8	3	2	5	4	7
7	7	4	1	6	3	8	5	2
8	8	7	2	1	4	3	6	5

Table 2.6. Irreducible representations of $\mathbb{G} = Q_8$.

	ρ_0	ρ_1	ρ_2	ρ_3	ρ_4
1	1	1	1	1	$\begin{pmatrix} 1 & 0 \\ 0 & 1 \end{pmatrix}$
2	1	1	-1	-1	$\begin{pmatrix} i & 0 \\ 0 & -i \end{pmatrix}$
3	1	-1	1	-1	$\begin{pmatrix} 0 & 1 \\ -1 & 0 \end{pmatrix}$
4	1	-1	-1	1	$\begin{pmatrix} 0 & i \\ i & 0 \end{pmatrix}$
5	1	1	1	1	$\begin{pmatrix} -1 & 0 \\ 0 & -1 \end{pmatrix}$
6	1	1	-1	-1	$\begin{pmatrix} -i & 0 \\ 0 & i \end{pmatrix}$
7	1	-1	1	-1	$\begin{pmatrix} 0 & -1 \\ 1 & 0 \end{pmatrix}$
8	1	-1	-1	1	$\begin{pmatrix} 0 & -i \\ -i & 0 \end{pmatrix}$

All representations $j = 0, 1, 2, 3, 4$ are self-dual, as can be verified by examining the duality maps, which are computed as

$$\Omega^0 = 1, \quad \Omega^1 = 1, \quad \Omega^2 = 1, \quad \Omega^3 = 1, \quad \Omega^4 = \begin{pmatrix} 0 & -1 \\ 1 & 0 \end{pmatrix}, \tag{2.84}$$

which implies

$$\alpha_0 = \alpha_1 = \alpha_2 = \alpha_3, \quad \alpha_4 = -1$$
$$d_0 = d_1 = d_2 = d_3 = 1, d_4 = -2. \tag{2.85}$$

The independent nonzero $3j$-symbols are

$$C_{000} = C_{011} = C_{022} = C_{033} = C_{044} = C_{234} = 1,$$

$$C_{044} = \begin{pmatrix} 0 & -\frac{i}{\sqrt{2}} \\ \frac{i}{\sqrt{2}} & 0 \end{pmatrix}, \quad C_{144} = \begin{pmatrix} 0 & -\frac{i}{\sqrt{2}} \\ -\frac{i}{\sqrt{2}} & 0 \end{pmatrix},$$

$$C_{244} = \begin{pmatrix} \frac{1}{\sqrt{2}} & 0 \\ 0 & \frac{1}{\sqrt{2}} \end{pmatrix}, \quad C_{344} = \begin{pmatrix} \frac{i}{\sqrt{2}} & 0 \\ 0 & -\frac{i}{\sqrt{2}} \end{pmatrix}. \tag{2.86}$$

The fusion rules are thus obtained by $\delta_{111} = \delta_{122} = \delta_{133} = \delta_{144} = \delta_{155} = \delta_{234} = \delta_{255} = \delta_{355} = \delta_{455} = 1$.

The independent nonzero symmetrized $6j$-symbols (2.50) are

$$G_{000}^{000} = 1, G_{111}^{000} = 1, G_{222}^{000} = 1, G_{333}^{000} = 1, G_{444}^{000} = -\frac{i}{\sqrt{2}},$$

$$G_{011}^{011} = 1, G_{233}^{011} = 1, G_{322}^{011} = 1, G_{444}^{011} = -\frac{i}{\sqrt{2}}, G_{022}^{022} = 1,$$

$$G_{133}^{022} = 1, G_{444}^{022} = -\frac{i}{\sqrt{2}}, G_{033}^{033} = 1, G_{444}^{033} = -\frac{i}{\sqrt{2}},$$

$$G_{044}^{044} = -\frac{1}{2}, G_{144}^{044} = -\frac{1}{2}, G_{244}^{044} = -\frac{1}{2}, G_{344}^{044} = -\frac{1}{2},$$

$$G_{123}^{123} = 1, G_{444}^{123} = -\frac{1}{\sqrt{2}}, G_{144}^{144} = -\frac{1}{2}, G_{244}^{144} = \frac{1}{2},$$

$$G_{344}^{144} = \frac{1}{2}, G_{244}^{244} = -\frac{1}{2}, G_{344}^{244} = \frac{1}{2}, G_{344}^{344} = -\frac{1}{2}. \tag{2.87}$$

All other nonzero $6j$-symbols are obtained through the tetrahedral symmetry in Eq. (1.4).

2.3 Levin-Wen models as topological gauge field theories

Constructed from the data $\{d, \delta, G\}$ derived from finite group representations, Levin-Wen models can be understood as topological gauge field theories in the dual formulation. By the Fourier transformation, they can be mapped to Kitaev models [54].

Let us first briefly gauge field theories on a spatial discrete graph. Originally it was formulated on a regular lattice, but the formulation can be easily adapted to an arbitrary graph. In this dissertation, we focus on trivalent graphs.

The fundamental concept is the gauge invariance. Let us consider a gauge group $\mathbb{G}$ and a gauge transformation $g(\mathbf{x}) \in \mathbb{G}$ which depends on the space point $\mathbf{x}$. A "charged" matter field $\varphi^\alpha(\mathbf{x})$ is transformed under a finite (generally linear) representation of $g(\mathbf{x})$ at the same space point $\mathbf{x}$ by $\varphi^\alpha(\mathbf{x}) \mapsto \mathcal{D}_{\alpha\beta}[g(\mathbf{x})]\varphi^\beta(\mathbf{x})$, where $\mathcal{D}_{\alpha\beta}(g(\mathbf{x}))$ is the corresponding matrix representation, and α ranges in the representation space of $\mathcal{D}$.

Now we consider discrete models. If we discretize the space by a graph, with a continuum space point replaced by a vertex $\mathbf{v}$ on the graph, then the derivative terms of the "charged"

matter field are replaced by finite differences. For example, a local action contains the nearest neighboring interaction

$$S_{\text{mat}} = \beta_m \sum_{(\mathbf{v}, \mathbf{v}')} \overline{\varphi_{\mathbf{v}}^{\alpha}} \varphi_{\mathbf{v}'}^{\alpha}, \tag{2.88}$$

where the bar denotes the complex conjugate.

The above action has only global gauge invariance. For the local gauge invariance, we need to introduce a gauge field $a_{\mathbf{v}\mathbf{v}'} \in \mathbb{G}$ associated to each oriented link between $\mathbf{v}$ and $\mathbf{v}'$. The use of the elements of the group instead of the Lie algebra will make the local gauge invariance explicit and simple. It also affords to formulate the models with a discrete gauge group. The local gauge invariant action is

$$S_{\text{mat}} = \beta_m \sum_{(\mathbf{v}, \mathbf{v}')} \overline{\varphi_{\mathbf{v}}^{\alpha}} \mathcal{D}_{\alpha\beta}(a_{\mathbf{v}\mathbf{v}'}) \varphi_{\mathbf{v}'}^{\beta}. \tag{2.89}$$

The local gauge invariance requires $a_{\mathbf{v}\mathbf{v}'}$ to transform as

$$a_{\mathbf{v}\mathbf{v}'} \mapsto g_{\mathbf{v}} a_{\mathbf{v}\mathbf{v}'} g_{\mathbf{v}'}^{-1}, \tag{2.90}$$

together with the constraint

$$a_{\mathbf{v}\mathbf{v}'} = a_{\mathbf{v}'\mathbf{v}}. \tag{2.91}$$

We also need a gauge invariant term for the gauge fields in the action. Let us consider the product of the gauge fields along a close curve $C = \mathbf{v}_1 \mathbf{v}_2 \ldots \mathbf{v}_n \mathbf{v}_1$ on the graph, called the holonomy along C:

$$a_C = a_{\mathbf{v}_1} a_{\mathbf{v}_2} \ldots a_{\mathbf{v}_n} a_{\mathbf{v}_1}. \tag{2.92}$$

The gauge transformation

$$a_C \mapsto g_{\mathbf{v}_1} a_C g_{\mathbf{v}_1} \tag{2.93}$$

occurs within the same conjugacy class of the group. Then the character of any representation will give a gauge invariant function. In fact, from the group theory, any gauge invariant function can be decomposed into the characters of irreducible representations along some closed curves. For the matrix group $SU(n)$ or $SO(n)$, if we choose the fundamental representation U, and the closed curve along the boundary of each plaquette, we arrive at the Wilson's action

$$S_{\text{J}} = \beta_J \sum_{\mathbf{p}} \frac{1}{\dim_U} \operatorname{Re} \chi_U(a_{\mathbf{p}}), \tag{2.94}$$

where $a_{\mathbf{p}}$ is the holonomy for the plaquette $\mathbf{p}$, and $\dim_U$ the dimension of the fundamental representation U.

There is a another formulation in terms of the irreducible representations. Suppose $\mathbb{G}$ is Lie group. When β_J is large, the holonomy $a_{\mathbf{p}}$ will fluctuate around the unit element of the group. The Wilson's action in this case corresponds to the continuum limit of the Yang-Mills action. Taking account of only quadratic terms in the fluctuating fields leads to the heat kernel action

$$\exp\left(-S_J(\mathbf{p})\right) = \sum_r \dim_r \chi_r(a_{\mathbf{p}}) \exp\left(-\frac{\dim_U C_r}{\beta_J}\right), \tag{2.95}$$

where $\{r\}$ are the irreducible representations of $\mathbb{G}$ and C_r is the values of the Casimir operator in r.

Gauge theories on a discrete graph also admit a finite gauge group. To compare with Levin-Wen models later, we take the Hamiltonian approach in the following. The Hilbert space is spanned by the gauge fields $a_{\mathbf{e}}$ assigned to the graph links $\mathbf{e}$. A gauge transformation $g_{\mathbf{v}}$ acting on the Hilbert space as

$$L(g): \left|\underset{\mathbf{v'}}{\overset{a_{\mathbf{e}}}{\rightarrow}}\underset{\mathbf{v}}{}\right\rangle \rightarrow \left|\underset{\mathbf{v'}}{\overset{g_{\mathbf{v}}a_{\mathbf{e}}g_{\mathbf{v'}}^{-1}}{\rightarrow}}\underset{\mathbf{v}}{}\right\rangle. \tag{2.96}$$

Note that any basis vector with the direction of an edge reversed and corresponding group element inversed at the same time is treated as the same as the original one.

The action of any gauge transformation can be decomposed into local operators defined at each vertex. Let $L(g_{\mathbf{v}})$ be the action of the gauge transformation with $g_{\mathbf{v}}$ at vertex $\mathbf{v}$ and the $g_{\mathbf{v'}} = 1$ being the identity element of $\mathbb{G}$ at all other vertices $\mathbf{v'} \neq \mathbf{v}$:

$$L(g_v): \left|\underset{a_1}{\overset{a_3}{}}\underset{a_2}{}\right\rangle \rightarrow \left|\underset{g_{\mathbf{v}}a_1}{\overset{g_{\mathbf{v}}a_3}{}}\underset{g_{\mathbf{v}}a_2}{}\right\rangle. \tag{2.97}$$

We define the local gauge invariance projection $A_{\mathbf{v}}$ at vertex $\mathbf{v}$

$$A_{\mathbf{v}} = \frac{1}{|\mathbb{G}|} \sum_{g_{\mathbf{v}} \in \mathbb{G}} L(g_{\mathbf{v}}), \tag{2.98}$$

as an average of all local gauge transformations. It projects onto the states that are invariant under any local gauge transformation $L(g_{\mathbf{v}}')$ because $L(g_{\mathbf{v}}')A_{\mathbf{v}} = |\mathbb{G}|^{-1} \sum_{g_{\mathbf{v}} \in \mathbb{G}} L(g_{\mathbf{v}}'g_{\mathbf{v}}) = |\mathbb{G}|^{-1} \sum_{g_{\mathbf{v}} \in \mathbb{G}} L(g_{\mathbf{v}}) = A_{\mathbf{v}}$.

The Levin-Wen models derived from finite group representations can be mapped to gauge theories by a Fourier transformation, and become Kitaev's quantum double models (or toric code models).

The Fourier transformation maps between the group elements and the irreducible representations. Take $\mathbb{G} = U(1)$ for example, local Hilbert basis $\{|\theta\rangle\}$ $(0 \leq \theta < 2\pi)$ is mapped to $\{|n\rangle\}$ by

$$|n\rangle = \frac{1}{2\pi} \int_0^{2\pi} e^{in\theta} |\theta\rangle, \qquad (2.99)$$

where $e^{in\theta}$ is the irreducible representation labeled by integer n. This map can be generalized to any finite group or Lie group.

Then the first term Q_v in Levin-Wen Hamiltonian is mapped to the gauge invariance projeciton $A_\mathbf{v}$ in Eq. (2.98). It prefers the conservation law due to the gauge symmetry at $\mathbf{v}$. For $\mathbb{G} = U(1)$, $L(\theta_\mathbf{v})$ is mapped to $e^{i(n_1+n_2+n_3)\theta_\mathbf{v}}$, and $A_\mathbf{v}$ is mapped to

$$\frac{1}{2\pi} \int_0^{2\pi} e^{i(n_1+n_2+n_3)\theta_\mathbf{v}} = \delta_{n_1+n_2+n_3,0}. \qquad (2.100)$$

In general, if we apply the gauge invariance projection at $\mathbf{v}$ in Levin-Wen Hilbert space, then any gauge transformation at $\mathbf{v}$ will result in a trivial phase 1, as we have seen in the previous section. This happens only when the tensor product of $j_1 \otimes j_2 \otimes j_3$ around v can be decomposed into the trivial representation, in which any group element transforms as the identity map. Hence we arrive at $\delta_{j_1 j_2 j_3}$, which equals to 1 if $j_1 \otimes j_2 \otimes j_3$ contains the trivial representation and 0 otherwise.

The second term B_p is mapped to a projection prefers zero flux at plaquette p. In the group element basis, the projection can be written as the Kronecker delta funciton $\delta_{a_1 a_2 \ldots, \mathbf{1}}$, which is 1 if the product of all group elements around the plaquett p equals the identity element $\mathbf{1}$ of the group, and 0 otherwise. The local operator B_p^s is the Wilson loop operator associated to the irreducible representation s. Indeed, the Wilson loop operator acting on a plaquette with a flux $a_1 a_2 \ldots$ results in a phase $\chi_s(a_1 a_2 \ldots)$. Then $B_p = D^{-1} \sum_s d_s B_p^s$ is mapped to

$$\frac{1}{|\mathbb{G}|} \sum_s \dim(j) \chi_s(a_1 a_2 \ldots) = \delta_{a_1 a_2 \ldots, \mathbf{1}}, \qquad (2.101)$$

where $D = \sum_s \dim(j)^2$ equals the group order $|\mathbb{G}|$.

Though the Fourier transformation applies to Lie group, throughout the dissertation we will focus on the finite group cases since the GSD goes to infinity in the Lie group case.

CHAPTER 3

CONCRETE CONSTRUCTION OF
LEVIN-WEN MODELS WITH
QUANTUM GROUPS

In last chapter, starting with irreducible representations of a finite group $\mathbb{G}$, we have constructed the symmetrized $3j$-symbols, and then the symmetrized $6j$-symbols. The construction can be generalized to quantum groups, and more generally, the unitary spherical tensor categories. For example, the $3j$-symbols constructed in the previous chapter describe the group representation category $Rep_{\mathbb{G}}$. In this chapter, we construct the symmetrized $6j$-symbol from the unitary spherical fusion categories, in the $3j$-symbol approach. "Unitary spherical" means some extra conditions on the tensor categories that lead to the tetrahedral symmetry (1.4). See Ref. [47, 17] for the introduction of unitary spherical tensor categories in mathematical literature. In this chapter, we present the categorical concepts in terms of tensors, so that they are accessible to physicists and are computational.

3.1 $6j$-symbols from unitary spherical tensor categories

We describe the structure of a unitary spherical fusion categories in terms of $3j$-symbols. In the following, we generalize the definition of symmetric $3j$-symbols by generalizing the symmetry conditions. Let I be a set of finitely many labels (e.g., inequivalent classes of irreducible representations of a finite group $\mathbb{G}$). Throughout this chapter, we assume all these labels represent some finite-dimensional complex vector spaces. There is a dual map $\wedge : I \to I; j \mapsto j^*$ with the double map $\wedge^2 = \mathrm{id}_I$ taking any label $j \in I$ back to itself. There is a special label denoted by 0 such that $0^* = 0$, representing one-dimensional complex vector space (i.e., $\mathcal{C}$, the one-dimensional space of complex numbers), and for each pair of dual objects j and j^*, there is a map $\omega_j : j^* \otimes j \to 0$ and its inverse $\omega_j^{-1} : 0 \to j \otimes j^*$, satisfying

$$\text{(diagram)} = j^* \text{(diagram)} \quad , \quad \text{(diagram)} = \text{(diagram)} j \quad . \tag{3.1}$$

where the cup presents the ω_j and the cap the ω_j^{-1}, as explained in Eq (2.16) and (2.17).

The composition $\omega_j \circ \omega_{j^*}^{-1}$ evaluates to a complex number. If $j \neq j^*$, then we can rescale ω_j to $\eta\,\omega_j$, where η^2 is determined by

$$\eta \times \left(\!j\!\right)j^* = \eta^{-1} \times \left(\!j^*\!\right)j, \tag{3.2}$$

for all $j \neq j^* \in I$. Note that η is determined up to a sign ± 1. By this rescaling, we have *sphericity condition*:

$$\left(\!j\!\right)j^* = \left(\!j^*\!\right)j, \tag{3.3}$$

for all $j \in I$.

Let us define the quantum dimension d_j for each j by

$$\mathrm{d}_j \equiv \left(\!j\!\right)j^*, \tag{3.4}$$

and require the *unitarity condition* that d_j is real. Throughout this chapter we assume d_j is nonzero, so d_j could be either positive or negative. Let us denote the sign by $\alpha_j = \mathrm{sign}(\mathrm{d}_j)$, and call it the *Frobenius-Schur indicator*. If $j \neq j^*$, we choose the sign in η in Eq (3.2) such that $\alpha_j = \alpha_{j^*} = 1$. If $j = j^*$, α_j could be either 1 or -1 which can not be changed by rescaling ω_j.

Now we describe the symmetrized $3j$-symbols. There is a function δ_{ijk} taking values of either 0 or 1 for any triple of $i, j, k \in I$, satisfying $\delta_{ijk} = \delta_{jki} = \delta_{k^*j^*i^*}$ and $\delta_{jj^*0} = 1$. The δ_{ijk} is called the *fusion rule* and in general could take integers greater than one, which we will only discuss in Appendix C. If $\delta_{ijk} = 1$, we say the triple (i, j, k) is *admissible*.

We require the *trimodality* condition

$$\alpha_i \alpha_j \alpha_k = 1 \tag{3.5}$$

if $\delta_{ijk} = 1$.

Following the similar procedure as in the previous chapter, for any admissible triple (j_1, j_2, j_3), we can define the $3j$-symbols

$$C_{j_1 j_2 j_3} : j_1 \otimes j_2 \otimes j_3 \to 0 \tag{3.6}$$

by the resolution of identity:

$$\text{(diagram)} = \sum_{j_3} \mathrm{d}_{j_3} \text{(diagram)} \, , \tag{3.7}$$

where the two trivalent vertices present the composition of $3j$-symbols and duality maps as in Eq. (2.33). They are satisfy the *normalization condition*

$$\text{(diagram)} = 1, \tag{3.8}$$

and the *pivotal condition*:

$$\text{(diagram)} = \text{(diagram)} \, , \tag{3.9}$$

Just as in Section 2.1.2, the $3j$-symbols are not independent under cyclic permutations. We require the *cyclic condition*

$$\text{(diagram)} = \text{(diagram)} \, . \tag{3.10}$$

Define the *symmetrized $6j$-symbol* by the evaluation of the diagram in Eq. (2.50). Follow the same reasoning as in Section 2.1, we have the same transformation rules (2.61), (2.60), and (2.62) under the complex conjugation. However, to prove the last equality of the tetrahedral symmetry, we apply the complex conjugation on ω_j and $C_{j_1 j_2 j_3}$ by:

$$\omega_j \mapsto \omega_j^{\dagger} \equiv \alpha_j \omega_{j^*}^{-1} \tag{3.11}$$

and

$$C_{j_1 j_2 j_3} \mapsto C^\dagger_{j_1 j_2 j_3} \qquad \equiv \qquad , \qquad (3.12)$$

which become Eqs (2.57) and (2.58) for finite group representations. Finally we arrive at the three identities in Eq (1.4).

3.2   Examples

Quantum groups can be obtained from Lie algebras. Just like that the algebra generated by s_x, s_y, and s_z of the Lie algebra $\mathfrak{su}(2)$ is the group algebra of $SU(2)$ (called the universal enveloping algebra of $\mathfrak{su}(2)$), the quantum group $\mathcal{U}_q(\mathfrak{su}(2))$ is similar but it is an algebra generated by

$$s_x, s_y, q^{s_z}. \qquad (3.13)$$

(called the q-deformed universal enveloping algebra of $\mathfrak{su}(2)$.) By "generated" we mean that each element in $\mathcal{U}_q(\mathfrak{su}(2))$ is a finite sum of products of the above generators. We will get back (group algebra of) $SU(2)$ in some sense as $q \to 1$.

When q is taken to be a primitive root of unity, $U_q(\mathfrak{su}(2))$ has some finitely many irreducible representations with nonzero quantum dimensions (3.4), by which we can construct the symmetrized $6j$-symbols as described in the previous section. An efficient way to construct these data is through the Jone-Wentzl projectors in Temperley-Lieb algebra (see ref [17] for example). In this section, we present two simple examples for $\mathcal{U}_q(\mathfrak{su}(2))$.

3.2.1   Semion theory

Semion theory takes the q-deformation parameter $q = \exp(\pi \mathrm{i}/3)$. It has the same fusion rule as that from the group $\mathbb{Z}_2$ representation theory, but can not be obtained from any group representation theory.

Set $I = \{\mathbb{C}, \mathbb{C}^2\}$ (or, $\{0, 1\}$ for short). Denote by $\{e_1, e_2\}$ the basis of the vector space $\mathbb{C}^2$.

Both 0 and 1 are self-dual. The duality maps are

$$\omega_0 = 1, \quad \omega_1 : 1 \mapsto -Ae_1 \otimes e_2 + A^{-1}e_2 \otimes e_1, \tag{3.14}$$

where $A = q^{1/2} = \exp(\pi i/6)$. The inverse of ω_1 is

$$\omega_1^{-1} : e_1 \otimes e_1 \mapsto 0, e_2 \otimes e_2 \mapsto 0,$$
$$e_1 \otimes e_2 \mapsto A, e_2 \otimes e_1 \mapsto -A^{-1}. \tag{3.15}$$

The dagger of ω_1 is

$$\omega_1^\dagger = -\omega_1^{-1} \tag{3.16}$$

such that $\omega_1^\dagger \circ \omega_1 > 0$.

From the duality maps we obtain $\Delta_0 = 1, \Delta_1 = \omega_1^{-1} \circ \omega_1 = -1$ and thus $\alpha_0 = 1$, and $\alpha_1 = -1$.

The nonzero $3j$-symbols are

$$C_{000} : 1 \otimes 1 \otimes 1 \mapsto 1$$
$$C_{011} : 1 \otimes e_1 \otimes e_1 \mapsto 0, \quad 1 \otimes e_2 \otimes e_2 \mapsto 0,$$
$$1 \otimes e_1 \otimes e_2 \mapsto iA, 1 \otimes e_2 \otimes e_1 \mapsto -iA^{-1}. \tag{3.17}$$

where the normalization factors are fixed by the normalization conditions of $3j$-symbols. The other nonzero $3j$-symbols C_{101} and C_{110} are obtained by the cyclic condition.

The nonzero symmetrized $6j$-symbols are

$$G_{000}^{000} = 1, G_{111}^{000} = i, G_{011}^{011} = -1. \tag{3.18}$$

The other nonzero symmetrized $6j$-symbols are obtained through the tetrahedral symmetry.

3.2.2   Fibonacci theory

Taking q-deformation parameter $q = -\exp(\pi i/5)$, there are four irreducible representations with nonzero quantum dimensions, denoted by 0,1,2, and 3. The Fibonacci theory takes only two of them, 0 and 2, which are closed under fusion rule.

Set $I = \{\mathbb{C}, \mathbb{C}^4\}$ (or, $\{0,2\}$ for short). Denote by $\{e_{11}, e_{12}, e_{21}, e_{22}\}$ the basis of the vector space $\mathbb{C}^4$.

Both 0 and 2 are self-dual. The duality maps are

$$\omega_0 = 1, \quad \omega_2 : 1 \mapsto -\frac{1}{A^4+1} e_{11} \otimes e_{22} + \frac{A^4}{A^4+1} e_{22} \otimes e_{11} - \frac{A^2}{A^4+1} e_{12} \otimes e_{12}$$

$$- \frac{A^2}{A^4+1} e_{21} \otimes e_{21} + A^2 e_{12} \otimes e_{21} + \frac{1}{A^2} e_{21} \otimes e_{12}, \qquad (3.19)$$

where $A = q^{1/2} = \exp(\pi i/6)$. The inverse ω_2^{-1} is given by

$$
\begin{array}{llll}
e_{11} \otimes e_{11} \mapsto 0 & e_{11} \otimes e_{12} \mapsto 0 & e_{12} \otimes e_{11} \mapsto 0 & e_{12} \otimes e_{12} \mapsto -\frac{1}{A^4+1} \\
e_{11} \otimes e_{21} \mapsto 0 & e_{11} \otimes e_{22} \mapsto A^2 & e_{12} \otimes e_{21} \mapsto -\frac{A^2}{A^4+1} & e_{12} \otimes e_{22} \mapsto 0 \\
e_{21} \otimes e_{11} \mapsto 0 & e_{21} \otimes e_{12} \mapsto -\frac{A^2}{A^4+1} & e_{22} \otimes e_{11} \mapsto \frac{1}{A^2} & e_{22} \otimes e_{12} \mapsto 0 \\
e_{21} \otimes e_{21} \mapsto -\frac{A^4}{A^4+1} & e_{21} \otimes e_{22} \mapsto 0 & e_{22} \otimes e_{21} \mapsto 0 & e_{22} \otimes e_{22} \mapsto 0
\end{array}
$$
$$(3.20)$$

The dagger of ω_2 is

$$\omega_2^\dagger = -\omega_2^{-1} \qquad (3.21)$$

such that $\omega_1^\dagger \circ \omega_1 > 0$.

From the duality maps we obtain $\Delta_0 = 1, \Delta_2 = \omega_2^{-1} \circ \omega_2 = \phi \equiv \frac{\sqrt{5}+1}{2}$ and thus $\alpha_0 = 1$, and $\alpha_2 = 1$.

The nonzero $3j$-symbols are C_{000} given by

$$1 \otimes 1 \otimes 1 \mapsto 1, \qquad (3.22)$$

C_{022} given by

$$
\begin{array}{ll}
1 \otimes e_{11} \otimes e_{11} \mapsto 0 & 1 \otimes e_{11} \otimes e_{12} \mapsto 0 \\
1 \otimes e_{11} \otimes e_{21} \mapsto 0 & 1 \otimes e_{11} \otimes e_{22} \mapsto \frac{A^2}{\sqrt{N_1}} \\
1 \otimes e_{12} \otimes e_{11} \mapsto 0 & 1 \otimes e_{12} \otimes e_{12} \mapsto -\frac{1}{(A^4+1)\sqrt{N_1}} \\
1 \otimes e_{12} \otimes e_{21} \mapsto -\frac{A^2}{(A^4+1)\sqrt{N_1}} & 1 \otimes e_{12} \otimes e_{22} \mapsto 0 \\
1 \otimes e_{21} \otimes e_{11} \mapsto 0 & 1 \otimes e_{21} \otimes e_{12} \mapsto -\frac{A^2}{(A^4+1)\sqrt{N_1}} \\
1 \otimes e_{21} \otimes e_{21} \mapsto -\frac{A^4}{(A^4+1)\sqrt{N_1}} & 1 \otimes e_{21} \otimes e_{22} \mapsto 0 \\
1 \otimes e_{22} \otimes e_{11} \mapsto \frac{1}{A^2\sqrt{N_1}} & 1 \otimes e_{22} \otimes e_{12} \mapsto 0 \\
1 \otimes e_{22} \otimes e_{21} \mapsto 0 & 1 \otimes e_{22} \otimes e_{22} \mapsto 0
\end{array}
$$
$$, \qquad (3.23)$$

and C_{222} given by

$$
\begin{aligned}
&e_{11} \otimes e_{11} \otimes e_{11} \mapsto 0 &\quad& e_{11} \otimes e_{11} \otimes e_{12} \mapsto 0 \\
&e_{11} \otimes e_{11} \otimes e_{21} \mapsto 0 && e_{11} \otimes e_{11} \otimes e_{22} \mapsto 0 \\
&e_{11} \otimes e_{12} \otimes e_{11} \mapsto 0 && e_{11} \otimes e_{12} \otimes e_{12} \mapsto 0 \\
&e_{11} \otimes e_{12} \otimes e_{21} \mapsto 0 && e_{11} \otimes e_{12} \otimes e_{22} \mapsto \frac{A^5}{(A^4+1)\sqrt{N_2}} \\
&e_{11} \otimes e_{21} \otimes e_{11} \mapsto 0 && e_{11} \otimes e_{21} \otimes e_{12} \mapsto 0 \\
&e_{11} \otimes e_{21} \otimes e_{21} \mapsto 0 && e_{11} \otimes e_{21} \otimes e_{22} \mapsto \frac{A^7}{(A^4+1)\sqrt{N_2}} \\
&e_{11} \otimes e_{22} \otimes e_{11} \mapsto 0 && e_{11} \otimes e_{22} \otimes e_{12} \mapsto -\frac{A}{(A^4+1)\sqrt{N_2}} \\
&e_{11} \otimes e_{22} \otimes e_{21} \mapsto -\frac{A^3}{(A^4+1)\sqrt{N_2}} && e_{11} \otimes e_{22} \otimes e_{22} \mapsto 0 \\
&e_{12} \otimes e_{11} \otimes e_{11} \mapsto 0 && e_{12} \otimes e_{11} \otimes e_{12} \mapsto 0 \\
&e_{12} \otimes e_{11} \otimes e_{21} \mapsto 0 && e_{12} \otimes e_{11} \otimes e_{22} \mapsto -\frac{A}{(A^4+1)\sqrt{N_2}} \\
&e_{12} \otimes e_{12} \otimes e_{11} \mapsto 0 && e_{12} \otimes e_{12} \otimes e_{12} \mapsto \frac{1-A^4}{A(A^4+1)^2\sqrt{N_2}} \\
&e_{12} \otimes e_{12} \otimes e_{21} \mapsto \frac{A-A^5}{(A^4+1)^2\sqrt{N_2}} && e_{12} \otimes e_{12} \otimes e_{22} \mapsto 0 \\
&e_{12} \otimes e_{21} \otimes e_{11} \mapsto 0 && e_{12} \otimes e_{21} \otimes e_{12} \mapsto \frac{A-A^5}{(A^4+1)^2\sqrt{N_2}} \\
&e_{12} \otimes e_{21} \otimes e_{21} \mapsto \frac{A^3-A^7}{(A^4+1)^2\sqrt{N_2}} && e_{12} \otimes e_{21} \otimes e_{22} \mapsto 0 \\
&e_{12} \otimes e_{22} \otimes e_{11} \mapsto \frac{A}{(A^4+1)\sqrt{N_2}} && e_{12} \otimes e_{22} \otimes e_{12} \mapsto 0 \\
&e_{12} \otimes e_{22} \otimes e_{21} \mapsto 0 && e_{12} \otimes e_{22} \otimes e_{22} \mapsto 0 \\
&e_{21} \otimes e_{11} \otimes e_{11} \mapsto 0 && e_{21} \otimes e_{11} \otimes e_{12} \mapsto 0 \\
&e_{21} \otimes e_{11} \otimes e_{21} \mapsto 0 && e_{21} \otimes e_{11} \otimes e_{22} \mapsto -\frac{A^3}{(A^4+1)\sqrt{N_2}} \\
&e_{21} \otimes e_{12} \otimes e_{11} \mapsto 0 && e_{21} \otimes e_{12} \otimes e_{12} \mapsto \frac{A-A^5}{(A^4+1)^2\sqrt{N_2}} \\
&e_{21} \otimes e_{12} \otimes e_{21} \mapsto \frac{A^3-A^7}{(A^4+1)^2\sqrt{N_2}} && e_{21} \otimes e_{12} \otimes e_{22} \mapsto 0 \\
&e_{21} \otimes e_{21} \otimes e_{11} \mapsto 0 && e_{21} \otimes e_{21} \otimes e_{12} \mapsto \frac{A^3-A^7}{(A^4+1)^2\sqrt{N_2}} \\
&e_{21} \otimes e_{21} \otimes e_{21} \mapsto \frac{A^5-A^9}{(A^4+1)^2\sqrt{N_2}} && e_{21} \otimes e_{21} \otimes e_{22} \mapsto 0 \\
&e_{21} \otimes e_{22} \otimes e_{11} \mapsto \frac{A^3}{(A^4+1)\sqrt{N_2}} && e_{21} \otimes e_{22} \otimes e_{12} \mapsto 0 \\
&e_{21} \otimes e_{22} \otimes e_{21} \mapsto 0 && e_{21} \otimes e_{22} \otimes e_{22} \mapsto 0 \\
&e_{22} \otimes e_{11} \otimes e_{11} \mapsto 0 && e_{22} \otimes e_{11} \otimes e_{12} \mapsto \frac{A}{(A^4+1)\sqrt{N_2}} \\
&e_{22} \otimes e_{11} \otimes e_{21} \mapsto \frac{A^3}{(A^4+1)\sqrt{N_2}} && e_{22} \otimes e_{11} \otimes e_{22} \mapsto 0 \\
&e_{22} \otimes e_{12} \otimes e_{11} \mapsto -\frac{1}{(A^7+A^3)\sqrt{N_2}} && e_{22} \otimes e_{12} \otimes e_{12} \mapsto 0 \\
&e_{22} \otimes e_{12} \otimes e_{21} \mapsto 0 && e_{22} \otimes e_{12} \otimes e_{22} \mapsto 0 \\
&e_{22} \otimes e_{21} \otimes e_{11} \mapsto -\frac{1}{(A^5+A)\sqrt{N_2}} && e_{22} \otimes e_{21} \otimes e_{12} \mapsto 0 \\
&e_{22} \otimes e_{21} \otimes e_{21} \mapsto 0 && e_{22} \otimes e_{21} \otimes e_{22} \mapsto 0 \\
&e_{22} \otimes e_{22} \otimes e_{11} \mapsto 0 && e_{22} \otimes e_{22} \otimes e_{12} \mapsto 0 \\
&e_{22} \otimes e_{22} \otimes e_{21} \mapsto 0 && e_{22} \otimes e_{22} \otimes e_{22} \mapsto 0
\end{aligned}
\tag{3.24}
$$

The normalization factors $N_1 = \phi$ and $N_2 = \frac{1}{2}\left(3\sqrt{5}-7\right)$ are fixed by the normalization conditions of $3j$-symbols. The other nonzero $3j$-symbols are obtained by the cyclic condition.

The fusion rule is

$$
\delta_{000} = \delta_{022} = \delta_{222} = 1, \delta_{002} = 0 \tag{3.25}
$$

(called the Fibonacci fusion rule[17]), and the nonzero $6j$-symbols G are given by

$$G_{000}^{000} = 1, G_{022}^{022} = G_{222}^{022} = 1/\phi,$$

$$G_{222}^{000} = 1/\sqrt{\phi}, G_{222}^{222} = -1/\phi^2, \tag{3.26}$$

The other nonzero symmetrized $6j$-symbols are obtained through the tetrahedral symmetry.

CHAPTER 4

TOPOLOGICAL OBSERVABLES IN
GROUND STATES: GROUND
STATE DEGENERACY

The GSD is an important topological observable and partially characterizes the topological phases. Topological observables (correlators) are those invariant under the smooth deformation of the space-time manifold, or, in discrete case, under mutations of discrete spatial graph. In this chapter, we study the GSD of Levin-Wen models by mutation symmetry.

Usually the GSD is examined as a topological invariant [47, 48, 50] of the 3-manifold $S^1 \times M$. In a Hamiltonian approach accessible to physicists, we will explicitly demonstrate that the GSD in the Levin-Wen model depends only on the topology of M on which the system lives and, therefore, is a topological invariant of the surface M. We also show that the ground state of any Levin-Wen Hamiltonian on a sphere is always nondegenerate. Moreover, we examine the Levin-Wen model associated with quantum group $\mathcal{U}_q(\mathfrak{su}(2))$, which is conjectured to be equivalent to the doubled Chern-Simons theory with gauge group $SU(2)$ at level k, and compute the GSD on a torus. Indeed, we find an agreement with that in the corresponding doubled Chern-Simons theory [37, 55]. This supports the above-mentioned conjectured equivalence between the doubled Chern-Simons theory and the LW model, at least in this particular case.

4.1   Graph mutations and fixed point states

Any ground state $|\Phi\rangle$ (there may be many) must be a simultaneous $+1$ eigenvector for all projectors Q_v and B_p. In this section we demonstrate the topological properties of the ground states on a closed surface with nontrivial topology.

Let us begin with *any two* arbitrary trivalent graphs $\Gamma^{(1)}$ and $\Gamma^{(2)}$ discretizing the same surface (e.g., a torus). It is known that they can be mutated to each other by a composition of the following elementary moves [56] (called the Pachner moves):

$$f_1 : \quad \rightarrow \quad , \tag{4.1}$$

$$f_2 : \quad \rightarrow \quad , \tag{4.2}$$

$$f_3 : \quad \rightarrow \quad . \tag{4.3}$$

See Fig. 4.1 for instance.

The Hilbert spaces are defined on the two different graphs, respectively, as described in the previous section. They are quite different from each other, and have different sizes in general. Correspondingly, Levin-Wen models are defined on these two graphs. Denote by $\mathcal{H}^{(1)}$ the Hilbert space on $\Gamma^{(1)}$, and $\mathcal{H}^{(2)}$ on $\Gamma^{(2)}$.

To the elementary moves f_1, f_2, and f_3, we associate linear maps between the corresponding Hilbert spaces as follows:

$$\hat{T}_1 : \left| \begin{matrix} j_1 & & j_4 \\ & j_5 & \\ j_2 & j_3 & \end{matrix} \right\rangle \rightarrow \sum_{j_5'} v_{j_5} v_{j_5'} G^{j_1 j_2 j_5}_{j_3 j_4 j_5'} \left| \begin{matrix} j_1 & & j_4 \\ & j_5 & \\ j_2 & & j_3 \end{matrix} \right\rangle, \tag{4.4}$$

$$\hat{T}_2 : \left| \begin{matrix} j_1 & & j_3 \\ & & \\ & j_2 & \end{matrix} \right\rangle \rightarrow \sum_{j_4 j_5 j_6} \frac{v_{j_4} v_{j_5} v_{j_6}}{\sqrt{D}} G^{j_2 j_3 j_1}_{j_6 j_4 j_5^*} \left| \begin{matrix} j_1 & j_6 & j_3 \\ j_4 & j_5 & \\ & j_2 & \end{matrix} \right\rangle, \tag{4.5}$$

$$\hat{T}_3 : \left| \begin{matrix} j_1 & j_6 & j_3 \\ j_4 & j_5 & \\ & j_2 & \end{matrix} \right\rangle \rightarrow \frac{v_{j_4} v_{j_5} v_{j_6}}{\sqrt{D}} G^{j_3^* j_2^* j_1^*}_{j_4^* j_6 j_5^*} \left| \begin{matrix} j_1 & & j_3 \\ & & \\ & j_2 & \end{matrix} \right\rangle. \tag{4.6}$$

Note that since we can reverse any edge by conjugating the corresponding label, the above formulas do not depend on the edge directions.

Between the Hilbert spaces $\mathcal{H}^{(1)}$ and $\mathcal{H}^{(2)}$ on any two graphs, there is a mutation transformation by a composition of these elementary maps. In particular, $B_p = D^{-1} \sum_s \mathrm{d}_s B_p^s$ is a special example. In fact, on the particular triangle plaquette p as in (4.6), we can verify $B_{p=\triangledown} = \hat{T}_2 \hat{T}_3$, by using the pentagon identity in (1.4).

The topology-preserving mutation transformations (4.4), (4.5), and (4.6) can be used to discuss the topological properties of Levin-Wen models, via the observables that persist under these mutations. In the following, we discuss the behavior the ground states under mutations. We show the following properties:

1. The mutations are unitary in the ground-state subspace.

2. The ground states are invariant under mutations.

Firstly, mutations are unitary in the ground-state subspace. We emphasize that these are maps between the Hilbert spaces on two different graphs. It suffices to check that the
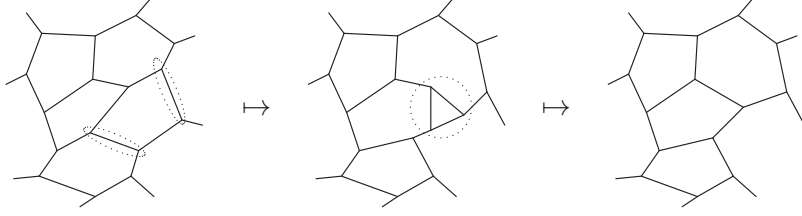
Figure 4.1. A mutation two graphs that discretize the same manifold. The left one is mutated to the middle one by a composition of f_1 moves, and the middle one is mutated to the right one by a f_3 move.

elementary maps $\hat{T}_1$, $\hat{T}_2$, and $\hat{T}_3$ are unitary. We first show $\hat{T}_1^\dagger = \hat{T}_1$, $\hat{T}_2^\dagger = \hat{T}_3$, and $\hat{T}_3^\dagger = \hat{T}_2$. In the matrix elements, we have:

$$\left\langle \begin{matrix} j_1 & j_4 \\ j_5 \\ j_2 & j_3 \end{matrix} \middle| \hat{T}_1^\dagger \middle| \begin{matrix} j_1 & j_4 \\ j_5 \\ j_2 & j_3 \end{matrix} \right\rangle \equiv \overline{\left\langle \begin{matrix} j_1 & j_4 \\ j_5 \\ j_2 & j_3 \end{matrix} \middle| \hat{T}_1 \middle| \begin{matrix} j_1 & j_4 \\ j_5 \\ j_2 & j_3 \end{matrix} \right\rangle} = \overline{v_{j_5} v_{j_5'} G_{j_3 j_4 j_5'}^{j_1 j_2 j_5}} = \overline{v_{j_5'} v_{j_5}} \alpha_{j_5} \alpha_{j_5'} G_{j_2 j_3 j_5^*}^{j_4 j_1 j_5'}$$

$$= v_{j_5'} v_{j_5} G_{j_2 j_3 j_5^*}^{j_4 j_1 j_5'} = \left\langle \begin{matrix} j_1 & j_4 \\ j_5 \\ j_2 & j_3 \end{matrix} \middle| \hat{T}_1 \middle| \begin{matrix} j_1 & j_4 \\ j_5 \\ j_2 & j_3 \end{matrix} \right\rangle, \qquad (4.7)$$

where in the fourth equality we used the symmetry condition in (1.4) and $\overline{v_j}\alpha_j = v_j$, and

$$\left\langle \begin{matrix} j_1 & j_3 \\ j_2 \end{matrix} \middle| \hat{T}_2^\dagger \middle| \begin{matrix} j_1 & j_6 & j_3 \\ j_4 & j_5 \\ j_2 \end{matrix} \right\rangle \equiv \overline{\left\langle \begin{matrix} j_1 & j_6 & j_3 \\ j_4 & j_5 \\ j_2 \end{matrix} \middle| \hat{T}_2 \middle| \begin{matrix} j_1 & j_3 \\ j_2 \end{matrix} \right\rangle} = \overline{\frac{v_{j_4} v_{j_5} v_{j_6}}{\sqrt{D}} G_{j_6^* j_4 j_5^*}^{j_2 j_3 j_1}}$$

$$= \frac{v_{j_4} v_{j_5} v_{j_6}}{\sqrt{D}} G_{j_4^* j_6 j_5^*}^{j_3^* j_2^* j_1^*} = \left\langle \begin{matrix} j_1 & j_3 \\ j_2 \end{matrix} \middle| \hat{T}_3 \middle| \begin{matrix} j_1 & j_6 & j_3 \\ j_4 & j_5 \\ j_2 \end{matrix} \right\rangle, \qquad (4.8)$$

where in the third equality we used the symmetry condition in (1.4), $G_{j_6^* j_4 j_5^*}^{j_2 j_3 j_1} \propto \delta_{j_4^* j_1 j_6}$, and $\alpha_{j_1} = \alpha_{j_4}\alpha_{j_6}$.

Now we verify unitary. $\hat{T}_1^\dagger \hat{T}_1 = \mathbf{1}$ and $\hat{T}_2^\dagger \hat{T}_2 = \hat{T}_3 \hat{T}_2 = \mathbf{1}$ are derived from the orthogonality condition in (1.4) (note that, since we have not used any information about the ground states in this argument, $\hat{T}_1$ and $\hat{T}_2$ are unitary on the entire Hilbert space). But $\hat{T}_3^\dagger \hat{T}_3 = \hat{T}_2 \hat{T}_3 = \mathbf{1}$ only holds in the ground-state subspace since we have already seen that $\hat{T}_2 \hat{T}_3 = B_{p=\triangledown}$, and we always have $B_{p=\triangledown} = \mathbf{1}$ in the ground states.

As a consequence of the unitarity, the Hamiltonian is hermitian. Indeed, each B_p consists of elementary $\hat{T}_1$, $\hat{T}_2$, and $\hat{T}_3$ maps. Particularly, on a triangle plaquette, we have $B_{p=\triangledown}^\dagger = (\hat{T}_2\hat{T}_3)^\dagger = \hat{T}_3^\dagger \hat{T}_2^\dagger = \hat{T}_2 \hat{T}_3 = B_{p=\triangledown}$.

The mutation transformations serve as the symmetry transformations in the ground states. If $|\Phi\rangle$ is a ground state then $\hat{T}|\Phi\rangle$ is also a ground state, where $\hat{T}$ is a composition of $\hat{T}_i$'s associated with elementary f moves from $\Gamma^{(1)}$ to $\Gamma^{(2)}$. This is equivalent to the

condition $\hat{T}(\prod_p B_p) = (\prod_{p'} B_{p'})\hat{T}$, which can be verified by the conditions in (1.4). (Here p and p' run over the plaquettes on $\Gamma^{(1)}$ and $\Gamma^{(2)}$, respectively. Also note that the B_p's are mutually-commuting projectors, i.e., $B_p B_p = B_p$, and thus $\prod_p B_p$ is the projector that projects onto the ground states.)

These mutation transformations look a little different from the usual ones since they may transform between the Hilbert spaces $\mathcal{H}^{(1)}$ and $\mathcal{H}^{(2)}$ on two different graphs $\Gamma^{(1)}$ and $\Gamma^{(2)}$. In general, $\Gamma^{(1)}$ and $\Gamma^{(2)}$ do not have the same number of vertices and edges. Thus $\mathcal{H}^{(1)}$ and $\mathcal{H}^{(2)}$ have different sizes. However, if we restrict to the ground-state subspaces $\mathcal{H}_0^{(1)}$ and $\mathcal{H}_0^{(2)}$, mutation transformations are invertible. In fact, they are unitary as we have just shown.

The tensor equations on the $6j$ symbols in (1.4) give rise to a simple result: each mutation that preserves the spatial topology of the two graphs induces a unitary symmetry transformation. During the mutations, local structures of the graphs are destroyed, while the spatial topology of the graphs is not changed. Correspondingly, the local information of the ground states may be lost, while the topological feature of the ground states is preserved. In fact, any topological feature can be specified by a topological observable $\hat{O}$ that is invariant under all mutation transformations $\hat{T}$ from $\mathcal{H}^{(1)}$ to $\mathcal{H}^{(2)}$: $\hat{O}'\hat{T} = \hat{T}\hat{O}$ (where $\hat{O}$ is defined on the graph $\Gamma^{(1)}$ and $\hat{O}'$ on $\Gamma^{(2)}$). This provides a systematic approach to study the topological properties in the discrete models.

Lastly, mutation transformations are unique. There may be many ways to mutate $\Gamma^{(1)}$ to $\Gamma^{(2)}$ using f_1, f_2 and f_3 moves. It turns out any two such mutations, say T and T', take a ground $|\Phi\rangle$ on $\Gamma^{(1)}$ to the same final state $T|\Phi\rangle = T'|\Phi\rangle$ on $\Gamma^{(2)}$. All these transformations are actually the same if the initial and final graphs $\Gamma^{(1)}$ to $\Gamma^{(2)}$ are fixed, i.e., independent of which way we choose to mutate the graph $\Gamma^{(1)}$ to $\Gamma^{(2)}$. Each ground state is invariant under mutations. Therefore the ground state Hilbert spaces on different graphs can be identified (up to a mutation transformation) and all graphs are equally good.

The invariance of the ground states under mutations implies that the degrees of freedom in the ground states do not depend on the specific structure of the graph. In this sense, the Levin-Wen model is the Hamiltonian version of some discrete TQFT (actually, Turaev-Viro type TQFT, see [48]). The fact that the degrees of freedom of the ground states depend only on the topology of the closed surface M is a typical characteristic of topological phases [20, 21, 22, 57, 26].

4.2   Ground state degeneracy

In this section we investigate the simplest nontrivial topological observable, the GSD. Since $\prod_p B_p$ is the projector that projects onto the ground states, taking a trace computes $\text{GSD} = \text{tr}(\prod_p B_p)$.

We can show that GSD is a topological invariant. Namely, in the previous section we mentioned that, by using (1.4), $\prod_p B_p$ is invariant under any mutation $\hat{T}$ between the Hilbert spaces $\mathcal{H}^{(1)}$ and $\mathcal{H}^{(2)}$: $\hat{T}^\dagger(\prod_{p'} B_{p'})\hat{T} = \prod_p B_p$. Taking a trace of both sides leads to $\text{tr}'(\prod_{p'} B_{p'}) = \text{tr}(\prod_p B_p)$, where the traces are evaluated on $\mathcal{H}^{(2)}$ and $\mathcal{H}^{(1)}$, respectively.

The independence of the GSD on the local structure of the graphs provides a practical algorithm for computing the GSD, since we may always use the simplest graph. see Fig. 4.2.

Expanding the GSD explicitly in terms of $6j$ symbols using (1.5) we obtain

$$
\begin{aligned}
\text{GSD} &= \sum_{j_1 j_2 j_3 j_4 j_5 j_6 \cdots} \left\langle \begin{matrix} j_1 & j_4 \\ & j_5 & \\ j_2 & j_3 \end{matrix} \middle| \left(\prod_p B_p \right) \middle| \begin{matrix} j_1 & j_4 \\ & j_5 & \\ j_2 & j_3 \end{matrix} \right\rangle \\
&= D^{-P} \sum_{s_1 s_2 s_3 s_4 \cdots} d_{s_1} d_{s_2} d_{s_3} d_{s_4} \cdots \sum_{j_1' j_2' j_3' j_4' j_5' \cdots} d_{j_1'} d_{j_2'} d_{j_3'} d_{j_4'} d_{j_5'} \cdots \times \\
&\quad \sum_{j_1 j_2 j_3 j_4 j_5 \cdots} d_{j_1} d_{j_2} d_{j_3} d_{j_4} d_{j_5} \cdots \left(G^{j_2 j_5 j_1}_{s_1^* j_1' j_5'} G^{j_1' j_2 j_5'}_{s_2^* j_5 j_2'} G^{j_5 j_1' j_2'}_{s_3^* j_2 j_1} \right) \left(G^{j_3 j_4 j_5^*}_{s_1^* j_5' j_4'} G^{j_4' j_5'^* j_3}_{s_2^* j_3' j_5^*} G^{j_5^* j_3' j_4'}_{s_4^* j_4 j_3} \right) \cdots .
\end{aligned}
$$

$$(4.9)$$

The formula needs some explanation. P is the total number of plaquettes of the graph. Each plaquette p contributes a summation over s_p together with a factor of $\frac{d_{s_p}}{D}$. In the picture in (4.9) the top plaquette is being operated on first by $B^{s_1}_{p_1}$, next the bottom plaquette by $B^{s_2}_{p_2}$, third the left plaquette by $B^{s_3}_{p_3}$, and finally the right plaquette by $B^{s_4}_{p_4}$. Although ordering of the B^s_p operators is not important (since all B_p's commute with each other), it is important to make an ordering choice (for all plaquettes on the graph) *once and for all*.

Each edge e contributes a summation over j_e and j_e' together with a factor of $d_{j_e} d_{j_e'}$. Each vertex contributes three $6j$ symbols.

The indices on the $6j$ symbols work as follows: since each vertex borders three plaquettes where B^s_p's are being applied, we pick up a $6j$ symbol for each corner. However, ordering is important: because we have an overall ordering of B^s_p's, at each vertex we get an induced ordering for the $6j$ symbols. Starting with the $6j$ symbol furthest left we have no primes on the top row. The bottom two indices pick up primes. All of these variables (primed or not) are fed into the next $6j$ symbol and the same rule applies: the bottom two indices pick up a prime with the convention $()'' = ()$.

<div align="center">(a)   (b)</div>
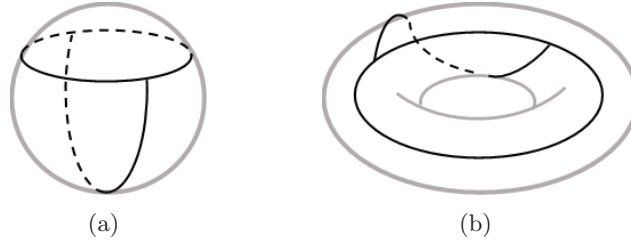
Figure 4.2. All trivalent graphs can be reduced to their simplest structures by compositions of elementary f moves. (a) On a sphere: 2 vertices, 3 edges, and 3 plaquettes. (b) On a torus: 2 vertices, 3 edges, and 1 plaquette.

By the calculation of the GSD, we have characterized a topological property of the phase using local quantities living on a graph discretizing M of nontrivial topology.

4.3   No degeneracy on a sphere

To calculate the GSD, we need to input the data $\{G_{kln}^{ijm}, d_j, \delta_{ijm}\}$ and evaluate the trace in (4.9). We start by computing the GSD in the simplest case of a sphere.

Let us consider the simplest graph as in Fig. 4.2(a). In the following we show that the ground state is nondegenerate on the sphere without referring to any specific structure in the model: $\mathrm{GSD}^{\mathrm{sphere}} = 1$. In fact, for more general graphs one can write down [58] the ground state as $\prod_p B_p |0\rangle$ up to a normalization factor, where in $|0\rangle$ all edges are labeled by string type 0.

We notice that the GSD on the open disk (which is topologically the same as the two-dimensional plane) can be studied using the same technique. This is because the open disk can be obtained by puncturing the sphere in Fig. 4.2(a) at the bottom. Although this destroys the bottom plaquette, we notice that the constraint $B_p = 1$ from the bottom plaquette is automatically satisfied as a consequence of the same constraint on all other plaquettes. The fact that $\mathrm{GSD}^{\mathrm{sphere}}(= \mathrm{GSD}^{\mathrm{disk}}) = 1$ indicates the nonchiral topological order in the Levin-Wen model.

Below we derive GSD $= 1$ on a sphere for a general Levin-Wen model, without referring to any specific structure of the data $\{d, \delta, G\}$. All we will use in the derivation are the general properties in Eq. (1.2) and Eq. (1.4).

The simplest trivalent graph on a sphere has three plaquettes and three edges, as illustrated in Fig. 4.2(a). Following the standard procedure as in (4.9), the GSD is expanded as

$$\text{GSD}^{\text{sphere}} = \sum_{j_1 j_2 j_3} \left\langle \begin{array}{c} j_1 \\ j_3 \\ j_2 \end{array} \middle| B_{p_2} B_{p_3} B_{p_1} \middle| \begin{array}{c} j_1 \\ j_3 \\ j_2 \end{array} \right\rangle$$

$$= \sum_{j_1 j_2 j_3} \left\langle \begin{array}{c} j_1 \\ j_3 \\ j_2 \end{array} \middle| \frac{1}{D} \sum_t d_t B_{p_2}^t \frac{1}{D} \sum_s d_s B_{p_3}^s \frac{1}{D} \sum_r d_r B_{p_1}^r \middle| \begin{array}{c} j_1 \\ j_3 \\ j_2 \end{array} \right\rangle$$

$$= \sum_{j_1 j_2 j_3 j_1' j_2' j_3'} \frac{1}{D} \sum_r d_r v_{j_1} v_{j_3} v_{j_1'} v_{j_3'} G_{r^* j_1'^* j_3'}^{j_2^* j_3 j_1^*} G_{r^* j_3'^* j_1'}^{j_2 j_1 j_3^*} \frac{1}{D} \sum_s d_s v_{j_1'} v_{j_2} v_{j_1} v_{j_2'} \times$$

$$G_{s^* j_2'^* j_1^*}^{j_3' j_1'^* j_2^*} G_{s^* j_1 j_2'}^{j_3'^* j_2 j_1'} \frac{1}{D} \sum_t d_t v_{j_2'} v_{j_3'} v_{j_2} v_{j_3} G_{t^* j_3 j_2^*}^{j_1^* j_2'^* j_3'} G_{t^* j_2 j_3}^{j_1 j_3'^* j_2'}, \tag{4.10}$$

where B_{p_1} is acting on the top bubble plaquette, B_{p_2} on the bottom bubble plaquette, and B_{p_3} on the rest plaquette outside the two bubbles.

All $6j$ symbols can be eliminated by using the orthogonality condition in Eq. (1.4) three times,

$$\sum_r d_r G_{r^* j_1'^* j_3'}^{j_2^* j_3 j_1^*} G_{r^* j_3'^* j_1'}^{j_2 j_1 j_3^*} = \frac{1}{d_{j_2}} \delta_{j_1' j_2 j_3'^*} \delta_{j_1 j_2 j_3^*}$$

$$\sum_s d_s G_{s^* j_2'^* j_1^*}^{j_3' j_1'^* j_2^*} G_{s^* j_1 j_2'}^{j_3'^* j_2 j_1'} = \frac{1}{d_{j_3'}} \delta_{j_1' j_2 j_3'^*} \delta_{j_1 j_2' j_3'^*}$$

$$\sum_t d_t G_{t^* j_3 j_2^*}^{j_1^* j_2'^* j_3'} G_{t^* j_2 j_3}^{j_1 j_3'^* j_2'} = \frac{1}{d_{j_1}} \delta_{j_1 j_2 j_3^*} \delta_{j_1 j_2' j_3'^*}, \tag{4.11}$$

and the GSD is a summation in terms of $\{d, \delta\}$:

$$\text{GSD}^{\text{sphere}} = \frac{1}{D^3} \sum_{j_1 j_2 j_3 j_1' j_2' j_3'} d_{j_1'} d_{j_2'} d_{j_3} \delta_{j_1 j_2 j_3^*} \delta_{j_1' j_2 j_3'^*} \delta_{j_1 j_2' j_3'^*}. \tag{4.12}$$

Summing over j_1', j_2', and j_3 using (1.2) finally leads to $\text{GSD}^{\text{sphere}} = 1$.

4.4 Ground state degeneracy for finite group theory

We compute the GSD in the Levin-Wen models constructed from finite group representations. As analyzed in Chapter 2, the ground states is invariant under gauge symmetry, and has trivial holonomy locally everywhere. On a closed spatial surface, the pure gauge fields have two types of physical d.o.f.: local holonomy around each plaquette, and the holonomy along the noncontractible loops of the surface. The former describes the magnetic field strength and the latter is oberseved in the Aharonov-Bohm effect. Since the ground states prefer trivial holonomy locally everywhere, the only physical d.o.f. left are the holonomy along the noncontractible loops.

Take the torus as our spatial surface. There are two noncontractible loops. If the torus is presented as a periodic square on the xy-plane, these two noncontractible loops are along

the periodic boundaries. See Fig. 4.3. The holonomies are the group elements a and b along the two boundary loops.

There are two global constraints on the holonomies: the gauge invariance condition and the requirement that the holonomy is trivial locally everywhere. The former implies that $\{a, b\}$ is equivalent to $\{gag^{-1}, gbg^{-1}\}$, as can be obtained by applying the gauge transformation at the reference point in Fig. 4.3. The latter implies $aba^{-1}b^{-1} = \mathbf{1}$.

Therefore the ground states have a basis

$$\left\{ \frac{1}{|\mathbb{G}|} \sum_g |gag^{-1}, gbg^{-1}\rangle \,\middle|\, aba^{-1}b^{-1} = \mathbf{1} \right\}. \tag{4.13}$$

The GSD on the torus is then

$$\text{GSD}_{\text{QD}}^{\text{torus}} = \left| \{(a,b) | a, b \in G; aba^{-1}b^{-1} = e\} / \sim \right|, \tag{4.14}$$

where $\sim$ in the quotient is the equivalence by conjugation,

$$(a,b) \sim (hah^{-1}, hbh^{-1}) \quad \text{for all } h \in G.$$

In general on any surface, the GSD is

$$\text{GSD} = \left| \frac{\text{Hom}(\pi_1(M), G)}{G} \right|, \tag{4.15}$$

where $\text{Hom}(\pi_1(\mathcal{M}), G)$ is the space of homomorphisms from the fundamental group $\pi_1(M)$ to G, and G in the quotient acts on this space by conjugation.

It is worthwhile to note that the number (4.14) is also the total number of irreducible representations [59] of the quantum double $D(G)$ of the group G. On the other hand, the quasiparticles in the model are classified [14] by the quantum double $D(G)$. Thus, the GSD on a torus is equal to the number of particle species in this example. In the next chapter, we shall prove this statement in generic Levin-Wen models.

4.5 Ground state degeneracy for quantum group $\mathcal{U}_q(\mathfrak{su}(2))$

Now let us take the example using the quantum group $\mathcal{U}_q(\mathfrak{su}(2))$ (with q being primitive root of unity). $\mathcal{U}_q(\mathfrak{su}(2))$ has finitely many irreducible representations, and thus the GSD we calculate is finite. We take the string types to be these representations, denoted by $0, 1, ..., k$, and the data $\{G_{kln}^{ijm}, d_j, \delta_{ijm}\}$ can be constructed by these representations as described in Chapter 3.

Below we compute $\text{GSD} = (k+1)^2$, both analytically and numerically.
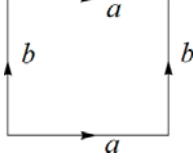
Figure 4.3. Holonomies $\{a, b\}$ along the noncontractible loops. The four corner points are identified as the same reference point. The two noncontractible loops start and end at this reference point.

For simplicity, we only consider the cases when the quantum dimensions are positive. Explicitly, they are

$$d_j = \frac{\sin \frac{(j+1)\pi}{k+2}}{\sin \frac{\pi}{k+2}}$$

$$D = \sum_{j=0}^{k} d_j^2 = \frac{k+2}{2 \sin^2 \frac{\pi}{k+2}}. \tag{4.16}$$

The branching rule is $\delta_{rst} = 1$ if

$$\begin{cases} r + s + t \text{ is even} \\ r + s \geq t, s + t \geq r, t + r \geq s \\ r + s + t \leq 2k \end{cases} \tag{4.17}$$

and $\delta_{rst} = 0$ otherwise. The explicit formula for the $6j$ symbol can be found in [60, 61]. However, we do not need the detailed data of the $6j$ symbol in the following computation of the GSD.

On a torus any trivalent graph can be reduced to the simplest one with two vertices and three edges, as in Fig. 4.2(b). On this graph the GSD consists of six local $6j$ symbols.

$$\text{GSD} = D^{-1} \sum_{s j_1 j_2 j_3 j_1' j_2' j_3'} d_s d_{j_1} d_{j_2} d_{j_3} d_{j_1'} d_{j_2'} d_{j_3'}$$
$$\left(G^{j_1 j_2 j_3^*}_{s j_3'^* j_2'} G^{j_3'^* j_1 j_2'}_{s j_2 j_1'} G^{j_2 j_3'^* j_1'}_{s j_1 j_3^*} \right) \left(G^{j_2^* j_3 j_1^*}_{s j_1'^* j_3'} G^{j_3' j_1'^* j_2^*}_{s j_2' j_1^*} G^{j_1 j_1'^* j_3'}_{s j_3 j_2^*} \right). \tag{4.18}$$

Reordering the $6j$ symbols yields

$$\text{GSD} = D^{-1} \sum_{s j_1 j_2 j_3 j_1' j_2' j_3'} d_s \left(v_{j_1} v_{j_3} v_{j_1'} v_{j_3'} G^{j_2^* j_3 j_3^*}_{s^* j_1'^* j_3'} G^{j_2 j_3'^* j_1'}_{s^* j_1 j_3^*} \right) \times$$
$$\left(v_{j_1'} v_{j_2} v_{j_1} v_{j_2'} G^{j_3' j_1'^* j_2^*}_{s^* j_2'^* j_1^*} G^{j_3'^* j_1 j_2'}_{s^* j_2 j_1'} \right) \left(v_{j_2'} v_{j_3'} v_{j_2} v_{j_3} G^{j_1^* j_1'^* j_3'}_{s^* j_3 j_2^*} G^{j_1 j_2 j_3^*}_{s^* j_3'^* j_2'} \right)$$
$$= D^{-1} \sum_{s j_1 j_2 j_3 j_1' j_2' j_3'} d_s \left(v_{j_1} v_{j_3} v_{j_1'} v_{j_3'} G^{j_2^* j_3 j_3^*}_{s^* j_1'^* j_3'} G^{j_2^* j_1^* j_3}_{s j_3' j_1'^*} \right) \times$$
$$\left(v_{j_1'} v_{j_2} v_{j_1} v_{j_2'} G^{j_3' j_1'^* j_2^*}_{s^* j_2'^* j_1^*} G^{j_3' j_2^* j_1'^*}_{s j_1^* j_2'} \right) \left(v_{j_2'} v_{j_3'} v_{j_2} v_{j_3} G^{j_1^* j_1'^* j_3'}_{s^* j_3 j_2^*} G^{j_1 j_1' j_3 j_2^*}_{s j_2^* j_3} \right), \tag{4.19}$$

where the symmetry condition in (1.4) was used in the second equality.

Let us compare the formula in (4.19) with that in (4.10). We set $j = j^*$ for all j and drop all stars, since all irreducible representations of $\mathcal{U}_q(\mathfrak{su}(2))$ are self-dual. Then we find that the summation (4.19) has the same form as the trace of $D^{-1} \sum_s d_s B^s_{p_2} B^s_{p_3} B^s_{p_1}$ on the graph on a sphere as in (4.10),

$$
\mathrm{tr}^{\mathrm{torus}}\!\left(\frac{1}{D} \sum_s d_s B^s_p\right)
$$

$$
= \sum_{j_1 j_2 j_3} \left\langle \ \overset{j_1}{\underset{j_2}{\leftarrow j_3}} \ \middle|\ \frac{1}{D} \sum_s d_s B^s_{p_2} B^s_{p_3} B^s_{p_1} \ \middle|\ \overset{j_1}{\underset{j_2}{\leftarrow j_3}} \ \right\rangle
$$

$$
= \mathrm{tr}^{\mathrm{sphere}}\!\left(\frac{1}{D} \sum_s d_s B^s_{p_2} B^s_{p_3} B^s_{p_1}\right), \tag{4.20}
$$

where B^s_p is defined on the only plaquette p on the torus (see Fig. 4.2(b)), while $B^s_{p_1} B^s_{p_2} B^s_{p_3}$ is defined on the same graph on a sphere as in (4.10) (see Fig. 4.2(a)).

The GSD on a torus becomes a trace on a sphere. The latter is easier to deal with since the ground state on a sphere is nondegenerate. The counting of ground states on a torus turns into a problem dealing with excitations on the sphere.

In the following we evaluate the summation in the representation of elementary excitations. Let us introduce a new set of operators $\{\hat{n}^r_p\}$ by a transformation,

$$
n^r_p = \sum_s s_{r0} s_{rs} B^s_p, \quad B^s_p = \sum_r \frac{s_{rs}}{s_{r0}} n^r_p. \tag{4.21}
$$

Here, s_{rs} is a symmetric matrix (referred to as the modular S-matrix for $\mathcal{U}_q(\mathfrak{su}(2))$),

$$
s_{rs} = \frac{1}{\sqrt{D}} \frac{\sin \frac{(r+1)(s+1)\pi}{k+2}}{\sin \frac{\pi}{k+2}}, \tag{4.22}
$$

and has the properties

$$
s_{rs} = s_{sr}, \quad s_{r0} = d_r/\sqrt{D}
$$

$$
\sum_s s_{rs} s_{st} = \delta_{rt}
$$

$$
\sum_w \frac{s_{wr} s_{ws} s_{wt}}{s_{w0}} = \delta_{rst}. \tag{4.23}
$$

Eq. (4.21) can be viewed as a finite discrete Fourier transformation between $\{\hat{n}^r_p\}$ and $\{B^s_p\}$. By properties (4.23), we see that $\{\hat{n}^r_p\}$ are mutually orthonormal projectors, and they form a resolution of the identity:

$$
\hat{n}^r_p \hat{n}^s_p = \delta_{rs} \hat{n}^r_p, \quad \sum_r \hat{n}^r_p = \mathrm{id} \tag{4.24}
$$

In particular, $\hat{n}^0_p = \frac{1}{D} \sum_s d_s B^s_p$ is the operator B_p in the Hamiltonian. The operator $\hat{n}^r_p$ projects onto the states with a quasiparticle (labeled by r type) occupying the plaquette p.

Expressed as common eigenvectors of $\{\hat{n}_p^r\}$, the elementary excitations are classified by the configuration of these quasiparticles.

Particularly, on the graph on a sphere as in (4.20), the Hilbert space has a basis of $\{|r_1, r_2, r_3\rangle\}$, where only those r_1, r_2, and r_3 that satisfy $\delta_{r_1 r_2 r_3} = 1$ are allowed. Each basis vector $|r_1, r_2, r_3\rangle$ is an elementary excitation with the quasiparticles labeled by r_1, r_2, and r_3 occupying the plaquettes p_1, p_2, and p_3. The configuration of quasiparticles are globally constrained by $\delta_{r_1 r_2 r_3} = 1$ (see Section 7.3). Therefore, tracing opertors $\{\hat{n}_p^r\}$ leads to

$$\operatorname{tr}(\hat{n}_{p_2}^{r_2} \hat{n}_{p_3}^{r_3} \hat{n}_{p_1}^{r_1}) = \delta_{r_2 r_3 r_1}. \tag{4.25}$$

Applying this rule reduces the summation (4.20) to

$$\operatorname{tr}(\frac{1}{D} \sum_s d_s B_{p_2}^s B_{p_3}^s B_{p_1}^s)$$

$$= \operatorname{tr}(\frac{1}{D} \sum_s d_s \sum_{r_1 r_2 r_3} \frac{S_{s r_1} S_{s r_2} S_{s r_3}}{S_{r_1 0} S_{r_2 0} S_{r_3 0}} \hat{n}_{p_2}^{r_2} \hat{n}_{p_3}^{r_3} \hat{n}_{p_1}^{r_1})$$

$$= \sum_{r_1 r_2 r_3} \frac{1}{D} \sum_s d_s \frac{S_{s r_1} S_{s r_2} S_{s r_3}}{S_{r_1 0} S_{r_2 0} S_{r_3 0}} \delta_{r_1 r_2 r_3}. \tag{4.26}$$

Then we substitute (4.16), (4.17) and (4.22) in and obtain

$$\begin{aligned}
\mathrm{GSD}_{\mathcal{U}_q(\mathfrak{su}(2))}^{\text{torus}} &= \sum_{r_1, r_2, r_3 = 0}^{k} \frac{\sin \frac{\pi}{k+2} \delta_{r_1 + r_2 + r_3, 2k}}{\sin \frac{(r_1+1)\pi}{k+2} \sin \frac{(r_2+1)\pi}{k+2} \sin \frac{(r_3+1)\pi}{k+2}} \\
&= \sum_{r=0}^{k} \sum_{s=0}^{r} \frac{\sin \frac{\pi}{k+2}}{\sin \frac{(r+1)\pi}{k+2} \sin \frac{(s+1)\pi}{k+2} \sin \frac{(r-s+1)\pi}{k+2}} \\
&= (k+1)^2. \tag{4.27}
\end{aligned}$$

(Here, we omit a rigorous proof of the last equality.)

We can also verify $\mathrm{GSD} = (k+1)^2$ by a direct numerical computation. We take

$$\begin{cases}
q = \exp(2\pi i/3) & \text{at } k = 1 \\
q = \exp(3\pi i/4) & \text{at } k = 2 \\
q = \exp(6\pi i/5) & \text{at } k = 3
\end{cases} \tag{4.28}$$

We can construct the data as described in Chapter 3. By this choice, the quantum dimensions d_j take the values as in (4.16), and we compute the summation (4.18) at

$$\begin{cases}
\mathrm{GSD} = 4 & \text{at } k = 1 \\
\mathrm{GSD} = 9 & \text{at } k = 2 \\
\mathrm{GSD} = 16 & \text{at } k = 3,
\end{cases} \tag{4.29}$$

which verifies $\mathrm{GSD} = (k+1)^2$ in the particular cases.

It is widely believed that when the string types in the Levin-Wen model are irreps from a quantum group at level k, then the associated TQFT is given by doubled Chern-Simons theory associated with the corresponding Lie group at level $\pm k$ [62, 55]. This equivalence tells us that in this case the Levin-Wen model can be viewed as a Hamiltonian realization of the doubled Chern-Simons theory on a lattice, and it provides an explicit picture of how the Levin-Wen model describes doubled topological phases.

Along these lines, our result is consistent [63] with the result $\mathrm{GSD}_{CS} = k + 1$ for Chern-Simons $SU(2)$ theory at level k on a torus. This can be seen since the Hilbert space associated to doubled Chern-Simons should be the tensor product of two copies of Chern-Simons theory at level $\pm k$.

CHAPTER 5

TOPOLOGICAL OBSERVABLES
IN GROUND STATES:
S AND T MATRICES

In the previous chapter, we studied the GSD as the simplest topological observable of Levin-Wen models, which partially characterize the topological phases. In this chapter, we study other topological observables: the modular matrices S and T. We may do this, since so far we have only considered local mutations. On a higher-genus surface, we should consider the "large transformations" of the surface.

In this chapter, we shall first construct the topological observables under modular transformations of a torus, then solve their eigen–problems to acquire the expected fractional topological numbers, i.e., the matrices S and T. See Ref. [64]. These fractional topological numbers are related to the fractional statistics of quasiparticles in the elementary excitations. Actually, there is believed to exist a correspondence between the topological degrees of freedom in the ground states of the system on a torus and the local degrees of freedom of the quasiparticles in the elementary excitations. We shall come back to address this correspondence in Chapter 7.

5.1 $SL(2, Z)$ transformations of the torus

Consider the graph Γ on which the model is defined. In Section 4.1, we constructed the mutation transformations that changes the local structure of the graph but preserve the graph topology. Under such mutations, the topological degrees of freedom of the ground states are intact. All such transformations are local. The ground–state projector $\prod_p B_p$ can also be constructed from such mutations.

Here, on the other hand, we look into the large transformations that alter the graph structure globally but still preserve the graph topology and find richer topological observables invariant under these large transformations.

Again, since we are not interested in the local transformations of the graph, we need only to work on the simplest graph of torus as in Fig. 4.2(b).

The transformations that change the topology are the familiar modular transformations, which form the group $SL_2(\mathbb{Z})$ that is generated by

$$\mathcal{S} = \begin{pmatrix} 0 & -1 \\ 1 & 0 \end{pmatrix}, \quad \mathcal{T} = \begin{pmatrix} 1 & 1 \\ 0 & 1 \end{pmatrix}, \tag{5.1}$$

satisfying relations $(\mathcal{ST})^3 = \mathcal{S}^2$ and $\mathcal{S}^4 = 1$. See Fig. 5.1.

To cast the modular transformations in the form of $6j$ symbols, let us redraw the torus in Fig. 4.2(b), in the coordinate frame in Fig. 5.1, which illustrates the $\mathcal{S}$ and $\mathcal{T}$ transformations on the torus. The $\mathcal{S}$ and $\mathcal{T}$ transformations on the subspace $\mathcal{H}^{B_f=1}$ are constructed by

$$\mathcal{S}: \left| \vcenter{\hbox{\includegraphics{a}}} \right\rangle \mapsto \sum_{k'} v_k v_{k'} G^{j^*i^*k}_{jik'} \left| \vcenter{\hbox{\includegraphics{b}}} \right\rangle \overset{\text{Rotation}}{\Longrightarrow} \sum_{k'} v_k v_{k'} G^{j^*i^*k}_{jik'} \left| \vcenter{\hbox{\includegraphics{c}}} \right\rangle, \tag{5.2}$$

and

$$\mathcal{T}: \left| \vcenter{\hbox{\includegraphics{d}}} \right\rangle \mapsto \sum_{k'} v_k v_{k'} G^{j^*i^*k}_{jik'} \left| \vcenter{\hbox{\includegraphics{e}}} \right\rangle \overset{\text{Twist}}{\Longrightarrow} \sum_{k'} v_k v_{k'} G^{j^*i^*k}_{jik'} \left| \vcenter{\hbox{\includegraphics{f}}} \right\rangle. \tag{5.3}$$

In the diagram above, we use the square with periodic boundary conditions to present the torus, with a simplest graph labeled by i, j, and k.

The operators in Eqs. (5.2) and (5.3) give the representations of the $\mathcal{S}$ and $\mathcal{T}$ matrices in Eq. (5.1) in the basis $\{|i,j,k\rangle\}$ (with constraint $\delta_{ijk} = 1$).

We can lay the ground states in the basis composed of the eigenvectors $\{\Phi_k\}$ of $\mathcal{T}$,

$$\mathcal{T}|\Phi_\alpha\rangle = \theta_\alpha |\Phi_\alpha\rangle \tag{5.4}$$

where θ_α is a $U(1)$ phase, and $\alpha = 1, 2, ..., \text{GSD}$ labels the degenerate ground states. These eigenvectors will be identified with the quantum double types as will be discussed in the next section.

$\mathcal{T}$ also has other eigenvectors, whose eigenvalues are zero. These zero eigenvectors are actually the excited states of the model, and we are not going to dwell on them in this chapter.

Hence, one can regard the eigenvalues θ_α of $\mathcal{T}$ as a set of topological numbers of the model. Another set of topological numbers are the $\mathcal{S}$–matrix of the topological sectors,

$$\tilde{S}_{\alpha\beta} = \langle \Phi_\alpha | \mathcal{S} | \Phi_\beta \rangle. \tag{5.5}$$
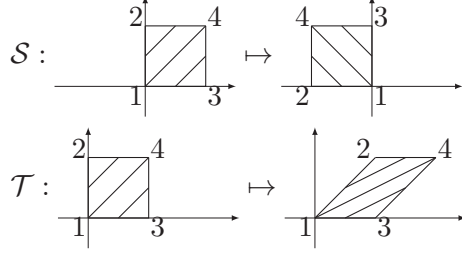
Figure 5.1. $\mathcal{S}$ and $\mathcal{T}$ transformations of a torus. The four corners are identified as the same point. *str* rotates the torus by 90°. $\mathcal{T}$ twists the upper boundary 2-4 along the 1-2 axis by one turn.

where $\alpha, \beta = 1, 2, ..., \mathrm{GSD}$. This matrix is orthonormal:

$$\sum_\beta \tilde{S}_{\alpha\beta} \overline{\tilde{S}_{\beta\gamma}} = \delta_{\alpha\gamma}. \tag{5.6}$$

Above all, apart from GSD, we obtain two more sets of topological numbers, $\{\theta_\alpha\}$, and $\{\tilde{S}_{\alpha\beta}\}$, to characterize the topological phases in our model.

We remark that those $\tilde{S}_{\alpha\beta}$ and θ_α are the topological observables in the ground states, not excitations.

5.2 Topological charge of ground states: Quantum double

The eigenstates of $\mathcal{T}$ are classified by the quantum double of the input data $\{\mathrm{d}, \delta, G\}$, as given by

$$|\mathcal{J}\rangle = \frac{1}{\sqrt{D}} \sum_{ijk} \frac{v_i v_k}{v_j} z^{\mathcal{J}}_{jijk} \left| \begin{array}{c} \vcenter{\hbox{$\displaystyle\substack{j\\k\\i\quad i\\j}$}} \end{array} \right\rangle, \tag{5.7}$$

where $\mathcal{J}$ are the quantum double types, and z^J is the half braiding tensor that characterize each $\mathcal{J}$, as introduced in Appendix A. Note that the coefficients are not symmetric along the two directions, because the twist $\mathcal{T}$ is not. With the normalization factor $1/\sqrt{D}$, they form a orthonormal basis $\langle \mathcal{J}|\mathcal{K}\rangle = \delta_{\mathcal{J},\mathcal{K}}$.

Here, we sketch the proof that $|\mathcal{J}\rangle$ are eigenvectors of $\mathcal{T}$. Under the twist $\mathcal{T}$, $|\mathcal{J}\rangle$ transforms as

$$\mathcal{T}|\mathcal{J}\rangle = \frac{1}{\sqrt{D}} \sum_{ijkk'} \frac{v_i v_k}{v_j} z^{\mathcal{J}}_{jijk} v_k v_{k'} G^{j^*i^*k}_{jik'} \left| \begin{array}{c} \vcenter{\hbox{$\displaystyle\substack{j\\i\\k'\quad k'\\j}$}} \end{array} \right\rangle \tag{5.8}$$

By the tetrahedral symmetry we have $G^{j^*i^*k}_{jik'} = G^{ik'j^*}_{ik^*j}$. Using the symmetry (A.4), we arrive at

$$
\mathcal{T}|\mathcal{J}\rangle = \sum_{ijk'} \frac{v_i v_k}{v_j} \overline{z^{\mathcal{J}}_{ji^*jk'}} \left| \begin{array}{c} \vcenter{\hbox{$\displaystyle$}} \end{array} \right\rangle
$$

$$
= \frac{1}{\sqrt{D}} \sum_{ijk} \frac{v_i v_k}{v_j} \overline{z^{\mathcal{J}}_{jk^*ji^*}} \left| \begin{array}{c} \vcenter{\hbox{$\displaystyle$}} \end{array} \right\rangle
$$

$$
= \theta_J |\mathcal{J}\rangle, \tag{5.9}
$$

where in the second equality we relabel k'^*ji to ijk, and in the last equality we use $\overline{z^{\mathcal{J}}_{jk^*ji^*}} = \theta_J z^{\mathcal{J}}_{jijk}$ for $\delta_{ijk} = 1$. $\theta_{\mathcal{J}}$ is a $U(1)$ number called the twist of the quantum double type $\mathcal{J}$. See Appendix A.

Above all, $\mathcal{T}$ has eigenvectors $|\mathcal{J}\rangle$ labeled by the quantum double types $\mathcal{J}$, with the eigenvalues being the twist of $\mathcal{J}$.

5.3 S and T matrices

In the basis $|\mathcal{J}\rangle$, we obtain the modular matrices:

$$
\tilde{S}_{\mathcal{JK}} = \langle \mathcal{J}|\mathcal{S}|\mathcal{K}\rangle = \frac{1}{D} \sum_{ijkk'} d_k d_{k'} G^{j^*i^*k}_{jik'} \overline{z^{\mathcal{J}}_{ij^*ik'^*}} z^{\mathcal{K}}_{jijk}
$$

$$
= \frac{1}{D} \sum_{ijk} d_k z^{\mathcal{J}}_{ijik} z^{\mathcal{K}}_{jijk}, \tag{5.10}
$$

and

$$
T_{\mathcal{JK}} = \delta_{\mathcal{JK}} \theta_{\mathcal{J}}, \tag{5.11}
$$

where we used $G^{j^*i^*k}_{jik'} = G^{j^*ik'}_{ji^*k}$ and the symmetry condition (A.3) in the last equality. This is exactly the (normalized) modular S matrix defined in Eq. (A.8).

We start with the large modular transformations $\mathcal{S}$ and $\mathcal{T}$ of torus, and we arrive at the modular S and T matrices for the quantum double types as defined in Append A.

5.4   Physical meaning of the quantum double charge

Consider the Levin-Wen models constructed from finite group representations. Let $\mathbb{G} = \mathbb{Z}_N$. As discussed in Appendix A, the quantum double types are labeled by pairs (g, j), where $g = 0, 1, \ldots, N - 1$ is the group elements, and $j = 0, 1, \ldots, N - 1$ are the irreducible representations and are thus, the string types we use to define the model. The quantum double charge (g, j) of the ground states can be understood as a charge-flux composite.

For $\mathbb{G} = \mathbb{Z}_2$ example, there are four quantum double types, denoted by $\mathbf{1}, e, m,$ and $em,$ as defined by Eq. (A.10) in Appendix A. The four ground states in the basis $\left| \vcenter{\hbox{$\begin{smallmatrix} & j & \\ & k & \\ i & & i \\ & j & \end{smallmatrix}$}} \right\rangle$ are

$$|\mathbf{1}\rangle = \frac{1}{\sqrt{2}}(|i = 0, j = 0, k = 0\rangle + |i = 1, j = 0, k = 1\rangle)$$

$$|e\rangle = \frac{1}{\sqrt{2}}(|i = 0, j = 1, k = 1\rangle + |i = 1, j = 1, k = 0\rangle)$$

$$|m\rangle = \frac{1}{\sqrt{2}}(|i = 0, j = 0, k = 0\rangle - |i = 1, j = 0, k = 1\rangle)$$

$$|em\rangle = \frac{1}{\sqrt{2}}(|i = 0, j = 1, k = 1\rangle + |i = 1, j = 1, k = 0\rangle). \tag{5.12}$$

If we rewrite the state $|ijk\rangle$ by $|j\rangle \otimes |i\rangle$ (k depends on i and j by the constraint $i + j + k = 0 \mod 2$), we see that the four ground states are expressed in terms of the charge-flux composites:

$$|\mathbf{1}\rangle = |0\rangle \otimes |\delta_1\rangle$$

$$|e\rangle = |1\rangle \otimes |\delta_1\rangle$$

$$|m\rangle = |0\rangle \otimes |\delta_{-1}\rangle$$

$$|em\rangle = |1\rangle \otimes |\delta_{-1}\rangle. \tag{5.13}$$

where $|\delta_g\rangle = \frac{1}{\sqrt{N}} \sum_i \exp(2\pi\mathrm{i}ig/N)|i\rangle$ is a Fourier transformation of $|i\rangle$ and present the magnetic flux g.

To see the physical meaning the quantum double charge of the ground states, we cut the torus along one noncontractible loop and get a cylinder. Take the simplest graph as illustrated in Eq. (5.2), see Fig. 5.2. The quantum double charge $\mathcal{J}$ of the ground state $|\mathcal{J}\rangle$ can be understood as the charge flow $\mathcal{J}$ through the cylinder.

The twist $\theta_{\mathcal{J}}$ can be understood as the topological spin of the charge-flux composite. In fact, $\mathcal{T}$ will twist the upper boundary loop of the cylinder in Fig. 5.2 once, and then identify it with the lower boundary loop again. In the ground state $|g, j\rangle$ in the $\mathbb{Z}_N$ example, this results in winding the charge j around the flux g and thus, an Aharonov-Bohm phase $\exp(2\pi\mathrm{i}jg/N)$.

This understanding establishes the connection between the topological charges of the ground states and of the excitations. In the following chapters, we will show that the quasiparticles in excitations carry quantum numbers also classified by the quantum double. In the ground state $|g, j\rangle$ in the $\mathbb{Z}_N$ example, if we create a pair of fluxons carrying the flux h and $h^{-1} = N - h$, move the fluxon h around the cylinder once, and then annihilate the fluxon pair, the ground state should acquire an amplitude of $\exp(2\pi\mathrm{i}jh/N)$.
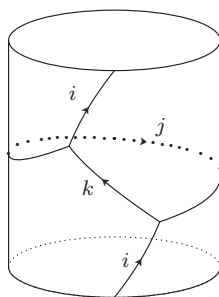
Figure 5.2. Cylinder obtained by cutting a torus, with the simplest trivalent graph.

CHAPTER 6

OPERATOR APPROACH TO FLUXON EXCITATIONS

The Levin-Wen models are exactly solvable because all Q_v and B_p are projection operators and are simultaneously commuting with each other. Therefore, the ground states are the simultaneous eigenstates of $Q_v = 1$ and $B_p = 1$ for all v and p. The elementary excited states are the simultaneous eigenstates of all Q_v and B_p, with their eigenvalues either 0 or 1. There are two types of quasiparticles, as identified by the eigenvalues of Q_v and B_p. We say there is a charge at vertex v in a $Q_v = 0$ eigenstate, and a fluxon at p in a $B_p = 0$ eigenstate. A charge at v and a fluxon at a plaquette p may combine to form a dyon, which is simply a charge-fluxon composite in abelian case. It is well known that any single charge (or single fluxon) state on a sphere is excluded by some global constraints on Q_v and B_p.

In this chapter, we focus on the subspace with $Q_v = 1$ for all v, and study the fluxons. We first show how to identify the topological charges in the fluxon excitations and then construct manipulation operators of the fluxons [65]. These manipulation operators may be used to simulate the topological quantum computation.

6.1 Particle species of fluxons

Fluxons localized at p are classified by the fusion algebra (1.7) of B_p^s. It is called the fusion algebra because the multiplication rule is determined by the fusion rule. From this algebra, we can derive a set of orthonormal projection operators to identify particle species of the fluxons.

In particular, we are interested in two well known classes of Levin-Wen models, constructed from the representations of (1) Finite groups, and (2) Quantum groups (including the quantum double of finite groups, and q-deformed Lie groups with q parameter being a primitive root of unity). In both cases, we have an extra condition that $\delta_{ijk} = \delta_{jik}$ and thus, the algebra (1.7) is abelian. (More generally, this condition holds for the models constructed

from braided tensor categories.) In this dissertation we assume $\delta_{ijk} = \delta_{jik}$ unless specified. The general situation is discussed in Appendix B.

Let us start with the abelian fusion algebra (1.7). It uniquely determines a $N \times N$ matrix X_j^J, called the *fusion characters*, satisfying

$$X_{j*}^J = \overline{X_j^J} \tag{6.1}$$

$$X_i^J X_j^J = \sum_k \delta_{ijk*} X_k^J X_0^J \tag{6.2}$$

$$\sum_j X_j^J \overline{X_j^K} = \delta_{J,K}, \sum_J X_i^J \overline{X_j^J} = \delta_{i,j}. \tag{6.3}$$

See Appendix B for the proof. X_j^J can be viewed as normalized one-dimensional representations of the fusion algebra, as observed in Eq (6.2). The factor X_0^J on the RHS of Eq (6.2) normalizes X_j^J to satisfy Eq. (6.3).

The matrix X_j^J determines a set of orthonormal projections operators n_p^J at p:

$$n_p^J := \sum_s \overline{X_s^J X_0^J} B_p^s, \tag{6.4}$$

satisfying

$$n_p^J n_p^K = \delta_{J,K} n_p^J, \quad \sum_J n^J = \mathbb{1}. \tag{6.5}$$

These projection operators measure the particle species J of the fluxons at p. Each n^J projects onto the states with J-type fluxon at p. There is a special fluxon type, denoted by $J = 0$, corresponding to quantum dimensions by $X_j^0 = d_j/\sqrt{D}$. This type is trivial because $n_p^0 = B_p$ projects onto states without any fluxon at p. Each J comes with a conjugate J^* such that $X_j^{J^*} = \overline{X_j^J}$, and we say J^*-type fluxon is the antiparticle of J-type fluxon.

6.2 Manipulation of fluxons

How can we create fluxons in a ground state to obtain an elementary fluxon excitations? How can we manipulate these fluxons? To answer these questions, we introduce the creation, the annihilation, the hopping, and the braiding operators.

6.2.1 Creation operator

On a ground state, fluxons can not be singly created by a local operator. They must created in pairs. In the following we show how to create a fluxon pair of the opposite types, J and J^*.

We define the creation operator W_e^J on an edge e by

$$W_e^J \left| \left(\begin{array}{c} \\ j_e \end{array} \right) \right\rangle := \frac{\overline{X_0^J}\, \overline{X_{j_e}^J}}{X_0^0 X_{j_e}^0} \left| \left(\begin{array}{c} \\ j_e \end{array} \right) \right\rangle. \tag{6.6}$$

It is diagonal in the matrix form. In the diagram above, only two plaquettes are shown, with the rest part of the graph remained unaffected, and the shape of the plaquettes could be arbitrary.

By acting W_e^J on any ground state $|\Phi\rangle$, we get a fluxon-pair state with fluxon J^* on p_1 and J on p_2, where p_1 is plaquette left to the edge e and p_2 right to e:

$$n_{p_1}^K W_e^J |\Phi\rangle = \delta_{J^*,K} W_e^J |\Phi\rangle$$
$$n_{p_2}^K W_e^J |\Phi\rangle = \delta_{J,K} W_e^J |\Phi\rangle$$
$$n_{p'}^K W_e^J |\Phi\rangle = \delta_{K,0} W_e^J |\Phi\rangle. \tag{6.7}$$

These properties can be proved using the conditions (1.4) on $6j$-symbols.

The definition of W_e^J does not depend on the direction of the edge e. In fact, if we reverse the direction of e, j_e in Eq. (6.6) is replaced by j_e^*. $X_{j_e^*}^J = X_{j_e}^{J^*}$ implies $W_e^J = W_{e^{-1}}^{J^*}$, where e and e^{-1} are the same edge with opposite direction. Both W_e^J and $W_{e^{-1}}^{J^*}$ create the same fluxon pairs across the edge, as they should, see Fig. 6.1.

From Eq. (6.6), we see that W_e^0 is the identity operator when $J = 0$, which agrees with that creating a trivial fluxon pair changes nothing. The hermitian of W_e^J creates a conjugate pair of fluxons because $X_j^{J^*} = \overline{X_j^J}$:

$$W_e^{J^*} = W_e^{J\dagger}. \tag{6.8}$$

The multiplication of W_e^J can be decomposed —

$$W^I W^J = \sum_K \Delta_{IJK^*} W^K, \quad \Delta_{IJK} = \sum_j \frac{X_0^I X_0^J}{X_0^K X_0^0} \frac{X_j^I X_j^J X_j^K}{X_j^0} - \tag{6.9}$$

by using Eq (6.3). Creating two fluxon pairs across the same edge yields a linear combination of fluxon-pair states.

The creation operator has a Fourier transformation. By the orthonormal conditions (6.3), we obtain the projection operator

$$E_e^k = \sum_J \frac{X_0^0 X_k^0}{X_0^J X_k^J} W_e^J \tag{6.10}$$

that projects onto states with label on the edge e to be k.

(a) $W_e^J|\Phi\rangle$ (b) $W_{e-1}^{J^*}$

Figure 6.1. Fluxon-pair state $W_e^J|\Phi\rangle$ generated from a ground state $|\Phi\rangle$. The creation operator does not depend on the edge direction. The fluxon-pair state $W_e^J|\Phi\rangle$ in (a) is the same as $W_{e-1}^{J^*}|\Phi\rangle$ in (b).

6.2.2   Annihilation and hopping operators

In the following we show how to annihilate and hop fluxons. Again, note that fluxons are created and annihilated in pairs locally.

Let us start with a ground state $|\Phi\rangle$, and consider a trivalent vertex and its three neighboring plaquettes p_0, p_1 and p_2, see Fig. 6.2(a).

In Fig. 6.2(b), W_2^J creates a J^*–J fluxon pair at p_0 and p_1, while W_3^J creates a J^*–J fluxon pair at p_1 and p_2. Now p_1 is occupied by two fluxons, J from W_2^J, and J^* from W_3^J. The resulting state may be no longer an eigenstate of certain $n_{p_1}^K$, because J and J^* may couple to more than one types of fluxons. However, since $n_{p_1}^K$ are orthonormal projections, we can decompose the state $W_3^J W_2^J|\Phi\rangle$ to $\sum_K n_{p_1}^K W_3^J W_2^J|\Phi\rangle$. In other words, $n_{p_1}^K$ projects onto the state $n_{p_1}^K W_3^J W_2^J|\Phi\rangle$ with only K-fluxon at p_1. When $W_3^J W_2^J|\Phi\rangle$ collapses to an $n_{p_1}^K = 1$ eigenstate $n_{p_1}^K W_3^J W_2^J|\Phi\rangle$, we say the two fluxons J and J^* couple to a new fluxon K.

Particularly, $n_{p_1}^0$ kills any nontrivial fluxon at p_1. In the above example, $n_{p_1}^0$ projects onto a fluxon-pair state, with J^* at p_0 and J at p_2. In this killing process, $n_{p_1}^0$ plays the role of annihilation operator. The annihilation occurs only if the two fluxons at p_1 are antiparticles of each other.

The above process is also a hopping process, in which the hopping operator $n_{p_1}^0 W_3^J$ moves the fluxon J from p_1 to p_2. In this process, a J-fluxon is created at p_2 while a J-fluxon is annihilated at p_1.

The hopping operator must satisfy some topological property: hopping along two homotopic paths (without any nontrivial fluxon enclosed by the two paths) leads to the same final state. Consider again the above example. We apply the hopping operator $n_{p_1}^0 W_3^J$ to the fluxon pair state $W_2^J|\Phi\rangle$, and obtain a fluxon pair state. The *path independence* requires

$$n_{p_1}^0 W_3^J W_2^J|\Phi\rangle = W_1^J|\Phi\rangle, \tag{6.11}$$
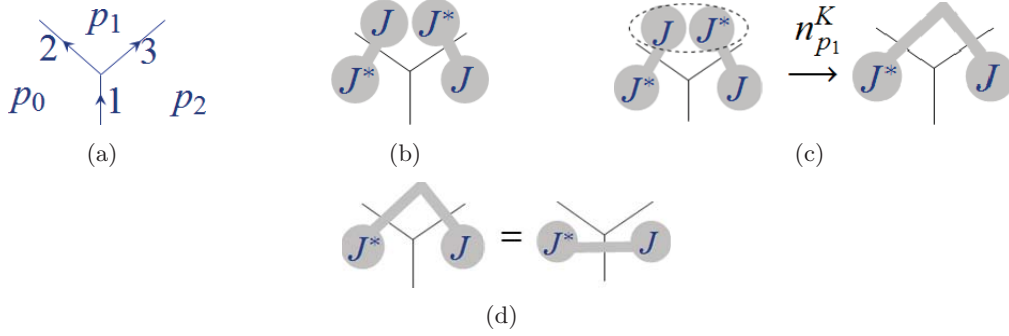
Figure 6.2. (a) Three neighboring plaquettes around a trivalent vertex. (b) Create two fluxon pairs across the edge 2 and 3. (c) Annihilate fluxons at p_1 by $n_{p_1}^0$. (d) The final fluxon-pair state in (c) is equal to that obtained by directly creating a fluxon pair across edge 1. This implies $n_{p_1}^0 W_2^J$ is path independent, and thus is a hopping operator of fluxon J at p_1.

around any trivalent vertex. This property can be verified by using the conditions (1.4) on $6j$-symbols.

The hopping operators induce a string operator that creates a pair of fluxons far apart. We choose a path along plaquettes $p_1, p_2, \ldots,$ and p_{n+1}, going across edges $e_1, e_2, ...,$ and e_n, as illustrated below:

$$p_1 \quad \Big|_{e_1} \quad p_2 \quad \Big|_{e_2} \quad \cdots \quad \Big|_{e_n} \quad p_{n+1} \tag{6.12}$$

This is a string consisting of plaquettes. First we create a fluxon pair on the neighboring plaquettes across e_1, with J^*-fluxon at p_1 and J-fluxon at p_2. Then we move the J-fluxon to p_n by a sequence of hopping operators, and the finial state is

$$n_{p_n}^0 W_{e_n}^J \ldots n_{p_2}^0 W_{e_2}^J W_{e_1}^J |\Phi\rangle. \tag{6.13}$$

The two fluxons are at the starting plaquette p_1 and the ending plaquette p_{n+1} of the string. The string operator in Eq. (6.13) only depends on the two ends of the string because of the path independence of the hopping operator.

6.2.3 Fluxons as flux tubes

Fluxons can be viewed as Faraday's "flux tubes" geometrically. As will be shown in Section 6.3, in the models constructed from finite group representations, the fluxons are "flux tubes" classified by the conjugacy classes of the finite group.

In Appendix C of Ref. [43], B_p^s can be graphically presented as fusing a loop labeled by s to the boundary edges of the plaqutte p. This loop has a physical meaning in gauge

theory language: B_p^s is the Wilson loop operator that creates a Wilson loop labeled by s around p.

In an excitation $|\Psi\rangle$ with a fluxon J at p, B_p^s takes the eigenvalue $\chi_s([J])$, with $[J]$ a conjugacy class. The J fluxon can be viewed as a flux tube piercing the plaquette p, as illustrated in Fig. 6.3(a).

Particularlly the fluxon pair state $W_e^J|\Phi\rangle$ is characterized by a flux tube loop piercing the two occupied plaquettes and going around the edge e, see Fig. 6.3(b).

In general, Levin-Wen models can be viewed as generalized discrete gauge theory where the gauge group is generalized to some algebra (weak Hopf algebra), each B_p^s is the generalized Wilson loop operator, and the fluxons are the generalized "flux tubes." With the created fluxon pair viewed as the flux tube around the edge, Eqs (6.4) and (6.10) can be viewed as the electromagnetic duality: Wilson loops generate magnetic flux labeled by J, while magnetic flux loops generate electric flux labeled by j. See Fig. 6.3(b).

6.3   Examples

Before discussing the properties of the fluxons, we study two examples: the models constructed from finite group representations, and from quantum group representations. We shall examine the fusion characters X_j^J in these two examples.

6.3.1   Finite group theory

In the Levin-Wen models constructed from the representations of a finite groups $\mathbb{G}$, the string types are taken to be all irreducible representations j of $\mathbb{G}$. For simplicity, we assume $\mathbb{G}$ is multiplicity free. The quantum dimension $d_j = \alpha_j \dim(V_j)$ is the dimension of the representation space V_j, where the Frobenius-Schur indicator $alpha_j = -1$ if the representation j is pseudoreal and 1 otherwise. $j = 0$ is the trivial representation that maps any $g \in \mathbb{G}$ to 1. The fusion rule δ_{ijk} is 1 if the trivial representation 0 appears in the decomposition of the tensor product representation $i \otimes j \otimes k$, and 0 otherwise (assuming $\mathbb{G}$ is multiplicity free). The construction of data $\{d, \delta, G\}$ has been explained in Chapter 2.

Such models using $\mathbb{G}$ is the dual formulation of a lattice gauge theory with the finite gauge group $\mathbb{G}$. We use the irreducible representations of $\mathbb{G}$ as the fundamental degrees of freedom, while the standard formulation use the group elements (i.e., the discrete gauge fields). The Levin-Wen model constructed from $\mathbb{G}$ representations can be mapped to Kitaev's quantum double model based on the same $\mathbb{G}$, see [54].

The fluxons are classified by the conjugacy classes. The number of conjugacy classes is equal to the number of irreducible representations, as expected by the analysis in Section

(a) flux tubes   (b) Single fluxon-pair state   (c) Two-fluxon-pair state

(d) Annihilation at plaquette 2
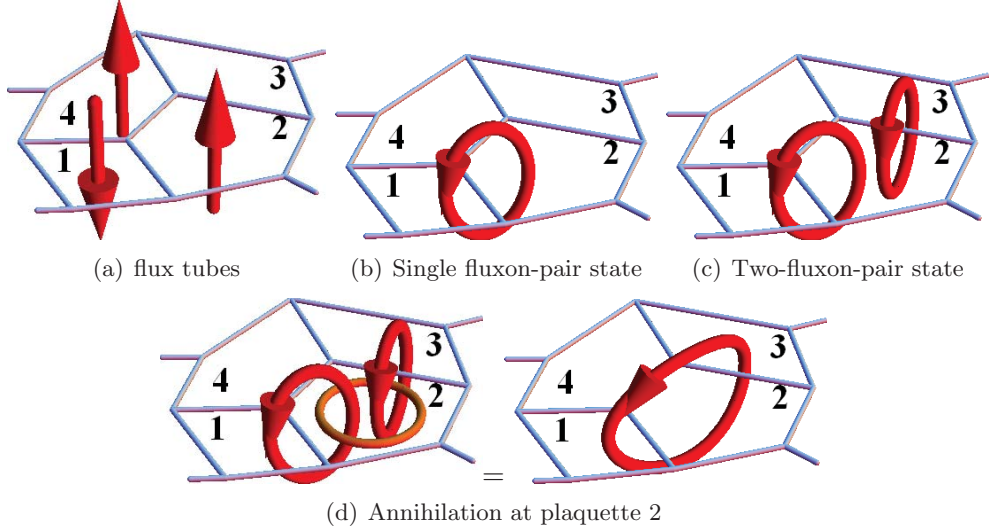
Figure 6.3. (color online.) Geometric structure of an elementary excitation $|\Psi\rangle$. A fluxon J is viewed as a flux tube piercing its occupied plaquette and going out of the surface, while a fluxon J^* is viewed as a flux tube coming into the surface. (a). Two fluxons I and J occupy plaquettes 2 and 4, and a fluxon K^* occupies plaqutte 1. (b). Single fluxon-pair state $W_e^J|\Phi\rangle$. The fluxon pair created by W_e^J on a ground state $|\Phi\rangle$ is viewed as a flux tube loop piercing the two occupied plaquettes and going around the edge e. (c) Two fluxon pairs in $W_{e_1}^J W_{e_2}^J|\Phi\rangle$. Two fluxon pairs are created on the ground state $|\Phi\rangle$, presented by two flux loops labeled by J. (d) Annihilation of fluxons at plaquatte 2. Yellow loop around the plaquette present the projection operator n_2^0, which annihilate the flux tubes at plaquette 2. After the annihilation, a fluxon pair state remains.

6.1. Denote by C^J the conjugacy classes of $\mathbb{G}$, and by $g^J \in \mathbb{G}$ a representative of each class J. The fusion characters X_j^J are normalized characters:

$$X_j^J = \sqrt{\frac{|C^J|}{|\mathbb{G}|}} \chi_j(g^J)\alpha_j, \tag{6.14}$$

where $|\mathbb{G}|$ is the order of $\mathbb{G}$, and $|C^J|$ the cardinality of C^J. The Frobenius-Schur indicator α_j appears such that $X_0^0 X_j^0 = \alpha_j \dim(j) = d_j$. The orthogonality relations (6.3) for X_j^J are thus, those for character functions χ_j with respect to conjugacy classes C^J.

The operator $n_p^0 = B_p$ in the Hamiltonian prefers zero holonomy around the plaquette p. In the ground states, zero holonomy everywhere implies a flat connection. Hence, the ground-state subspace is identified with the module space of flat connections on the spatial surface.

Denote by J the conjugacy class of the finite group, and g^J the representative element in the class. Then the creation operator W_e^J of a fluxon-pair is

$$W_e^J : \left|\ \overbrace{}^{j_e}\ \right\rangle \mapsto \frac{|C^J|}{\dim(j)}\overline{\chi_j(g^J)}\left|\ \overbrace{}^{j_e}\ \right\rangle, \tag{6.15}$$

where $|C^J|$ is the cardinality of the conjugacy class J, and $\dim(j)$ the dimension of the representation space of j.

In the gauge theory language, W_e^J changes the holonomies of the two neighboring plaquettes across the edge e by the conjugacy class J. To see this, consider the Fourier transformation between the basis of group elements and the representation elements:

$$\left\langle \boxtimes_{g_e} \Big| \Y_{j_e;\alpha\beta} \right\rangle = \rho_{\alpha\beta}^j(g_e), \tag{6.16}$$

where $\rho^j(g_e)$ is the representation matrix and α, β the matrix indexes. The creation operator W_e^J results in a multiple of $\chi_j(g^J)$. Since $\frac{\dim(j)}{|\mathbb{G}|}\sum_h \rho_{\alpha\beta}^j(g_e h g^J h^{-1}) = \chi_j(g^J)\rho_{\alpha\beta}^j(g_e)$, we see that the creation operator in the group element basis is

$$W_e^J : \left| \Y_{g_e} \right\rangle \mapsto \frac{|C^J|}{|G|}\sum_{h\in\mathbb{G}} \left| \Y_{g_e h g^J h^{-1}} \right\rangle$$

$$= \sum_{h\in J}\left| \Y_{g_e h} \right\rangle. \tag{6.17}$$

Therefore a fluxon-pair state can be expressed as $\sum_{h\in J} h \otimes h^{-1}$, with h the holonomy along two plaquettes. If the finite group is nonabelian and the conjugacy class J has more than one elements, the two fluxons are entangled. See Fig. 6.4.

For example, the cyclic group $\mathbb{G} = \mathbb{Z}_N$ group has N irreducible representations $j = 0, 1, \ldots, N-1$, with $j^* = N - j$ and $d_j = 1$ for all j. The fusion rule is

$$\delta_{ijk} = \begin{cases} 1 & \text{if } i + j + k = 0 \bmod N \\ 0 & \text{otherwise} \end{cases} \tag{6.18}$$

The $6j$ symbol is given by

$$G_{j_4 j_5 j_6}^{j_1 j_2 j_3} = \delta_{j_1 j_5 j_6}\delta_{j_2 j_4 j_6^*}\delta_{j_3^* j_4 j_5}\delta_{j_1 j_2 j_3} \tag{6.19}$$

Since $\mathbb{Z}_n$ is abelian, each group element itself forms a conjugacy class. Hence, the fluxons are classified by the group elements. The characters are given by $\chi_j(n) = \exp(inj/N)$.

Another example is the simplest nonabelian group, the dihedral group $\mathbb{G} = D_3$ (also known as the symmetry group S_3). It has three irreducible representations $j = 0, 1, 2$. Since all of them are real representations, the quantum dimension d_j is the dimension of representation space V_j: $d_0 = d_1 = 1$ and $d_2 = 2$.

The fusion rules are given by $\delta_{000} = \delta_{011} = \delta_{022} = \delta_{122} = \delta_{222} = 1$. See Section 2.2.2 for detailed construction.

The fluxons are classified by the three conjugacy classes, with the character table presented in Table 6.1.
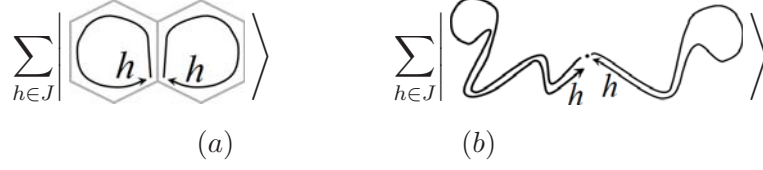
Figure 6.4. Fluxon-pair state labeled by conjugacy class J. (a) A fluxon-pair created across the middle edge. (b) When two fluxons are separated far apart, the pairing of the holonomies around the two plaquettes will not be broken.

Table 6.1. Character table of $\mathbb{G} = D_3$.

	C^1	C^2	C^3
$\chi_{j=0}$	1	1	1
$\chi_{j=1}$	1	1	-1
$\chi_{j=2}$	2	-1	0

6.3.2   Quantum group theory

Consider models constructed from the representations of a q-deformed Lie group $\mathcal{U}_q(\mathfrak{g})$, with the parameter q a primitive root of unity. While the usual Lie group has the infinitely many irreducible representations, the q-deformed Lie group has finitely many (semisimple) irreducible representations with nonzero quantum dimensions. The states in this class are also known as the spin-network states, which intends to formulate the metric field of the 2+1D quantum gravity.

The input data of $6j$-symbols may be constructed from the irreducible representations (with nonzero quantum dimensions) of $\mathcal{U}_q(\mathfrak{g})$. For example, Reshetikhin and Kirillov derived the $6j$-symbol from the representation theory of $\mathcal{U}_q(\mathfrak{sl}_2)$. Later, a much simpler approach through the Kauffman brackets (or, through Temperley-Lieb algebra) was developed. For detailed construction, see Chapter 3.

For the example of the semion theory, there are two string types denoted by $j = 0, 1$, with quantum dimensions $d_0 = 1, d_1 = -1$. The fusion rule is the $\delta_{000} = \delta_{011} = 1$ and $\delta_{001} = \delta_{111} = 0$.

The fusion character X_j^J is determined by δ_{ijk}:

$$X_0^{J=0} = 1, \ X_1^{J=0} = -1, \ X_0^{J=1} = 1, \ X_1^{J=1} = 1. \tag{6.20}$$

Note that $X_1^{J=0} = -1$ to match $d_1 = -1$.

6.4 Topological charge in fluxon excitations: Quantum double

In Section 6.1 we discussed one type of quantum numbers – the orthonormal projections to identify the particle species of fluxon types. However, to fully characterize many-fluxon excitations, we need more quantum numbers. Consider the many-fluxon states with N fluxons occupying N fixed plaquettes, with the fluxons $J_1, J_2, \ldots, J_N$ at $p_1, p_2, \ldots, p_N$. Such states are degenerate, and the fluxon type projection n_p^J can not distinguish those degenerate states.

We need more quantum numbers to describe the collective behavior of many fluxons, i.e., we need to know not only the fluxon type at each plaquette, but also the relative degree of freedom (d.o.f.) among these fluxons. For this purpose, in the following, we figure out the quantum number of the subsystem of two fluxons at the neighboring plaquettes.

Consider two neighboring plaquettes p_1 and p_2. For simplicity, we assume both are triangle plaquettes. At these two plaquettes, the local operators $B_1^s B_2^t$ are given by

$$\left\langle \begin{array}{c} j_6 \ j_2' \ j_5' \ j_7 \\ j_1' \\ j_3' \ j_4' \end{array} \middle| B_1^s B_2^t \middle| \begin{array}{c} j_6 \ j_2 \ j_5 \ j_7 \\ j_1 \\ j_3 \ j_4 \end{array} \right\rangle$$

$$= v_{j_1} v_{j_2} v_{j_3} v_{j_4} v_{j_5} v_{j_1'} v_{j_2'} v_{j_3'} v_{j_4'} v_{j_5'} \sum_{j_1''} \mathrm{d}_{j_1''}$$

$$\times G^{j_5 j_2^* j_1}_{s j_1'' j_2'^*} G^{j_6 j_3^* j_2}_{s j_2' j_3'^*} G^{j_4^* j_1^* j_3}_{s j_3' j_1''^*} G^{j_3' j_4^* j_1''^*}_{t j_1'^* j_4'} G^{j_7 j_5^* j_4}_{t j_4' j_5'} G^{j_2''^* j_1' j_5}_{t j_5' j_1'^*}, \tag{6.21}$$

from which we obtain the fluxon projection operator $n_1^J n_2^K = \sum_{rs} \overline{X_s^J X_0^J X_t^K X_0^K}\, B_1^s B_2^t$, with n_1^J for fluxon J at the left plaquette, and n_2^K for fluxon K at the right one.

In addition to $n_1^J n_2^K$, it is possible to construct other local observables, say P_{12}, that measures the total quantum number of the two-plaquette subsystem, which commute with the Hamiltonian. By "local" we mean that P_{12} only changes local labels j_1, j_2, j_3, j_4, and j_5 around the bounday of the two plaquettes, similar to $n_1^J n_2^K$. Since the relative d.o.f. between two fluxons should live on the middle edge, we can start by assuming that P_{12} has a general form of

$$\left\langle \begin{array}{c} j_6 \ j_2' \ j_5' \ j_7 \\ \tilde{j}_1 \\ j_3' \ j_4' \end{array} \middle| P_{12} \middle| \begin{array}{c} j_6 \ j_2 \ j_5 \ j_7 \\ j_1 \\ j_3 \ j_4 \end{array} \right\rangle$$

$$= \sum_{st} v_{j_2} v_{j_3} v_{j_4} v_{j_5} v_{j_2'} v_{j_3'} v_{j_4'} v_{j_5'} \sum_{j_1' j_1''} \mathrm{d}_{j_1''} \mathrm{d}_{j_1'} Z_{st j_1 \tilde{j}_1 j' j_1''}$$

$$\times G^{j_5 j_2^* j_1}_{s j_1' j_2'^*} G^{j_6 j_3^* j_2}_{s j_2' j_3'^*} G^{j_4^* j_1^* j_3}_{s j_3' j_1''^*} G^{j_3' j_4^* j_1''^*}_{t \tilde{j}_1^* j_4'} G^{j_7 j_5^* j_4}_{t j_4' j_5'} G^{j_2''^* j_1' j_5}_{t j_5' \tilde{j}_1^*}, \tag{6.22}$$

with $Z_{st j_1 \tilde{j}_1 j' j_1''}$ to be determined. In fact, P_{12} becomes $B_1^{s'} B_2^{t'}$ with the choice $Z_{st j_1 \tilde{j}_1 j' j_1''} = \frac{v_{j_1} v_{\tilde{j}_1}}{\mathrm{d}_{j_1'}} \delta_{j_1', j_1''} \delta_{s, s'} \delta_{t, t'}$. In Eq. (6.22), the $6j$ symbols are assigned as follows: the index j_1' is

localized near the top trivalent vertex and j_1'' near the bottom trivalent vertex. This is the most general form for an arbitrary action on the d.o.f. j_1 in the middle edge, while conserving the branching rule at all vertices.

The formula (6.22) of P_{12} can be simplified for our purpose. If we create a fluxon pair across the middle edge, the total quantum number should not be affected because no fluxon will be left if we fuse locally created fluxon pair together. Therefore, we require $P_{12}W_1^J = W_1^J P_{12}$ for all J. By the orthonormal condition (6.3), the above expression is nonzero only when $\tilde{j}_1 = j_1$. It means that only the boundary edges $2, 3, 4$ and 5 of the two-plaquette subsystem will be changed, just like that only the boundary edges of the plaquette p are changed by B_p^s.

Therefore, we arrive at

$$\sum_{st} \left\langle \left. \begin{matrix} j_6 \nearrow j_2' \quad j_5' \quad j_7 \\ \quad j_1 \\ j_3' \quad j_4' \end{matrix} \right| P_{12} \left| \begin{matrix} j_6 \quad j_2 \quad j_5 \quad j_7 \\ \quad j_1 \\ j_3 \quad j_4 \end{matrix} \right. \right\rangle$$

$$= \sum_{st} v_{j_2} v_{j_3} v_{j_4} v_{j_5} v_{j_2'} v_{j_3'} v_{j_4'} v_{j_5'} \sum_{j_1' j_1''} \mathrm{d}_{j_1''} \mathrm{d}_{j_1'} Z_{st j_1 j_1' j_1''}$$

$$\times G_{sj_1' j_2'}^{j_5 j_2^* j_1} G_{sj_2' j_3'}^{j_6 j_3^* j_2} G_{sj_3' j_1''}^{j_4^* j_1^* j_3} G_{tj_1^* j_4'}^{j_3' j_4^* j_1''^*} G_{tj_4' j_5'}^{j_7 j_5^* j_4} G_{tj_5' j_1^*}^{j_2''^* j_1' j_5}, \tag{6.23}$$

with $Z_{st j_1 j_1' j_1''}$ to be determined.

For P_{12} to be an observable, we require

$$P_{12} n_1^J = n_1^J P_{12}, \quad P_{12} n_2^J = n_2^J P_{12}. \tag{6.24}$$

The solutions to Eq (6.24) are given by the quantum double structure. See Appendix A. Each quantum double type $\mathcal{J}$ is characterized by a half braiding tensor $z^{\mathcal{J}}_{s j_1 t j_1'}$, giving rise to a solution:

$$Z_{st j_1 j_1' j''1} = z^{\mathcal{J}}_{s j_1 t j_1'} \overline{z^{\mathcal{J}}_{s j_1 t j_1''}}. \tag{6.25}$$

We can diagonalize these solutions and obtain the orthonormal projections $P_{12}^{\mathcal{J}}$, with the choice

$$Z^{\mathcal{J}}_{st j_1 j_1' j''1} = \sum_{\mathcal{K}} \overline{\tilde{S}_{\mathcal{J}0}} \tilde{S}_{\mathcal{J}\mathcal{K}} z^{\mathcal{J}}_{s j_1 t j_1'} \overline{z^{\mathcal{J}}_{s j_1 t j_1''}}, \tag{6.26}$$

Here, $\tilde{S}_{\mathcal{J}\mathcal{K}}$ is the modular S matrix for the quantum double data as defined in (A.8). These $Z^{\mathcal{J}}$ defines orthonormal:

$$P_{12}^{\mathcal{J}} P_{12}^{\mathcal{K}} = \delta_{\mathcal{J}\mathcal{K}} P_{12}^{\mathcal{J}}, \quad \sum_{\mathcal{J}} P_{12}^{\mathcal{J}} = \mathbf{1}. \tag{6.27}$$

They identify the total topological charge of the wo-fluxon subsystem.

If $P^{\mathcal{J}} = 1$ in an elementary excitation, we say the total charge of the two-fluxon subsystem is $\mathcal{J}$. Any fluxon type J is a quantum double type, and P_{12}^{J} can be expressed in terms of W and n^J:

$$P_{12}^{J} = \sum_{KL} n_1^K n_2^K (\sum_I W_e^I) n_1^0 n_2^J (\sum_I W_e^I) n_1^K n_2^K. \tag{6.28}$$

If we have a fluxon J at the left plaquette, but no fluxon at the right one, then the total charge must be equal to J. But there are more quantum double types than fluxon types: $\{J\} \subset \{\mathcal{J}\}$.

From Eq. (6.27), it seems that all possible topological charges are classified by the quantum double. However, in many cases, $P^{\mathcal{J}}$ may be zero in the entire space. The quantum double types are more than we can observed in an elementary fluxon excitations. In particular, if the input quantum dimensions $d_j = \pm 1$ for all j, then all fluxons are abelian, and the topological charges are classified by the fluxons, with $P_{12}^{\mathcal{J}} = 0$ if $\mathcal{J}$ is not equal to any of the fluxon types J. In a nonabelian case, the topological charges may be classified by the entire set of quantum double types. We will discuss these situations in details in the following two chapters.

Similarly, we can measure the total topological charge of a subsystem containing more than two fluxons. Consider three neighboring plaquettes as illustrated below. We define the projection operator $P_{123}^{\mathcal{J}}$ by

$$= \sum_{rst} v_{j_3} v_{j_4} v_{j_5} v_{j_6} v_{j_7} v_{j_8} v_{j_3'} v_{j_4'} v_{j_5'} v_{j_6'} v_{j_7'} v_{j_8'} \times$$

$$\sum_{j_1' j_1'' j_2' j_2''} d_{j_1'} d_{j_1''} d_{j_2'} d_{j_2''} Z_{rsj_1 j_1' j_1''}^{\mathcal{J}} Z_{stj_2 j_2' j_2''}^{\mathcal{J}} (G_{rj_1' j_3'^*}^{j_8 j_3^* j_1} G_{rj_3' j_4'^*}^{j_9 j_4^* j_3} G_{rj_4' j_1''^*}^{j_5^* j_1^* j_4}) \times$$

$$(G_{sj_1^* j_5'^*}^{j_4' j_5^* j_1''^*} G_{sj_5' j_2''^*}^{j_6^* j_2^* j_5} G_{sj_2' j_8'^*}^{j_7 j_8^* j_2} G_{sj_8' j_1}^{j_3'^* j_1' j_8}) (G_{tj_7' j_2}^{j_8'^* j_2' j_7} G_{tj_2' j_6'^*}^{j_5' j_6^* j_2''^*} G_{tj_6' j_7'^*}^{j_{10} j_7' j_6}), \tag{6.29}$$

where $z^{\mathcal{J}}$ is as given in Eq. (6.26). $P_{123}^{\mathcal{J}}$ measures the total charge of the three-fluxon subsystem. This definition is valid for any three fluxons on any graph. If the three fluxons are far apart from each other, we can move them to three neighboring plaquettes by the unitary hopping operators. If the three neighboring plaquettes have different shapes other than those in the above equation, $P_{123}^{\mathcal{J}}$ is defined in the same way only up to some unitary mutations T_1 in Eq. (4.4).

Following the same rules, the projection operator $P^{\mathcal{J}}$ can be defined in a subsystem containing an arbitrary finitely number of fluxons.

These topological charges are topological, because the measurement of the total charge only depends on the topology of the configuration space of fluxons. It may depend on the topology of how the subsystem boundary loops enclose the selected fluxons. See Fig. 6.5 for an example. The choice of the subsystems also depends on the topology of the spatial graph. See Fig. 6.6 for an example. In both examples, the two choices of the subsystem containing the three same fluxons cannot be smoothly deformed into each other, and thus the measurement $P_{123}^{\mathcal{J}}$ may have different results. Otherwise, the total topological charge is the same no matter how large the subsystem is, and how far apart the fluxons contained are.

Figure 6.5. Two ways to choose a subsystem containing three fixed fluxons on a sphere.

Figure 6.6. Two ways to choose a subsystem containing three fixed fluxons on a torus.

CHAPTER 7

FRACTIONAL EXCHANGE STATISTICS

In this chapter we study the fractional exchange statistics in the fluxon excitations [65], using the hopping operator as developed in Section 6.2.2. In Fig. 7.1, the two fluxons of types J_1 and J_2 are exchanged in the counterclockwise direction.

By the path independence of hopping operators, the effect of the exchange of two fluxons only depends on the topology of the configure space of all fluxons, and hence, the N-fluxon states form a representation space of the braid group B_N.

7.1   Hilbert space structure of many-fluxon states

To describe the Hilbert space of many-fluxon excitations, we determine the full quantum numbers as follows. We can specify the topological charge of each fluxon, i.e., the fluxon types. Then we can specify the total topological charge of the subsystems of several fluxons. But the total topological charges of all subsystems cannot be determined at the same time. For example, consider excitations with four fluxons, enumerated by $1, 2, 3$ and 4. We can measure the total topological charge of the first two fluxons by $P_{12}^{\mathcal{J}}$, or of fluxon 1 and 3 by $P_{13}^{\mathcal{J}}$. These two quantum numbers can not be determined at the same time: $P_{12}^{\mathcal{J}} P_{13}^{\mathcal{J}} \neq P_{13}^{\mathcal{J}} P_{12}^{\mathcal{J}}$. Therefore, we need to choose an appropriate set of quantum numbers without over-counting them.

Consider N-fluxon excitations, with their fluxon types $J_1, J_2, \ldots, J_N$ at N fixed plaquettes. The Hilbert space of such N-fluxon states has a basis presented by

$$(7.1)$$

The N external lines are labeled by the fluxon types $J_1, J_2, ..., J_N$ of the N fluxons. There are also $N - 3$ internal lines, labeled by the quantum double types $\mathcal{J}_1, \mathcal{J}_2, \ldots, \mathcal{J}_{N-3}$. $\mathcal{J}_1$ is the total topological charge of the first two fluxons, $\mathcal{J}_2$ of the first three, and $\mathcal{J}_{N-3}$ the first $N - 2$. The configuration of $\mathcal{J}$'s are constrained by the quantum double fusion rule:

Figure 7.1. Exchange of two fluxons in the counterclockwise direction by hopping operators.

J_1 and J_2 couple to $\mathcal{J}_1$, $\mathcal{J}_1$ and J_3 couple to $\mathcal{J}_2$, and so on. This fusion rule is determined by the modular S matrix of the quantum double types:

$$\delta_{\mathcal{J}_1 \mathcal{J}_2 \mathcal{J}_3} = \sum_{\mathcal{J}} \frac{\tilde{S}_{\mathcal{J}_1 \mathcal{J}} \tilde{S}_{\mathcal{J}_2 \mathcal{J}} \tilde{S}_{\mathcal{J}_3 \mathcal{J}}}{\tilde{S}_{0\mathcal{J}}}, \tag{7.2}$$

which takes values of 0 or 1. See Appendix A. Here, 0 in $\tilde{S}_{0\mathcal{J}}$ is the trivial quantum double type, which is identical to the trivial fluxon type. $\delta_{\mathcal{J}_1 \mathcal{J}_2 \mathcal{J}_3^*} = 0$ implies $\mathcal{J}_1$ and $\mathcal{J}_2$ cannot couple to $\mathcal{J}_3$. For simplicity, here we assume the multiplicity free fusion rules.

Therefore, the basis of N-fluxon Hilbert space on a sphere is

$$\{|J_1, J_2, \ldots, J_N; \mathcal{J}_1, \mathcal{J}_2, \ldots, \mathcal{J}_{N-3}\rangle | \delta_{J_1 J_2 \mathcal{J}_1^*} = 1, \delta_{J_3 \mathcal{J}_1 \mathcal{J}_2^*} = 1, \ldots, \delta_{J_{N-1} \mathcal{J}_{N-3} J_N} = 1\} \tag{7.3}$$

When the topology of the spatial graph is nontrivial (e.g. on a torus), we need to consider the topological d.o.f., which only depends on the topology. The ground states are degenerate. This degeneracy survives in the fluxon excitations, but the degeneracy may not be exactly the same as the GSD.

On a torus, the basis of N-fluxon Hilbert space is presented by

$$\tag{7.4}$$
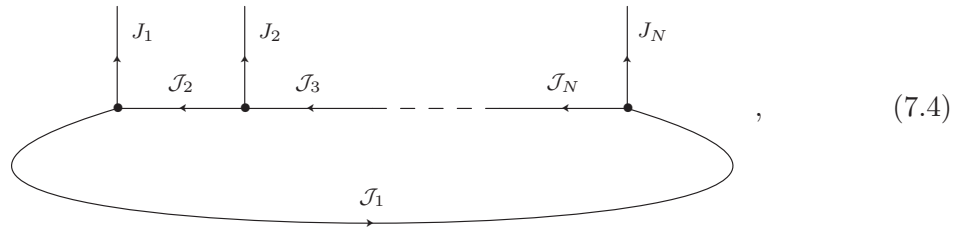
in which the N external lines are labeled by the fluxon types $J_1, J_2, \ldots$, and J_N of the N fluxons, and the N internal lines are labeled by N quantum double types $\mathcal{J} - 1, \mathcal{J}_2, \ldots$, and $\mathcal{J}_N$, satisfying the fusion rule at each vertex in the above diagram. The topological d.o.f. is encoded in the loop formed by internal lines $\mathcal{J}_1, \mathcal{J}_2, \ldots$, and $\mathcal{J}_N$. Formally, the basis is

$$\{|J_1, J_2, \ldots, J_N; \mathcal{J}_1, \mathcal{J}_2, \ldots, \mathcal{J}_N\rangle | \delta_{\mathcal{J}_1 \mathcal{J}_2^* J_1} = 1, \delta_{\mathcal{J}_2 \mathcal{J}_3^* J_2} = 1, \ldots, \delta_{\mathcal{J}_N \mathcal{J}_1^* J_N} = 1\}. \tag{7.5}$$

7.2   Hilbert space structure using finite groups

7.2.1   Full quantum numbers of fluxon excitations

In the Levin-Wen models constructed from finite group representations, the fluxon types are classified by the conjugacy classes, as we have seen in Section 6.3.1. In general, the full quantum numbers of fluxon excitations are classified by not only the conjugacy classes, but the quantum double types. An elementary excitation with more than two fluxons is described by the fluxon types ar all plaquettes, as well as the relative d.o.f. between these fluxons. Let us consider two situations with an abelian group and with a nonabelian group.

In a discrete pure gauge theory with an abelian group, the only observables are the magentic fluxes. In Levin-Wen models (from finite group representations), two fluxons couple to a new fluxon with the two fluxon types adding up to be the new fluxon type.

On the other hand, in a pure nonabelian gauge theory, the story is different. When two nonabelian fluxons are put together, an electric charge may be observed as the total quantum number. Let us consider two fluxons in a N-fluxon excitation, and move a third fluxon around these two fluxons by one turn, then the total electric charge will contribute a phase to the wavefunction (or, a unitary braiding matrix in general).

For example, in the Levin-Wen models on a sphere using $\mathbb{G} = D_3$, there are 6 elements, denoted by $\{1, 2, 3, 4, 5, 6\}$, and the fluxon types are classified by the three conjugacy classes as $C_1 = \{1\}, C_2 = \{2, 3\}$, and $C_3 = \{4, 5, 6\}$.

As analyzed in the previous section, the fluxon-pair state corresponding to the second conjugacy class can be presented by $|2 \otimes 2\rangle + |3 \otimes 3\rangle$, with the two group elements representing the holonomies on the left and right plaquettes. See Fig. 6.4. Any gauge transformation at the reference point will result in a conjugation of the left and right holonomies at the same time, leading to either one of the following transformations:

$$(1). \ |2 \otimes 2\rangle \mapsto |2 \otimes 2\rangle, |3 \otimes 3\rangle \mapsto |3 \otimes 3\rangle,$$
$$\text{or } (2). \ |2 \otimes 2\rangle \leftrightarrow |3 \otimes 3\rangle. \tag{7.6}$$

The fluxon-pair state is invariant under any such gauge transformation. This is what we expect, since the total charge of all fluxons (on the sphere) must be trivial under the gauge symmetry.

When there are more than two fluxons in the system, locally in the subsystem, the state may be presented by $|2 \otimes 2\rangle - |3 \otimes 3\rangle$, with the holonomies around the two fluxons in C_2. Now it transforms in the nontrivial Z_2 representation under the gauge transformations (7.6). Such an excitation has the total $\mathbb{Z}_2$ charge of the two fluxons.

In general, the full quantum numbers in many-fluxon states are classified by the quantum double types (at most), including pure fluxons, electric charges, and dyons (i.e., charge-flux composites). They are measured by the projection operators $P^{\mathcal{J}}$ defined in (6.23) and (6.26). In the following section we examine the full quantum numbers in the example using $\mathbb{G} = D_3$.

7.2.2 Example:$\mathbb{G} = D_3$

The input data $\{d, \delta, G\}$ defining the Levin-Wen model are constructed in Section 2.2.2. The fluxon types are classified by the conjugacy classes $\{1\}$, $\{2, 3\}$, and $\{4, 5, 6\}$.

For a nonabelian group, they are the particle species of dyons. They are determined as follows. Denote by A the conjugacy classes of $\mathbb{G}$, and pick up a representative element $^A h$ in each class. For each conjugacy class, there is a centralizer $Z_A = \{g^A h = {}^A h g | g \in \mathbb{G}\}$. We can list all irreducible representations μ of Z_A. Quantum double type $\mathcal{J}$ are given by the pairs (A, μ), corresponding to all irreducible representations μ of Z_A for all conjugacy classes A. The quantum double types for D_3 are presented in Appendix A.

We enumerate these quantum double types by $1, 2, \ldots, 8$, with the 1 the trivial topological charge for the vacuum, 4 and 7 the fluxons types. The the fusion rule for the quantum double types are given by

$$
\begin{array}{llllllll}
\delta_{111} = 1 & \delta_{122} = 1 & \delta_{133} = 1 & \delta_{144} = 1 & \delta_{155} = 1 & \delta_{166} = 1 & \delta_{177} = 1 & \delta_{188} = 1 \\
\delta_{233} = 1 & \delta_{244} = 1 & \delta_{255} = 1 & \delta_{266} = 1 & \delta_{278} = 1 & \delta_{333} = 1 & \delta_{345} = 1 & \delta_{346} = 1 \\
\delta_{356} = 1 & \delta_{377} = 1 & \delta_{378} = 1 & \delta_{388} = 1 & \delta_{444} = 1 & \delta_{456} = 1 & \delta_{477} = 1 & \delta_{478} = 1 \\
\delta_{488} = 1 & \delta_{555} = 1 & \delta_{577} = 1 & \delta_{578} = 1 & \delta_{588} = 1 & \delta_{666} = 1 & \delta_{677} = 1 & \delta_{678} = 1 \\
\delta_{688} = 1
\end{array}
\tag{7.7}
$$

In the model defined on a sphere, the lowest excitations are the fluxon-pair states: $|J_1 = 4, J_2 = 4\rangle$ and $|J_1 = 7, J_2 = 7\rangle$.

The three-fluxon states are $|J_1, J_2, J_3\rangle$ that satisfy $\delta_{J_1 J_2 J_3} = 1$. There are two kinds of such states: $|J_1 = 4, J_2 = 4, J_3 = 4\rangle$ and $|J_1 = 4, J_2 = 7, J_3 = 7\rangle$, up to the permutations on the free fluxons.

The four-fluxon states are $|J_1, J_2, J_3, J_4; \mathcal{J}\rangle$ with $\mathcal{J}$ the total charge of the first two fluxons, satisfying $\delta_{J_1 J_2 \mathcal{J}} = 1$ and $\delta_{J_3 J_4 \mathcal{J}} = 1$. The results are presented in Table 7.1. We see that although all fluxons carry no charge, the subsystem of two fluxons takes all possible charges.

7.3 Quantum group theory

Take the example of the Levin-Wen models constructed from the Fibonacci data described in Section 3.2.2.

Table 7.1. Basis of four-fluxon states for $\mathbb{G} = D_3$

states #	1	2	3	4	5	6	7	8	9	10	11	12	13	14	15	16
J_1	4	4	4	4	4	4	4	7	7	7	7	7	7	7	7	7
J_2	4	4	4	7	7	7	7	4	4	4	4	7	7	7	7	7
J_3	4	4	7	4	4	7	7	4	4	7	7	4	7	7	7	7
J_4	4	4	7	7	7	4	4	7	7	4	4	4	7	7	7	7
$\mathcal{J}$	2	4	4	7	8	7	8	7	8	7	8	4	3	4	5	6

The quantum double types are $\{0, 2, \bar{2}, 2\bar{2}\}$. 0 denotes the trivial charge meaning no quasiparticle. 2 denotes the chiral Fibonacci anyon, $\bar{2}$ the anti-chiral Fibonacci anyon, and $2\bar{2}$ the doubled Fibonacci anyon, the composite of 2 and $\bar{2}$. The only nontrivial fluxon type is $2\bar{2}$. This is a general feature in models constructed from nontrivial quantum groups (or, modular tensor category): all fluxons are doubled anyons.

The quantum double types are "direct product" of two copies of Fibonacci anyons with opposite chiralities, with the fusion rule: $\delta_{i\bar{j},k\bar{l},m\bar{n}} = \delta_{ikm}\delta_{jln}$. These quantum double types are also denoted by $\{\mathbf{1}, \tau, \bar{\tau}, \tau\bar{\tau}\}$ in the literature.

On a sphere, the lowest excitations are the fluxon-pair states $|J_1 = \tau\bar{\tau}, J_2 = \tau\bar{\tau}\rangle$, and the second lowest excitations are three fluxon states $|J_1 = \tau\bar{\tau}, J_2 = \tau\bar{\tau}, J_3 = \tau\bar{\tau}\rangle$. The four-fluxon states have the basis with the 4-fold degeneracy:

$$|J_1 = \tau\bar{\tau}, J_2 = \tau\bar{\tau}, J_3 = \tau\bar{\tau}, J_4 = \tau\bar{\tau}; \mathcal{J} = \mathbf{1}\rangle,$$
$$|J_1 = \tau\bar{\tau}, J_2 = \tau\bar{\tau}, J_3 = \tau\bar{\tau}, J_4 = \tau\bar{\tau}; \mathcal{J} = \tau\rangle,$$
$$|J_1 = \tau\bar{\tau}, J_2 = \tau\bar{\tau}, J_3 = \tau\bar{\tau}, J_4 = \tau\bar{\tau}; \mathcal{J} = \bar{\tau}\rangle,$$
$$|J_1 = \tau\bar{\tau}, J_2 = \tau\bar{\tau}, J_3 = \tau\bar{\tau}, J_4 = \tau\bar{\tau}; \mathcal{J} = \tau\bar{\tau}\rangle, \tag{7.8}$$

with $\mathcal{J}$ the total charge of the first two fluxons.

The basis of N-fluxon excitations on a sphere are labeled by $\mathcal{J}_1, \mathcal{J}_2, \ldots, \mathcal{J}_{N-3}$ on the internal links among the N fluxons, as in Eq (7.1).

7.4   Fractional exchange statistics of fluxons

The basis (7.1) allows us to calculate the fractional exchange statistics of fluxons. The transformation of degenerate N-fluxon states under the exchange of any two fluxons can be computed using the hopping operators we have developed in Chapter 6. They form a representation of the Braid group B_N, because of the path independence of the hopping operators.

For example, let us study in the model constructed from Fibonacci data. Consider the four-fluxon states on a sphere. If we exchange two fluxons in the counterclockwise direction by the hopping operators, we obtain the braiding matrices in the basis (7.8):

$$\sigma_1 = \sigma_3 = \begin{pmatrix} 1 & 0 & 0 & 0 \\ 0 & e^{\frac{3i\pi}{5}} & 0 & 0 \\ 0 & 0 & e^{-\frac{3i\pi}{5}} & 0 \\ 0 & 0 & 0 & 1 \end{pmatrix},$$

$$\sigma_2 = \begin{pmatrix} \varphi^2 & e^{-\frac{3i\pi}{5}}\varphi^{3/2} & e^{\frac{3i\pi}{5}}\varphi^{3/2} & \varphi \\ e^{-\frac{3i\pi}{5}}\varphi^{3/2} & e^{-\frac{i\pi}{5}}\varphi^2 & \varphi & e^{\frac{2i\pi}{5}}\varphi^{3/2} \\ e^{\frac{3i\pi}{5}}\varphi^{3/2} & \varphi & e^{\frac{i\pi}{5}}\varphi^2 & e^{-\frac{2i\pi}{5}}\varphi^{3/2} \\ \varphi & e^{\frac{2i\pi}{5}}\varphi^{3/2} & e^{-\frac{2i\pi}{5}}\varphi^{3/2} & \varphi^2 \end{pmatrix}, \tag{7.9}$$

where $\varphi = \frac{\sqrt{5}-1}{2}$. σ_1 exchanges the fluxon 1 and 2, σ_2 exchanges 2 and 3, and σ_3 exchanges 3 and 4. They generate the representation of the braid group B_4.

We emphasize that the braiding matrices are nontrivial only in the presense of at least three fluxons on a sphere, because of the global constraint that the total topological charge of all fluxons (on a sphere) is trivial. In Levin-Wen models, all fluxons have trivial topological spin, and thus the braiding matrices are nontrivial only for excitations with at least four fluxons. These braiding matrices are unique up to similar transformations, which are equivalently basis transformations of the four-fluxon states. On a torus, however, there could be nontrivial braiding matrices of two-fluxon states, because the topological charge of the fluxons are coupled to the topological d.o.f., as can be seen in the basis (7.4). The two-fluxon states on a torus has nine-fold degeneracy. The 9×9 braiding matrix has eigenvalues of

$$1, 1, 1, 1, 1, e^{\frac{3i\pi}{5}}, e^{\frac{3i\pi}{5}}, e^{\frac{-3i\pi}{5}}, e^{\frac{-3i\pi}{5}}. \tag{7.10}$$

The total charge of the two fluxons is τ in the $e^{\frac{3i\pi}{5}}$ eigenstates, and $\bar{\tau}$ in the $e^{\frac{-3i\pi}{5}}$ eigenstates.

7.5 The S and T matrices

Fluxon types $\{J\}$ are parts of topological charges $\{\mathcal{J}\}$ in the fluxon excitations. To fully understand the topological properties of fluxon excitations, we consider the fractional exchange statistics that topological charges $\mathcal{J}$ obey. We can prepare a four-fluxon excitation $|J_1 = \tau\bar{\tau}, J_2 = \tau\bar{\tau}, J_3 = \tau\bar{\tau}, J_4 = \tau\bar{\tau}; \mathcal{J}\rangle$ with the fluxons 1 and 2 together at two neighboring plaquettes, and fluxons 3 and 4 together. Then we can treat the composite of fluxon 1 and 2 as one quasiparticle of type $\mathcal{J}$, and the composite of fluxon 3 and 4 as another quasiparticle of type $\mathcal{J}^*$.

In the first composite quasiparticle $\mathcal{J}$, if we exchange fluxon 1 and 2, the topological charge $\mathcal{J}$ of the composite will not be changed. This enables us to detect the intrinsic topological property of $\mathcal{J}$. Exchanging fluxon 1 and 2 twice takes the state back to itself, up to certain $U(1)$ phase. Indeed, both initial and final states are uniquely labeled by the quantum numbers $J_1, J_2, \ldots; \mathcal{J}, \ldots$. See Fig. 7.2. We define this phase as the topological spin of $\mathcal{J}$. The topological spin computes to be the twist $\theta_{\mathcal{J}}$ of quantum double types $\mathcal{J}$, as defined in Appendix A.

In the model constructed from the Fibonacci data, we have $\theta_{\mathbf{1}} = 1, \theta_\tau = e^{3\pi i/5}, \theta_{\bar{\tau}} = e^{-3\pi i/5}, \theta_{\tau\bar{\tau}} = 1$.

We can also compute the S matrix. We start with a ground state (it does not matter which ground state we choose) and generate four fluxons with two composite quasiparticles $\mathcal{J}$ and $\mathcal{J}^*$ in the above way, and generate another four fluxons with two composte quasiparticles $\mathcal{K}$ and $\mathcal{K}^*$. We first exchange $\mathcal{J}$ and $\mathcal{K}$ twice, and then annihilate $\mathcal{J}$ with $\mathcal{J}^*$, and $\mathcal{K}$ with $\mathcal{K}^*$. In the process, the ground state acquires an amplitude, denoted by $S_{\mathcal{J}\mathcal{K}}$. See Fig. 7.3 for the entire process.

If we normalize it by $\frac{1}{D}$, we obtain

$$\tilde{S}_{\mathcal{J}\mathcal{K}} = \frac{1}{D} S_{\mathcal{J}\mathcal{K}} = \frac{1}{D} \sum_{ijk} d_k z^{\mathcal{J}}_{ijik} z^{\mathcal{K}}_{jijk}. \tag{7.11}$$

Compare with Eq 5.10, we conclude [64] the correspondence between the generate ground states on a torus and the quasiparticles in the excitations are as follows: (1) the GSD is euqal to the number of the particle species of quasiparticles; (2) the modular matrices S and T that characterize the ground states are identical to those that characterize the fractional statistics of quasiparticles.
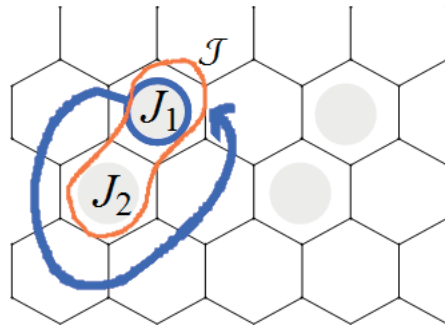
Figure 7.2. Exchanging fluxon J_1 and J_2 twice yields a $U(1)$ phase, interpreted as the topological spin. Practically, we move the fluxon J_1 around J_2 by one turn. Four fluxons are shown in the diagram, with the total charge the subsystem of fluxon J_1 and J_2 is $\mathcal{J}$.
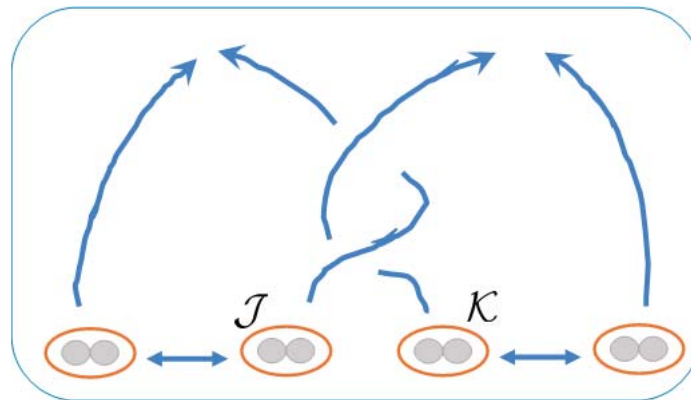
Figure 7.3. The amplitude $S_{\mathcal{J}\mathcal{K}}$ evaluated in a ground state. Initially we generate eight fluxons, partitioned into four composites of topological charges $\mathcal{J}^*$, $\mathcal{J}$, $\mathcal{K}$, and $\mathcal{K}^*$. $\mathcal{J}^*$ is paired to $\mathcal{J}$, and $\mathcal{K}$ is paired to $\mathcal{K}^*$. Then we exchange $\mathcal{J}$ and $\mathcal{K}$ twice. Finally, we annihilate $\mathcal{J}$ with $\mathcal{J}^*$, and $\mathcal{K}$ with $\mathcal{K}^*$. The entire amplitude is defined as $S_{\mathcal{J}\mathcal{K}}$.

CHAPTER 8

FRACTIONAL EXCLUSION STATISTICS

By now it is well-known that (quasi-)particles in strongly entangled many-body systems may exhibit exotic quantum statistics (see [66] for a review), other than the usual Bose-Einstein and Fermi-Dirac ones. In addition to the anyonic or braiding exchange statistics [27, 29] in two-dimensional systems, statistical weight of many-body quantum states may also obey new combinatoric counting rules [67, 66], in which the number of available single-particle states, when adding one more quasiparticle into the system, linearly depends on the number of existing quasiparticles. A typical new feature of the generalized Pauli exclusion principle is mutual exclusion between different species, resulting in a matrix of statistical parameters [67], as well as unusual thermodynamics for ideal gases with only statistical interactions [66].

More precisely, following [66], in the case with only one species of quasiparticles, the number of N-particle states is assumed to be given by the binomial coefficient:

$$W_{G,N} = \binom{G_{\text{eff}} + (N-1)}{N}, \tag{8.1}$$

with $G_{\text{eff}} = G - \alpha(N-1)$ being the number of available single-particle states, while G is the number of single-particle states when $N = 1$. Then $\alpha = 0$ corresponds to bosons and $\alpha = 1$ fermions; other values of α gives rise to exotic exclusion statistics. Similarly, in the multispecies case, the number of many-particle states is assumed to be given by $(a, b = 1, \ldots, m$ labeling species)

$$W_{\{G_a, N_a\}} = \prod_a \binom{G_a + N_a - 1 - \sum_{b=1}^{m} \alpha_{ab} (N_b - \delta_{ab})}{N_a}. \tag{8.2}$$

Here, coefficients α_{ab} form the (mutual) statistics matrix.

It has been shown [68] that the thermodynamic ansatz [69] for one-dimensional solvable many-particle models is actually a special case of the exotic exclusion statistics. (See also [70, 71].) It has been also numerically verified that quasiparticle excitations in the fractional quantum Hall (FQH) systems indeed obey [72] Eq (8.1), or Eq (8.2) allowing mutual

exclusion between different species [73]. Moreover, either the Haldane or Jain hierarchy in the FQH effect can be theoretically understood from the exclusion statistics of quasiparticles [66, 74].

Recently there has been revived interest in the study of quasiparticle statistics in two-dimensional topological states of matter (including FQH systems), because of the possibility of using their braiding to do (fault tolerant) topological quantum computation (TQC) [14, 17]. In order to better know the error of TQC at finite temperature, it is necessary to better understand how exclusion statistics of quasiparticles emerges in two-dimensional topological matter, which governs the thermodynamics of the system.

In this chapter, we carry out the many-body state counting in an exactly solvable discrete model, i.e., the Levin-Wen model [43] (with a special set of data), that describes a two-dimensional topological quantum fluid [75] of Fibonacci anyons [76], with doubled Fibonacci anyons as fluxon excitations living on plaquettes. The Fibonacci anyons are the simplest nonabelian anyons. They occur as quasiparticles in the $k = 3$ Read-Rezayi state [77] in a FQH state with filling fraction $\nu = \frac{12}{5}$, and can be used for universal topological quantum computation [17]. (Recently, it is proposed [78] that the physics of interacting Fibonacci anyons may be studied in a Rydberg lattice gas.)

In this chapter, we first construct the number operator for fluxons in the model, which helps us identify the states with localized excitations. Then we numerically count the (many-body) states with fluxon-number N fixed, from $N = 1$ up to $N = 7$, for the system on a sphere and torus, respectively. The results exhibit a pattern closely related to the Fibonacci numbers, which in turn is put in the form of Eq (8.2); thus determining a topology-dependent statistical parameter matrix. Our work [79] reveals that exotic exclusion emerges among quasiparticles due to interplay between various "hidden" degrees of freedom in addition to fluxon locations. Finally, we briefly discuss the thermodynamics of the system.

8.1   Exclusion statistics on a sphere

Take the example of the Levin-Wen models with the Fibonacci data, as described in Section 7.3.

Let us count the N-fluxon states in the model with P plaquettes on a sphere. Pick up a set of N fixed plaquettes and denote it by $\mathcal{C} = \{p_1, p_2, ..., p_N\}$ $(N < P)$. The states with exactly N fluxons occupying the selected plaquettes are those $|\psi\rangle$ satisfying

$$n_p^j|\Psi\rangle = \delta_{j1}|\Psi\rangle, \quad \text{for } p \in \mathcal{C},$$

$$n_{p'}^j|\Psi\rangle = \delta_{j0}|\Psi\rangle, \quad \text{for } p' \notin \mathcal{C}. \tag{8.3}$$

Thus $\left(\prod_{p\in\mathcal{C}} n_p^1 \prod_{p'\notin\mathcal{C}} n_{p'}^0\right)$ is the projector onto the subspace of such states. Tracing this projection computes the total number of the N-fluxon states in the configuration $\mathcal{C}$:

$$w_{P,N,\mathcal{C}} = \text{tr}(\prod_{p\in\mathcal{C}} n_p^1 \prod_{p'\notin\mathcal{C}} n_{p'}^0). \tag{8.4}$$

We numerically compute Eq (8.4) on random graphs on spheres with $P(\geq 7)$ plaquettes, with the stable result presented in Table 8.1.

The pattern of the N-dependence is obvious:

$$w_{P,N,\mathcal{C}} = F_{N-1}^2, \tag{8.5}$$

where F_n is the Fibonacci number that satisfies the recurrence relation: $F_n = F_{n-1} + F_{n-2}$ with $F_1 = F_2 = 1$. Both numerically and analytically we have checked that Eq (8.5) is independent of the graph, of the total number P of plaquettes, as well as the locations of the N fluxons. In fact, the N-fluxon space has a basis (7.1) obeying the fusion rule as analyzed in Section 7.3. The appearance of the squared in Eq (8.5) is consistent with the conjecture that the Levin-Wen model describes a *doubled* topological phases [50, 80].

Summing over configurations $\mathcal{C}$ (i.e., over possible distributions of N plaquettes in a fixed graph), we get the total number of N-fluxon states:

$$W_{P,N}^{\text{sphere}} = \sum_{\mathcal{C}} w_{P,N,\mathcal{C}} = \binom{P}{N} F_{N-1}^2. \tag{8.6}$$

The first factor counts the ways to distribute N fluxons over P plaquettes. The second factor counts the configurations of the link degrees of freedom, which are not unique, given N and $\mathcal{C}$. The independence of $w_{P,N,\mathcal{C}}$ on P and $\mathcal{C}$ implies the degeneracy of the excited states is topological in the sense that it does not depend on the detailed structure of the underlying graph, and not on the relative positions between the fluxons either. The origin of this property lies in the topological symmetry of the model under mutations of the underlying graph [80].

Table 8.1. State counting on sphere

Fluxon number N	0	1	2	3	4	5	6	7
State Counting $w_{P,N,\mathcal{C}}$	1	0	1	1	4	9	25	64

To find the exclusion statistics, we rewrite (8.6):

$$W_{P,N}^{\text{sphere}} = \binom{P}{N} \sum_{N_1,N_2=0}^{[\frac{1}{2}(N-2)]} \binom{N - N_1 - 2}{N_1}\binom{N - N_2 - 2}{N_2},\tag{8.7}$$

where $[x]$ is the greatest integer less than or equal to x.

Now Eq (8.2) is in the form of Eq (8.7), by introducing two additional pseudo-species $a = 1, 2$, which do not contribute to the total energy but are helpful for state-counting. This is similar to what was suggested for state counting in some conformal field theories [81]. Including the original fluxon species labeled by $a = 0$, from Eq (8.7) we read the exclusion statistics parameters α_{ab} $(a, b, = 0, 1, 2)$:

$$\alpha^{\text{sphere}} = \begin{pmatrix} 1 & 0 & 0 \\ -1 & 2 & 0 \\ -1 & 0 & 2 \end{pmatrix}.\tag{8.8}$$

The diagonal α_{aa} is the self-exclusion statistics for species a. The $\alpha_{00} = 1$ implies the hard-core boson behavior. This can be understood with Eq (6.5).

The pseudo-species provides a way to count configurations, in the presence of fluxons, of link degrees of freedom, which are not uniquely determined by the constraints (8.3). The value $\alpha_{11} = \alpha_{22} = 2$ implies that one pseudo-particle makes two single-particle states (or "seats") unavailable to an additional pseudo-particle. The negative mutual statistics $\alpha_{20} = \alpha_{30} = -1$ tells us that each fluxon present creates one vacant "seat" for each pseudo-species. So the maximum particle number of each pseudo-species is naturally $[(N - 1)/2]$. These results help us to understand the structure of the (many-body) Hilbert space for excited states of the system, and to derive analytically the state counting formula (8.7).

8.2 Exclusion statistics on a torus

We proceed and consider the model on a torus. The ground state degeneracy [80] is 4. Thus, the system exhibits the global topological degrees of freedom, and we can study their effects on excited states by counting the pseudo-particle states.

Pick up N plaquettes ($N < P$). The number of states with N fluxons on these plaquettes is computed numerically as in Table 8.2.

Table 8.2. State counting on torus

Fluxon number N	0	1	2	3	4	5	6
State Counting	2^2	1	3^2	4^2	7^2	11^2	18^2

The pattern of its dependence on N is

$$W_{P,N}^{\text{torus}} = \binom{P}{N} L_N^2, \tag{8.9}$$

with L_n the Lucas number, a modified version of the Fibonacci number, satisfying the recurrence relation $L_n = L_{n-1} + L_{n-2}$ with $L_1 = 1, L_2 = 3$.

We rewrite (8.9) in terms of binomial coefficients:

$$W_{P,N}^{\text{torus}} = \binom{P}{N} \sum_{N_1,N_2=0,1} \binom{1}{N_1}\binom{1}{N_2} \times$$
$$\sum_{N_3,N_4=0}^{[\frac{1}{2}(N-2)]} \binom{N-2N_1-N_3}{N_3}\binom{N-2N_2-N_4}{N_4}, \tag{8.10}$$

and get the exclusion statistics parameters α_{ab} $(a,b=0,1,2,3,4)$:

$$\alpha^{\text{torus}} = \begin{pmatrix} 1 & 0 & 0 & 0 & 0 \\ 0 & 1 & 0 & 0 & 0 \\ 0 & 0 & 1 & 0 & 0 \\ -1 & 2 & 0 & 2 & 0 \\ -1 & 0 & 2 & 0 & 2 \end{pmatrix}, \tag{8.11}$$

where we denote by $a = 0$ the fluxon species.

Eq. (8.10) shows that one needs to introduce four pseudo-species $a = 1,2,3,4$. The pseudo-species $a = 1,2$ are interpreted as the topological degrees of freedom on the torus, for the following reasons. The allowed "particle number" $N_1, N_2 = 0,1$ of these pseudo-species are independent of the number N of fluxons. Particularly when there is no fluxon present, the configurations $N_1, N_2 = 0,1$ characterize the four-degenerate ground states. Then the pseudo-species $a = 3,4$ provide a way to count the configurations of link degrees of freedom given a ground state and fluxon number.

The state counting of excitations on a torus is shown to be different from that on a sphere. Indeed, the mutual statistics parameters $\alpha_{31} = \alpha_{42} = 2$ imply that the number of configurations of link degrees of freedom $a = 3$ $(a = 4)$ are affected by the topological degrees of freedom $a = 1$ $(a = 2)$, respectively. On the other hand, the topological degrees of freedom are not affected by the fluxons present and the link degrees of freedom. So the degenerate ground states can be used to label the sectors of excitations. We note that in the sector with $N_1 = N_2 = 1$, the state counting for fluxons is exactly the same as that on sphere.

8.3 Statistical thermodynamics

Now we assume that only fluxons can be thermally excited. In the thermodynamic limit, the Hilbert space dimension of N-fluxon states (occupying N fixed plaquettes) is asymptotically

$$\text{on sphere:} \quad \lim_{N\to\infty} F_{N-1}^2 \sim \phi^{2N-2}/5,$$
$$\text{on torus:} \quad \lim_{N\to\infty} L_N^2 \sim \phi^{2N}. \tag{8.12}$$

(ϕ^2 is called the quantum dimension of the fluxon.) On a torus, for example, the canonical partition function is

$$Z^{\text{torus}} = \sum_{N=0}^{P} \binom{P}{N} L_N^2 e^{-N\epsilon/kT} \sim (\phi^2 e^{-\epsilon/kT} + 1)^P. \tag{8.13}$$

It can be interpreted as the grand canonical partition function of the many-fluxon system, which behaves like a fermionic system with a *temperature-independent fugacity* z given by the quantum dimension:

$$z = \phi^2. \tag{8.14}$$

The fugacity z counts the effective number of states per fluxon located at a plaquette. Note that z is irrational rather than integer. This is a manifestation that the many-fluxon states are highly entangled ones with long-range entanglement. They are superpositions of highly constrained j-configurations on the links, obviously not of the form of a direct product of localized fluxon states.

The statistical distribution of the average occupation number of fluxons is obtained from Eq (8.13):

$$\langle n \rangle = \langle N \rangle / P = \frac{1}{e^{\epsilon/kT}\phi^{-2} + 1}. \tag{8.15}$$

Many useful thermodynamic observables are then computable. Though the model is very simple, we believe that the features revealed in this paper should be quite general for emergent exotic exclusion statistics and thermodynamics for quasiparticle excitations in a wide class of two-dimensional topological phases.

CHAPTER 9

OTHER DISCRETE MODELS FOR
TOPOLOGICAL PHASES

9.1   Kitaev model

In this section, we introduce Kitaev's quantum double (QD) model [14] as a gauge field theory with finite gauge group $\mathbb{G}$ defined on graph in two spatial dimensions. The model is a Hamiltonian approach to the discrete topological gauge field theory. Two types of operators play the central role in the model: the gauge invariance constraint operator, and the gauge invariant operators.

The Hilbert space is spanned by the gauge fields $a_{\mathbf{e}}$ assigned to the graph links $\mathbf{e}$. The gauge transformations are defined at vertices, as discussed in Eqs. (2.96) and (2.97).

The Hamiltonian of Kitaev's QD model is

$$H = -\sum_{\mathbf{v}} A_{\mathbf{v}} - \sum_{\mathbf{p}} B_{\mathbf{p}}, \tag{9.1}$$

where the gauge invariant operator $A_{\mathbf{v}}$ at vertex $\mathbf{v}$ is defined by Eq (9.13), and $B_{\mathbf{p}}$ on plaquette $\mathbf{p}$ is defined by a Kronecker delta function:

$$B_{\mathbf{p}} \left| \begin{smallmatrix} a_3 \diagup\!\!\!\bigtriangleup\!\! a_2 \\ \diagup\overline{}\diagdown \\ a_1 \end{smallmatrix} \right\rangle = \delta_{a_1 a_2 a_3} \left| \begin{smallmatrix} a_3 \diagup\!\!\!\bigtriangleup\!\! a_2 \\ \diagup\overline{}\diagdown \\ a_1 \end{smallmatrix} \right\rangle. \tag{9.2}$$

Here, $a_1 a_2 a_3$ is the holonomy around the plaquette $\mathbf{p}$, and the delta function $\delta_a = 1$ if the group element a equals the identity element in $\mathbb{G}$ and 0 otherwise. Thus, $B_{\mathbf{p}}$ is a projector that measures whether the holonomy around the plaquette $\mathbf{p}$ is trivial or not. Though only triangle plaquettes and trivalent vertices are shown in Eqs. (2.96), (2.97), and (9.2), those operators are defined on all other types of vertices and plaquettes.

All $A_{\mathbf{v}}$ and $B_{\mathbf{p}}$ are mutually commuting projection operators, and hence, the model is exactly solvable.

The $A_{\mathbf{v}}$ prefers gauge symmetry at vertex $\mathbf{v}$. While the gauge symmetry broken states are interpreted as a "charged" particle. The energy cost of 1 to break the gauge symmetry

is interpreted as the on-site energy of the "charge" particle. These "charges" are classified by the irreducible representations of the gauge group $\mathbb{G}$.

Similarly, $B_\mathbf{p}$ prefers zero "magnetic" flux at plaquette $\mathbf{p}$. It costs a energy of 1 to obtain a nonzero "magnetic" flux, which is classified by the conjugacy classes of the gauge group.

In fact, the "charges" and the "magnetic" fluxes are classified by the orthonormal projection operators, respectively. Let us define

$$A_\mathbf{v}^j = \frac{\dim_j}{|\mathbb{G}|} \sum_{g_\mathbf{v} \in \mathbb{G}} \overline{\chi^j(g_\mathbf{v})} L(g_\mathbf{v}) \tag{9.3}$$

for an irreducible representation j of the group, and

$$n_\mathbf{p}^C : \left| \begin{smallmatrix} a_3 & \triangle & a_2 \\ & \triangle & \\ & a_1 & \end{smallmatrix} \right\rangle \mapsto \delta_{[a_1 a_2 a_3],C} \left| \begin{smallmatrix} a_3 & \triangle & a_2 \\ & \triangle & \\ & a_1 & \end{smallmatrix} \right\rangle, \tag{9.4}$$

for a conjugacy class C of the group. Here the delta function $\delta_{[a],C} = 1$ if the group element a belongs to C and 0 otherwise. These projection operators are orthonormal:

$$A_\mathbf{v}^j A_\mathbf{v}^{j'} = \delta_{j,j'} A_\mathbf{v}^j, \quad \sum_j A_\mathbf{v}^j = \mathbb{1}$$

$$n_\mathbf{p}^C n_\mathbf{p}^{C'} = \delta_{C,C'} n_\mathbf{p}^C, \quad \sum_C n_\mathbf{p}^C = \mathbb{1} \tag{9.5}$$

An eigenstate with $A_\mathbf{v}^j = 1$ is interpreted as the state with a "charge" j at vertex $\mathbf{v}$, and with $n_\mathbf{p}^C$ interpreted as a "magnetic" flux at $\mathbf{p}$.

As we have already seen in Section 2.3, Kitaev models are equivalent to Levin-Wen models with finite groups in the subspace of ground states and fluxon excitations, by a Fourier transformation [54]. Therefore, all results analyzed in this dissertation are valid in Kitaev model.

9.2 Dijkgraaf-Witten models

Kitaev models can be generalized.

In this section, we shall construct a twisted version [82] of Kitaev models in $(2+1)$–dimension, in which the topological charges are classified by the twisted quantum double, whereas the topological charges in the Kitaev model are classified by the usual quantum double. These models can be viewed as the Hamiltonian approach to Dijkgraaf-Witten gauge field theories [83]. They have exactly–soluble Hamiltonians on the Hilbert space spanned by planar graphs consisting of triangles whose edges are graced with group elements in a certain finite group.

9.2.1   Basic ingredients

The model is defined on a two–dimensional graph Γ consisting of triangles only (Fig. 9.1). Such a graph does not have any open edge and may be thought as a simplicial triangulation of certain two-dimensional Riemannian surface, e.g., a sphere; however, in this model, we shall take the graph as abstract without referring to its topological background except when we compare the model with other models, such as Dijkgraaf–Witten discrete topological gauge theories. Note that Fig. 9.1 is a crop of one such graph, so the open edges in the figure are not really open. We enumerate the vertices of Γ by any ordered set of labels. The enumerations of the vertices we choose are irrelevant as long as their relative order remains consistent during the calculation.

The model is characterized by a triple (H, G, α), which can be denoted by $H_{G,\alpha}$ for short. The first in the triple is the Hamiltonian H. The second ingredient G is a finite group. Each edge of Γ is graced with a group element of G. The Hilbert space is spanned by the configurations of group elements on the edges of Γ. Each edge (see Fig. 9.1) carries an arrow that goes from the vertex with a larger label to the one with a smaller label. To each edge e of the graph Γ, we assign a group element $g_e \in G$, and all possible assignments form the basis vectors of the Hilbert space.

$$\{g_1, g_2, ..., g_E\} \tag{9.6}$$

where E is the total number of edges in Γ.

It is convenient to denote both an edge and the group element on the edge by simply $[ab]$ with $a < b$ as the two boundary vertices of the edge. It is understood that $[ba] = [ab]^{-1}$. The inner product of the Hilbert space is the obvious one:

$$\left\langle \begin{array}{c} c' \\ \text{[b'c']} \bigtriangleup \text{[a'c']} \\ a' \quad b' \\ \text{[a'b']} \end{array} \middle| \begin{array}{c} c \\ \text{[bc]} \bigtriangleup \text{[ac]} \\ a \quad b \\ \text{[ab]} \end{array} \right\rangle = \delta_{[ab][a'b']}\delta_{[bc][b'c']}\delta_{[ac][a'c']} \cdots , \tag{9.7}$$

where only one triangle in Γ is drawn, and the "..." omits the δ–functions on all other triangles that are not shown. Note that three group elements on the three sides of a triangle, e.g., the $[ab], [bc]$ and $[ac]$ on the RHS of Eq. (9.7), are independent of each other in general, i.e., $[ab] \cdot [bc] \neq [ac]$. From now on, we shall neglect the group elements on the edges but keep only the vertex labels when we draw a basis vector.

The third element is a *normalized 3–cocycle* $\alpha \in H^3(G, U(1))$, i.e., a function $\alpha : G^3 \rightarrow U(1)$ that satisfies the *3-cocycle condition*
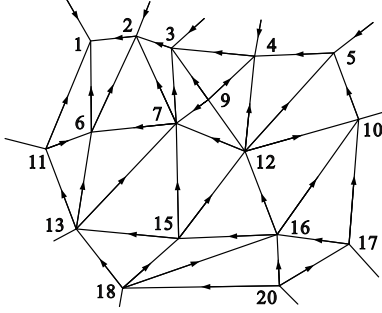
Figure 9.1. A portion of a graph that represent the basis vectors in the Hilbert space. Each edge carries an arrow and is assigned a group element denoted by $[ab]$ with $a < b$.

$$\alpha(g_1, g_2, g_3)\alpha(g_0 \cdot g_1, g_2, g_3)^{-1} \times$$

$$\alpha(g_0, g_1 \cdot g_2, g_3)\alpha(g_0, g_1, g_2 \cdot g_3)^{-1}\alpha(g_0, g_1, g_2) = 1 \tag{9.8}$$

for all $g_i \in G$, and satisfies the *normalization condition*

$$\alpha(1, g, h) = \alpha(g, 1, h) = \alpha(g, h, 1) = 1, \tag{9.9}$$

whenever $g, h \in G$ are arbitrary. We emphasize that this normalization condition is not an *ad hoc* condition we imposed as an extra on the 3–cocycles; rather, it is a natural condition that any group 3–cocycle can satisfy for the following reason. A 3–cocycle α is in fact an equivalence class of the 3–cocycles that can be scaled into each other by merely a 3–coboundary $\delta\beta$, where β is a 2–cochain. It can be shown that for any equivalence class of 3–cocycles, there always exists a representative that meets the normalization condition in Eq. (9.9), which is in turn justified.

Note that every group has a trivial 3-cocycle $\alpha_0 \equiv 1$ on the entire G. One can define a 3–cocycle on any subgraph composed of three triangles, which share a vertex and any two of which share an edge. Consider Fig. 9.2(a) as an example: The four vertices are in the order $v_1 < v_2 < v_3 < v_4$. We define the 3–cocycle for this subgraph by taking its three variables from left to right to be the three group elements, $[v_1v_2]$, $[v_2v_3]$ and $[v_3v_4]$, which are along
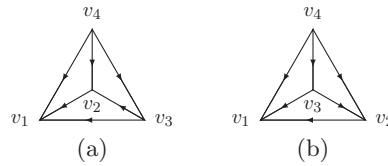
Figure 9.2. (a) The defining graph of the 3–cocycle $\alpha([v_1v_2], [v_2v_3], [v_3v_4])$. (b) For $\alpha([v_1v_2], [v_2v_3], [v_3v_4])^{-1}$.

the path from the least vertex v_1 to the greatest vertex v_4 passing v_2 and v_3 in order; hence, the 3–cocycle reads $\alpha([v_1v_2], [v_2v_3], [v_3v_4])$. If one lifts the vertex v_2 in Fig. 9.2(a) above the paper plane, the three triangles turn out to be on the surface of a tetrahedron. In this sense, one can think of the 3–cocycle as associated with a tetrahedron as well, which is useful when the graph is really interpreted as the triangulation of a Riemannian surface.

On the other hand, if one switches the vertices v_2 and v_3 in Fig. 9.2(a), one obtains Fig. 9.2(b), which defines the inverse 3–cocycle $\alpha([v_1v_2], [v_2v_3], [v_3v_4])^{-1}$. Whether a graph defines a 3–cocycle α or the inverse α^{-1} depends on the orientation of the four vertices in the graph by the following rule. One first reads off a list of the three vertices counter–clockwise from any of the three triangles of the defining graph of the 3–cocycle, e.g., (v_2, v_3, v_4) from Fig. 9.2(a) and (v_3, v_2, v_4) from Fig. 9.2(b). One then appends the remaining vertex to the beginning of the list, e.g., (v_1, v_2, v_3, v_4) from Fig. 9.2(a) and (v_1, v_3, v_2, v_4) from Fig. 9.2(b). If the list can be turned into ascending order by even permutations, such as (v_1, v_2, v_3, v_4) from Fig. 9.2(a), one has an α but an α^{-1} otherwise, as by (v_1, v_3, v_2, v_4) from Fig. 9.2(b).

We would like to warn the reader of some abuse of language in the rest of the chapter. For example, when we say "a 3–cocycle," we may refer to a class $[\alpha]$, a representative α, or the evaluation of α on a tetrahedron. For another example, although there is abstractly only one 3–cocycle condition as in Eq. (9.8), we may sometimes mean 3–cocycle conditions by the evaluation of the condition on different tetrahedra. Regardless, such usage should not cause any confusion contextually.

9.2.2 The Hamiltonian

The 3–cocycles will appear in the matrix elements of the model's Hamilton defined as follows.

$$H = -\sum_v A_v - \sum_f B_f, \tag{9.10}$$

where B_f is the face operator defined at each triangular face f, and A_v is the vertex operator defined on each vertex v. We now elaborate more on these operators.

The action of B_f on a basis vector is

$$B_f \left| \begin{array}{c} v_3 \\ \triangle \\ v_1 \quad v_2 \end{array} \right\rangle = \delta_{[v_1v_2]\cdot[v_2v_3]\cdot[v_3v_1]} \left| \begin{array}{c} v_3 \\ \triangle \\ v_1 \quad v_2 \end{array} \right\rangle. \tag{9.11}$$

The discrete delta function $\delta_{[v_1v_2]\cdot[v_2v_3]\cdot[v_3v_1]}$ is unity if $[v_1v_2] \cdot [v_2v_3] \cdot [v_3v_1] = 1$, where 1 is the identity element in G, and 0 otherwise. Note again that here, the ordering of v_1, v_2, and v_3 does not matter because of the identities $\delta_{[v_1v_2]\cdot[v_2v_3]\cdot[v_3v_1]} = \delta_{[v_3v_1]\cdot[v_1v_2]\cdot[v_2v_3]}$ and

$\delta_{[v_1v_2]\cdot[v_2v_3]\cdot[v_3v_1]} = \delta_{\{[v_1v_2]\cdot[v_2v_3]\cdot[v_3v_1]\}^{-1}} = \delta_{[v_3v_1]^{-1}\cdot[v_2v_3]^{-1}\cdot[v_1v_2]^{-1}} = \delta_{[v_1v_3]\cdot[v_3v_2]\cdot[v_2v_1]}$. In other words, in any state on which $B_f = 1$ on a triangular face f, the three group degrees of freedom around v are related by a *chain rule*:

$$[v_1v_3] = [v_1v_2] \cdot [v_2v_3] \tag{9.12}$$

for any enumeration v_1, v_2, v_3 of the three vertices of the face f.

The operator A_v is a summation

$$A_v = \frac{1}{|G|} \sum_{[vv']=g\in G} A_v^g, \tag{9.13}$$

which deserves explanation. The value $|G|$ is the order of the group G. The operator A_v^g acts on a vertex v with a group element $g \in G$ by replacing v by a new enumeration v' that is less than v but greater than all the enumerations that are less than v in the original set of enumerations before the action of the operator, such that $[v'v] = g$. A_v^g does not affect any vertex other than v but introduces a $U(1)$ phase, composed of 3–cocycles determined by v' and all the vertices adjacent to v before the action, to the resulted state. In a dynamical language, v' is understood as on the next "time" slice, and there is an edge $[v'v] \in G$ in the $(2+1)$ dimensional "spacetime" picture. Consider a trivalent vertex as an example (see Eq. (9.14)). Without loss of generality, we assume that the enumerations of the four vertices are in the order $v_1 < v_2 < v_3 < v_4$. The basis vector on the LHS of (9.14) is specified by six group elements, $[v_1v_3]$, $[v_2v_3]$, $[v_3v_4]$, $[v_1v_4]$, $[v_2v_1]$, and $[v_2v_4]$. The action of $A_{v_3}^g$ on this state reads

$$A_{v_3}^g \left| \begin{array}{c} \vphantom{v} \end{array} \right\rangle$$

$$= \delta_{[v_3'v_3],g} \alpha\left([v_1v_2], [v_2v_3'], [v_3'v_3]\right) \alpha\left([v_2v_3'], [v_3'v_3], [v_3v_4]\right)$$

$$\times \alpha\left([v_1v_3'], [v_3'v_3], [v_3v_4]\right)^{-1} \left| \begin{array}{c} \vphantom{v} \end{array} \right\rangle, \tag{9.14}$$

where on the RHS, the new enumerations are in the order $v_1 < v_2 < v_3' < v_3 < v_4$, and the following *chain rule* of group elements on the edges holds.

$$[v_1v_3'] = [v_1v_3] \cdot [v_3v_3'],$$
$$[v_2v_3'] = [v_2v_3] \cdot [v_3v_3'], \tag{9.15}$$
$$[v_3'v_4] = [v_3'v_3] \cdot [v_3v_4].$$

The phase factor consisting of three 3–cocycles on the RHS of Eq. (9.14) encodes the nonvanishing matrix elements of $B_{v_3}^{v_3'}$, namely

$$
\begin{aligned}
\left(A_{v_3}^g\right)&{}_{[v_1 v_3'][v_2 v_3'][v_3' v_4]}^{[v_1 v_3][v_2 v_3][v_3 v_4]} \left([v_1 v_2], [v_2 v_3], [v_1 v_3]\right) \\
&= \alpha\left([v_1 v_2], [v_2 v_3'], [v_3' v_3]\right) \alpha\left([v_2 v_3'], [v_3' v_3], [v_3 v_4]\right) \\
&\quad \times \alpha\left([v_1 v_3'], [v_3' v_3], [v_3 v_4]\right)^{-1}.
\end{aligned} \tag{9.16}
$$

For each vertex on the LHS of Eq. (9.14), we group its three neighboring enumerations together with the new enumeration v_3' in the ascending order. Hence, we have (v_1, v_2, v_3', v_3) for the lower vertex, (v_1, v_3', v_3, v_4) for the upper left vertex, and (v_2, v_3', v_3, v_4) for the upper right one, and then assign three 3-cocycles respectively to the three vertices: $\alpha\left([v_1 v_2], [v_2 v_3'], [v_3' v_3]\right)$, $\alpha\left([v_2 v_3'], [v_3' v_3], [v_3 v_4]\right)$, and $\alpha\left([v_1 v_3'], [v_3' v_3], [v_3 v_4]\right)^{-1}$. The chirality of a 3–cocyle, or in other words, whether a vertex contributes a 3–cocycle α or the inverse α^{-1}, is based on the following criteria. We write down a triple for the three neighboring enumerations around each vertex in the counterclockwise direction and append v_3' to the front, namely, (v_3', v_1, v_2, v_3) for the lower vertex, (v_3', v_1, v_3, v_4) for the upper left one, and (v_3', v_2, v_4, v_3) for the upper right one. If it takes an (odd) even number of steps to permute a list to the ascending order, the vertex contributes (the inverse of) the corresponding 3-cocycle in the action.

The matrix elements in Eq. (9.16) can be better motivated and understood in the following way. One may think that the graph evolves in "time" under the driver of the Hamiltonian. Focusing on the vertex operator only and considering the $A_{v_3}^g$ in Eq. (9.14), the action of the operator creates a new "time" slice by replacing the original vertex v_3 by v_3' and connects the two vertices in the "time" direction. This scenario is shown in Fig. 9.3, which is made three–dimensional $(2+1)$ to illustrate the "spacetime" picture and relate our model to Dijkgraaf–Witten discrete topological gauge theory.

As in Fig. 9.3, we can view the original three triangles on the LHS of Eq. (9.14) as a tetrahedron $v_1 v_2 v_3 v_4$ and the three new triangles as another tetrahedron $v_1 v_2 v_3' v_4$, of which the vertex v_3' lies inside $v_1 v_2 v_3 v_4$ because of the ordering $v_3' < v_3$. Since v_3' and v_3 are connected, there are three more tetrahedra effectively generated by the action of the vertex operator, namely $v_1 v_2 v_3' v_3$, $v_2 v_3' v_3 v_4$, and $v_1 v_3' v_3 v_4$. It looks like that the original tetrahedron is split into four tetrahedra. This splitting of tetrahedron implies the three chain rules in Eq. (9.15), which then enables us to endow the three tetrahedra $v_1 v_2 v_3' v_3$, $v_2 v_3' v_3 v_4$, and $v_1 v_3' v_3 v_4$, respectively, with the three 3–cocycles $\alpha\left([v_1 v_2], [v_2 v_3'], [v_3' v_3]\right)$, $\alpha\left([v_2 v_3'], [v_3' v_3], [v_3 v_4]\right)$, and $\alpha\left([v_1 v_3'], [v_3' v_3], [v_3 v_4]\right)^{-1}$, following the rule shown in Fig. 9.2.
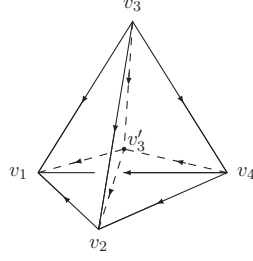
Figure 9.3. The topology of the action of $A_{v_3}^g$.

The operator $A_{v_3}^g$ in Eq. (9.14) is just an identity operator if $[v_3'v_3] = 1$, i.e., the identity in G. In fact, according to Eq. (9.14), we have the following matrix element

$$\alpha\left([v_1v_2], [v_2v_3'], 1\right) \alpha\left([v_2v_3'], 1, [v_3v_4]\right) \times \alpha\left([v_1v_3'], 1, [v_3v_4]\right)^{-1}, \tag{9.17}$$

which is unity, by the *normalization condition* (9.9).

The vertex operator in Eq. (9.14) can naturally extend its definition from a trivalent vertex to a vertex of any valence higher than three. The number of 3–cocyles in the phase factor brought by the action of A_v^g on a vertex is equal to the valence of the vertex. The chirality of each 3–cocycle in the phase factor follows the criteria described in the previous paragraph. It is clear that $A_v^{g=1} \equiv \mathbb{I}$ by the discussion above.

It can be shown that all B_f and A_v are projection operators and commute with each other (see Appendix A). As a result, the ground states and all elementary excitations are thus simultaneous eigenvectors of all these local operators. Moreover, the elementary excitations are identified as local quasiparticles that are classified by the the representations of the local operators.

9.2.3   Equivalent models

Now that a 3–cocycle defines a twisted quantum double model, one may wonder that since a 3–cocycle represents a whole equivalence class, whether two equivalent 3–cocycles, i.e., two representatives of the same equivalent class, define the same model. Let us consider two Hamiltonians $H_{G,\alpha}$ and $H_{G,\alpha'}$, respectively, defined by two equivalent 3–cocycles α and α' that are related by the 3–coboundary $\delta\beta$ of a normalized 2–cochain $\beta : G^2 \mapsto U(1)$ that satisfy $\beta(x,e) = 1 = \beta(e,x)$ for all $x \in G$,

$$\begin{aligned} \alpha'(g_0, g_1, g_2) &= \delta\beta(g_0, g_1, g_2)\alpha(g_0, g_1, g_2) \\ &= \frac{\beta(g_1, g_2)\beta(g_0, g_1g_2)}{\beta(g_0g_1, g_2)\beta(g_0, g_1)}\alpha(g_0, g_1, g_2), \end{aligned} \tag{9.18}$$

where $g_i \in G$, and δ is the coboundary operator. As each 3–cocycle is defined on three triangles (or equally a tetrahedron) such as in Fig 9.2, each 2–cochain β can be thought as

defined on a triangle. Hence, Eq. (9.18) can be viewed as a local "gauge" transformation on α.

We now check the relation between $H_{G,\alpha'}$ and $H_{G,\alpha}$. It suffices to check only the vertex operators $A_v^g(\alpha')$ and $A_v^g(\alpha)$ because the face operators B_f have merely δ–functions as matrix elements and are thus inert under the transformation in Eq. (9.18). Without loss of generality, we consider again the vertex operator on a trivalent vertex, as that in Eq. (9.14). By Eq. (9.18), We immediately obtain the following.

$$
A_3^g(\alpha')\left|\,\raisebox{-1em}{\begin{tikzpicture}\end{tikzpicture}}\,\right\rangle
$$

$$
=\frac{\alpha'([12],[23'],[3'3])\alpha'([23'],[3'3],[34])}{\alpha'([13'],[3'3],[34])}\left|\,\raisebox{-1em}{}\,\right\rangle
$$

$$
=\frac{\beta([12],[23])\beta([13],[34])}{\beta([23],[34])}\times\frac{\alpha([12],[23'],[3'3])\alpha([23'],[3'3],[34])}{\alpha([13'],[3'3],[34])}
$$

$$
\times\frac{\beta([23'],[3'4])}{\beta([12],[23'])\beta([13'],[3'4])}\left|\,\raisebox{-1em}{}\,\right\rangle, \tag{9.19}
$$

where the δ–function $\delta_{[3'3],g}$ is omitted for simplicity. The second term consisting of three α's is precisely the matrix element of $A_3^g(\alpha)$. If we move the first fraction of β in the second equality of the above equation to the LHS, we readily see that the action of $A_3^g(\alpha')$ on the rescaled state

$$
\frac{\beta([23],[34])}{\beta([12],[23])\beta([13],[34])}\left|\,\raisebox{-1em}{}\,\right\rangle
$$

matches perfectly the action of $A_3^g(\alpha)$ on the original state. The above rescaling is clearly a local $U(1)$ phase, which can be boiled down to the following local $U(1)$ transformation on the basis of the states of triangles:

$$
\left|\,\raisebox{-1em}{}\,\right\rangle\mapsto\beta([ab],[bc])^{\varepsilon(a,b,c)}\left|\,\raisebox{-1em}{}\,\right\rangle, \tag{9.20}
$$

where $\varepsilon(a,b,c)$ is a sign, which equals $+1$ if the enumerations $a<b<c$ are clockwise on the triangle and -1 otherwise. In this new basis, $A_v^g(\alpha')$ has the same matrix elements and thus the same spectrum as those of $A_v^g(\alpha)$ in the old basis.

There is a continuous deformation between any two 3–cocycles related by $\alpha'=\alpha\delta\beta$. Define a 2–cochain $\beta^{(t)}(x,y)=\beta(x,y)^t$, with $0\le t\le 1$, then $\alpha^{(t)}=\alpha\delta\beta^{(t)}$ is equivalent to

α for all $0 \leq t \leq 1$, with $\alpha^{(0)} = \alpha$ and $\alpha^{(1)} = \alpha'$. The corresponding transformation in Eq. (9.20) with β replaced by $\beta^{(t)}$ is a continuous local $U(1)$ transformation; hence, there is no phase transition in the one–parameter family of systems with the the Hamiltonian $H_{G,\alpha^{(t)}}$ from $0 \leq t \leq 1$. Thus, we can conclude that the two Hamiltonians $H_{G,\alpha'}$ and $H_{G,\alpha}$ arising from two equivalent 3–cocycles α' and α indeed describe the same topological phase.

CHAPTER 10

SUMMARY AND OUTLOOK

In this dissertation, we have discussed the exactly solvable discrete models for two-dimensional topological phases, and studied the robust, emergent properties in these models. We have developed a systematic approach for the concrete construction of Levin-Wen models based on $3j$-symbols, exploring the representation theory of finite groups and quantum groups. The construction reveals an unknown relationship between the Levin-Wen models and the discrete topological gauge field theories. We have also provided algorithms and examples to generate the desired set of data, allowing the numerical computations for various cases.

To study the topological observables (quantum numbers) of the ground states and excitations in the Levin-Wen models, we have developed an operator approach. In this approach we have been able to study systematically how exotic robust properties of topological phases emerge in the exactly solvable models. More concretely, what we have achieved are the following:

1. We have constructed and calculated two topological observables in the ground states: the GSD and the modular matrices S and T. We have calculated the topological GSD on a torus, and have proved that the ground state is nondegenerate on a sphere.

2. We found that the ground states are classified by the quantum double structure. The topological charges of ground states are determined by the quantum double types.

3. We have developed the operator approach to study the elementary fluxon excitations. We have seen how to generate a excitation from a ground state, and how to measure and manipulate the fluxons by operators. The topological charges in the excitations have been classified by the quantum double structure.

4. We have calculated the fractional exclusion statistics of the quasiparticles. This reveals the Hilbert space structure of fluxon excitations. We have seen that the excitations

are highly entangled because of the nonlocal feature of the internal quantum numbers which characterize the relative d.o.f. between fluxons.

5. We have calculated the fractional exchange statistics of quasiparticles, and have derived the modular matrices S and T from them.

6. We have shown the interesting correspondence between the quantum numbers of the degenerate ground states and those of the quasiparticle excitations: (1) the GSD is euqal to the particle species of quasiparticles; (2) the modular matrices S and T that characterize the ground states are identical to those that characterize the fractional statistics of quasiparticles. The ground states and the quasiparticles carry the same topological charges as classified by the quantum double structure.

Some of the above results have been reported [80, 82, 79]. The others will be published soon [51, 65, 64]. For simplicity, we have restricted ourselves mainly to the multiplicity-free cases of the fusion algebra for string types. (Namely the tensor $\delta_{j_1 j_2 j_3}$ takes only a value of 0 or 1.) We expect it will be straightforward to generalize our approach and results to the nonmultiplicity-free cases.

We have not discussed the holographic edge-bulk duality in this dissertation. Boundaries for the Kitaev models and Levin-Wen models have been somewhat studied in the literature [84, 85]. In some cases, the boundary states are gapless [86]. The general theory of the boundary states is still lacking, which is certainly worthwhile to pursue in the the framework presented here.

We emphasize that Chern-Simons field theories in continuum spacetime describing the chiral (time-reversal breaking) topological phases have no lattice counterpart. How to separate the two chiral and antichiral sectors in the discrete Levin-Wen model, which is known to be nonchiral, is still a challenge.

Finally, the models we have discussed may be related to (the effective theory of) symmetry enriched topological phases. Just like the Dijkraff-Witten models, which are known to be related to symmetry protected topological phases by a nonlocal transformation, we expect a similar relation could be uncovered between the (generalized) Levin-Wen models that have some internal gauge group structure and the symmetry enriched topological phases.

APPENDIX A

QUANTUM DOUBLE

Given the data $\{\mathrm{d}, \delta, G\}$, we define the half braiding tensor z by:

$$\sum_{lrs} \mathrm{d}_r \mathrm{d}_s z_{lnqr} z_{pmls} G_{nr^*t}^{m^*sl^*} G_{jn^*t}^{s^*pm} G_{q^*n^*k}^{m^*tr^*} = \delta_{jk}\delta_{mnj^*} \frac{1}{\mathrm{d}_j} z_{pjqt}, \tag{A.1}$$

for all p, q, j, k, t, m, n. $z_{pjqt}^{\mathcal{J}}$ is nonzero only if $\delta_{pjt^*} = 1 = \delta_{jqt^*}$. This defining equation is called the *naturality condition* of the half braiding tensor.

Let us enumerate all nonzero solutions $z_{pjqt}^{\mathcal{J}}$ by a label $\mathcal{J}$. If the solution $\mathcal{J}$ can not be decomposed into two nontrivial solutions by $z^{\mathcal{J}} = z^{\mathcal{J}_1} + z^{\mathcal{J}_2}$, we say the solution $\mathcal{J}$ is elementary. The algebraic theory of all elementary solutions is called the quantum double, with each elementary solution $\mathcal{J}$ called a quantum double type.

The quantum double is a mathematical structure in tensor categories that appears in mathematical literature [87]. The tensor z_{pjqt}^{J} appears in [43] as the Ω tensor, for the study of the fractional statistics in excitations of Levin-Wen models.

$z_{pjqt}^{\mathcal{J}}$ satisfies the orthonormal relation

$$\sum_l z_{ljqt}^{\mathcal{J}} \overline{z_{ljpt}^{\mathcal{J}}} = \delta_{pq} N_p^{\mathcal{J}} \delta_{jpt^*},$$

$$\sum_l z_{qjlt}^{\mathcal{J}} \overline{z_{pjlt}^{\mathcal{J}}} = \delta_{pq} N_p^{\mathcal{J}} \delta_{pjt^*}, \tag{A.2}$$

where $N_p^{\mathcal{J}}$ is an integer either 0 or 1.

$z_{pjqt}^{\mathcal{J}}$ satisfies the symmetry conditions

$$z_{pjqt}^{\mathcal{J}} = \sum_r \mathrm{d}_r G_{jq^*t}^{j^*pr^*} \overline{z_{qj^*pr}^{\mathcal{J}}} \tag{A.3}$$

$$\overline{z_{qj^*pr}^{\mathcal{J}}} = \sum_t \mathrm{d}_t G_{jt^*q}^{jrp^*} z_{pjqt}^{\mathcal{J}}, \tag{A.4}$$

where the second condition is a consequence of the first one together wit the orthogonality relation (1.4).

For each elementary solution $z^{\mathcal{J}}_{pjqt}$ to Eq. (A.1), $z^{\mathcal{J}}_{q^*j^*p^*t^*}$ is also an elementary solution. We call the corresponding quantum double type the dual of $\mathcal{J}$ and denote it by $\mathcal{J}^*$:

$$z^{\mathcal{J}^*}_{pjqt} = z^{\mathcal{J}}_{q^*j^*p^*t^*}, \tag{A.5}$$

by which we see $\mathcal{J}^{**} = \mathcal{J}$.

For each $\mathcal{J}$, we define the twist by

$$\theta_{\mathcal{J}} = \frac{1}{\mathrm{d}_q N^{\mathcal{J}}_q} \sum_t z^{\mathcal{J}}_{qqqt} \mathrm{d}_t \delta_{qqt^*}, \tag{A.6}$$

for any q with $N^{\mathcal{J}}_q = 1$. The RHS in Eq. (A.6) is independent of q, as long as $N^{\mathcal{J}}_q = 1$. $\theta_{\mathcal{J}}$ is a $U(1)$ number.

A useful property derived from the symmetry conditions (1.4) is

$$\overline{z^{\mathcal{J}}_{jijk}} = \theta_{\mathcal{J}} z^{\mathcal{J}}_{jk^*ji^*}. \tag{A.7}$$

The modular S matrix is

$$\tilde{S}_{\mathcal{J}\mathcal{K}} = \frac{1}{D} \sum_{ijk} \mathrm{d}_k z^{\mathcal{J}}_{ijik} z^{\mathcal{K}}_{jijk}, \tag{A.8}$$

with $1/D$ being the normalization factor. It satisfies:

$$\begin{aligned}
\tilde{S}_{\mathcal{J}\mathcal{K}} &= \tilde{S}_{\mathcal{K}\mathcal{J}} \\
\sum_{\mathcal{K}} \tilde{S}_{\mathcal{J}\mathcal{K}} \tilde{S}_{\mathcal{K}\mathcal{L}} &= \delta_{\mathcal{J},\mathcal{L}^*}.
\end{aligned} \tag{A.9}$$

We remark that the modular S matrix and the twist $\theta_{\mathcal{J}}$ are uniquely determined by the rank-3 tensor $z^{\mathcal{J}}_{pjpt}$, though the half braiding tensor $z^{\mathcal{J}}_{pjqt}$ may have nonzero components when $p \neq q$.

A.1 Example: quantum double of finite groups $\mathbb{Z}_N$ and D_3

The quantum double of finite groups $\mathbb{G}$ characterizes the particle species of charge-flux composites, where the fluxes are presented by the conjugacy classes of $\mathbb{G}$, while the charges are presented by the irreducible representations of (subgroups) of $\mathbb{G}$. For more details about the quantum double in algebra level, see [87, 88]. In this appendix, the z characterize the quantum double of $\mathbb{G}$ from the perspective of representation theory.

Given the $6j$-symbols constructed from finite group representations, the independent solutions to Eq. (A.1) are denoted by pairs (A, μ). A is a conjugacy class of $\mathbb{G}$, and μ is

an irreducible representation of the centralizer $Z_A = \{g \in \mathbb{G} | g h_A = h_A g\}$ where h_A is a arbitrary representative element in A but fixed once for all.

For abelian groups $\mathbb{G}$, each group element is itself a conjugacy class, so the quantum double charges are pairs (g, μ) of group elements and irreducible representations of $\mathbb{G}$. For example, let $\mathbb{G} = \mathbb{Z}_N$, the quantum double charges are (g, μ) for $g, \mu = 0, 1, \ldots, N-1$ and the z tensors are

$$z_{pjqt}^{(g,\mu)} = \delta_{p,\mu} \delta_{q,\mu} \exp(2\pi i g / N) \delta_{pjt^*} \delta_{jqt^*}, \tag{A.10}$$

where $\delta_{pjt^*} = 1$ if $p + j - t = 0$ mod N and 0 otherwise.

The quantum double types may be realized as charge-flux composites because there may exist a braiding operator that winds a particle carrying quantum number (g, j) around another particle carrying quantum number (h, k) such that the wavefuction of the system acquires a phase $\exp(ijh/N) \exp(ikg/N)$. This braiding operator is important to understand the quantum double types, we will not dwell on them here.

Take another example of $\mathbb{G} = D_3$. From Table 2.1, D_3 has three conjugacy classes $C_1 = \{1\}$, $C_2 = \{2, 3\}$, and $C_3 = \{4, 5, 6\}$. We pick up the representative elements $1, 2$, and 4 in these classes, and have the centralizers $Z_1 = 1, 2, 3, 4, 5, 6$, $Z_2 = 1, 2, 3$, and $Z_3 = 1, 4$. We see that $Z_1 = D_3$, $Z_2 \cong \mathbb{Z}_3$, and $Z_3 \cong \mathbb{Z}_2$ have one-dimensional irreducible representations as presented in Table A.1.

Let us relabel the irreducible representations ρ_0, ρ_1, and ρ_2 by $[+]$, $[-]$, and $[2]$, and the eight quantum double types are presented in Table A.2.

The z tensors for the eight quantum double types are

Table A.1. Irreducible representations of Z_2 and Z_3 in $\mathbb{G} = D_3$, here $\omega = \exp 2\pi i / 3$.

Z_2	1	2	3	Z_3	1	4
$[+]$	1	1	1	$[+]$	1	1
$[\omega]$	1	ω	$\overline{\omega}$	$[-]$	1	-1
$[\overline{\omega}]$	1	$\overline{\omega}$	ω			

Table A.2. Eight quantum double types (A, μ) for $\mathbb{G} = D_3$

flux A	charges μ		
$C_1 = \{1\}$	$[+]$	$[-]$	$[2]$
$C_2 = \{2, 3\}$	$[+]$	$[\omega]$	$[\overline{\omega}]$
$C_3 = \{4, 5, 6\}$	$[+]$	$[-]$	

$$z_{pjqt}^{(C_1,[+])} = \delta_{p,0}\delta_{q,0}\delta_{j,t}$$

$$z_{pjqt}^{(C_1,[-])} = \delta_{p,1}\delta_{q,1} \begin{pmatrix} 0 & 1 & 0 \\ 1 & 0 & 0 \\ 0 & 0 & -1 \end{pmatrix}_{jt}$$

$$z_{pjqt}^{(C_1,[2])} = \delta_{p,2}\delta_{q,2} \begin{pmatrix} 0 & 0 & 1 \\ 0 & 0 & -1 \\ 1 & -1 & 1 \end{pmatrix}_{jt}$$

$$z_{pjqt}^{(C_2,[+])} = \delta_{p,0}\delta_{q,0} \begin{pmatrix} 1 & 0 & 0 \\ 0 & 1 & 0 \\ 0 & 0 & -\frac{1}{2} \end{pmatrix}_{jt} + \delta_{p,1}\delta_{q,1} \begin{pmatrix} 0 & 1 & 0 \\ 1 & 0 & 0 \\ 0 & 0 & \frac{1}{2} \end{pmatrix}_{jt} -$$

$$\frac{\sqrt{3}}{2}i\delta_{p,0}\delta_{q,1}\delta_{j,3}\delta_{t,3} + \frac{\sqrt{3}}{2}i\delta_{p,1}\delta_{q,0}\delta_{j,3}\delta_{t,3}$$

$$z_{pjqt}^{(C_2,[\omega])} = \delta_{p,2}\delta_{q,2} \begin{pmatrix} 0 & 0 & 1 \\ 0 & 0 & -1 \\ e^{-\frac{2i\pi}{3}} & e^{\frac{i\pi}{3}} & e^{\frac{2i\pi}{3}} \end{pmatrix}_{jt}$$

$$z_{pjqt}^{(C_2,[\overline{\omega}])} = \delta_{p,2}\delta_{q,2} \begin{pmatrix} 0 & 0 & 1 \\ 0 & 0 & -1 \\ e^{\frac{2i\pi}{3}} & e^{-\frac{i\pi}{3}} & e^{-\frac{2i\pi}{3}} \end{pmatrix}_{jt}$$

$$z_{pjqt}^{(C_3,[+])} = \delta_{p,0}\delta_{q,0} \begin{pmatrix} 1 & 0 & 0 \\ 0 & -1 & 0 \\ 0 & 0 & 0 \end{pmatrix}_{jt} + \delta_{p,2}\delta_{q,2} \begin{pmatrix} 0 & 0 & 1 \\ 0 & 0 & 1 \\ 1 & 1 & 0 \end{pmatrix}_{jt} +$$

$$\delta_{p,0}\delta_{q,2}\delta_{j,3}\delta_{t,3} + \delta_{p,2}\delta_{q,0}\delta_{j,3}\delta_{t,3}$$

$$z_{pjqt}^{(C_3,[-])} = \delta_{p,1}\delta_{q,1} \begin{pmatrix} 0 & 1 & 0 \\ -1 & 0 & 0 \\ 0 & 0 & 0 \end{pmatrix}_{jt} + \delta_{p,2}\delta_{q,2} \begin{pmatrix} 0 & 0 & 1 \\ 0 & 0 & 1 \\ -1 & -1 & 0 \end{pmatrix}_{jt} +$$

$$i\delta_{p,1}\delta_{q,2}\delta_{j,3}\delta_{t,3} + i\delta_{p,2}\delta_{q,1}\delta_{j,3}\delta_{t,3} \tag{A.11}$$

APPENDIX B

REPRESENTATIONS OF THE FUSION ALGEBRA

The matrix X_j^J is obtained from the irreducible representations of the fluxon algebra (1.7). Let us denote by $\{\rho, V\}$ a matrix representation, where $\rho(B_p^s)$ is the representation matrix, and V the representation space. The irreducible representations have the following properties.

They satisfy *Schur's lemma.* (a). Given an irreducible representation $\{\rho, V\}$, if a matrix $T : V \to V$ commutes with $\rho(B_p^i)$ for all i, then $T = \alpha\mathbb{1}$ for some complex number α, where $\mathbb{1}$ is the identity matrix. (b). Given two inequivalent irreducible representations $\{\rho, V\}$ and $\{\rho', V'\}$, if a matrix $T : V \to V'$ commutes with B_p^i by $\rho'(B_p^i)T = T\rho(B_p^i)$ for all i, then $T = 0$.

Proof: Here, we prove part (a) only. Any eigenspace of T with eigenvalue α

$$U_\alpha = \{v \in V | Tv = \alpha v\} \tag{B.1}$$

is a subrepresentation. Indeed, for any $v \in U_\alpha$,

$$T\rho(B_p^i)v = \rho(B_p^i)Tv = \alpha\rho(B_p^i)v \tag{B.2}$$

implies $\rho(B_p^i)v \in U_\alpha$ for all i. Since V is irreducible, U_α must be either $\{0\}$ or V. Therefore, T has at most one eigenvalue, i.e., $T = \alpha\mathbb{1}$ for some complex number α.

If $\delta_{ijk} = \delta_{jik}$, then all irreducible representations are one-dimensional.

Proof: $\delta_{ijk} = \delta_{jik}$ implies that the fusion algebra is abelian:

$$B_p^i B_p^j = \sum_k \delta_{ijk^*} B_p^k = \sum_k \delta_{jik^*} B_p^k = B_p^j B_p^i, \tag{B.3}$$

and thus each $\rho(B_p^i)$ commutes with $\rho(B_p^j)$ for all j:

$$\rho(B_p^i)\rho(B_p^j) = \rho(B_p^j)\rho(B_p^i). \tag{B.4}$$

Applying Schur's lemma yields $\rho(B_p^i) = \alpha_i \mathbb{1}$ for some complex number α_i, where $\mathbb{1}$ is the identity matrix. Therefore, V can be decomposed into a direct sum of one-dimensional subrepresentations. Since $\{\rho, V\}$ is irreducible, it must be one-dimensional.

They satisfy *Peter-Weyl Theorem*. Let $\{\rho^J, V^J\}$ be all (inequivalent) irreducible representations that satisfy $\rho_{\alpha\beta}^J(B_p^{i^*}) = \overline{\rho_{\alpha\beta}^J(B_p^i)}$ (which follows from $B_p^{s^*} = B_p^{s\dagger}$). The matrix elements $\rho_{\alpha\beta}^J(B_p^i)$ form a orthonormal basis of functions over B_p^s.

Proof: First we check the orthogonal condition. If (ρ^J, V_J) and (ρ^K, V_K) are two irreducible representations, and $T: V_K \to V_J$ is a linear operator. Let us average T by

$$\tilde{T} = \sum_i \rho^J(B_p^i) T \rho^K(B_p^{i^*}), \tag{B.5}$$

such that it commutes with B_p^j for all j:

$$\begin{aligned}
\tilde{T}\rho^K(B_p^j) &= \sum_i \rho^J(B_p^i) T \rho^K(B_p^{i^*}) \rho^K(B_p^j) \\
&= \sum_i \rho^J(B_p^i) T \rho^K(B_p^{i^*} B_p^j) \\
&= \sum_{ik} \rho^J(B_p^i) T \rho^K(\delta_{i^* j k^*} B_p^k) \\
&= \sum_k \rho^J\left(\sum_i \delta_{jk^* i^*} B_p^i\right) T \rho^K(B_p^k) \\
&= \sum_k \rho^J(B_p^j B_p^{k^*}) T \rho^K(B_p^k) \\
&= \rho^J(B_p^j)\tilde{T}, \tag{B.6}
\end{aligned}$$

where in the fourth equality the cyclic condition $\delta_{i^* j k^*} = \delta_{jk^* i^*}$ was used.

By Schur's lemma,

$$\begin{aligned}
\tilde{T} &= 0 && \text{if } J \neq K \\
\tilde{T} &= c_{JK}\mathbf{1} && \text{if } J = K \tag{B.7}
\end{aligned}$$

for some complex number c_{JK}. Particularly, we set

$$T = |\mathbf{e}_\alpha^K\rangle\langle\mathbf{e}_\beta^J|, \tag{B.8}$$

in the basis $|e_\alpha^K\rangle$ of V_K and $|e_\beta^J\rangle$ of V_J, and Eq. (B.7) becomes

$$\begin{aligned}
\langle\mathbf{e}_\gamma^J|\tilde{T}|\mathbf{e}_\sigma^K\rangle &= \sum_i \langle\mathbf{e}_\gamma^J|\rho^J(B_p^i)|\mathbf{e}_\alpha^K\rangle\langle\mathbf{e}_\beta^J|\rho^K(B_p^{i^*})|\mathbf{e}_\sigma^K\rangle \\
&= \sum_i \rho_{\gamma\alpha}^J(B_p^i)\rho_{\beta\sigma}^K(B_p^{i^*}) \\
&= c_{JK}\delta_{JK}\delta_{\gamma\sigma}. \tag{B.9}
\end{aligned}$$

By relabeling i as j^*, we also have

$$\sum_{j^*} \rho_{\gamma\alpha}^J(B_p^{j^*}) \rho_{\beta\sigma}^K(B_p^j) = c_{JK}\delta_{JK}\delta_{\alpha\beta}. \tag{B.10}$$

Combining Eq. (B.9) and (B.10) together with the condition $(B_p^i)^\dagger = B_p^{i^*}$, we have

$$\sum_i \rho_{\gamma\alpha}^J(B_p^i)\overline{\rho_{\sigma\beta}^K(B_p^i)} = c_J\delta_{JK}\delta_{\gamma\sigma}\delta_{\alpha\beta}. \tag{B.11}$$

where c_J is a positive number determined by

$$c_J = \frac{1}{\dim(V^J)^2} \sum_i \sum_{\gamma,\alpha=1}^{\dim(V^J)} \left|\rho_{\gamma\alpha}^J(B_p^i)\right|^2. \tag{B.12}$$

Therefore we arrive at the orthonormal condition

$$\sum_i \frac{1}{\sqrt{c_J}} \rho_{\alpha\beta}^J(B_p^i) \overline{\frac{1}{\sqrt{c_K}}\rho_{\gamma\sigma}^K(B_p^i)} = \delta_{JK}\delta_{\alpha\gamma}\delta_{\beta\sigma}. \tag{B.13}$$

Now let us check the completeness condition. First, any representation (ρ, V) can be made unitary. Indeed, any (positive-definite, hermitian) inner product $\langle \cdot, \cdot \rangle$ of V determines new one

$$\langle\!\langle v, w \rangle\!\rangle := \sum_i \left\langle \rho(B_p^i)v, \rho(B_p^i)w \right\rangle, \tag{B.14}$$

such that the representation ρ is unitary:

$$\begin{aligned}
\langle\!\langle \rho(B_p^j)v, w \rangle\!\rangle &= \sum_i \left\langle \rho(B_p^i)\rho(B_p^j)v, \rho(B_p^i)w \right\rangle \\
&= \sum_{k,i} \delta_{ijk^*} \left\langle \rho(B_p^k)v, \rho(B_p^i)w \right\rangle \\
&= \sum_k \left\langle \rho(B_p^k)v, \rho(\sum_i \delta_{kj^*i^*}B_p^i)w \right\rangle \\
&= \sum_k \left\langle \rho(B_p^k)v, \rho(B_p^k)\rho(B_p^{j^*})w \right\rangle \\
&= \left\langle\!\left\langle v, \rho(B_p^{j^*})w \right\rangle\!\right\rangle
\end{aligned} \tag{B.15}$$

Second, (ρ, V) can be decomposed into a direct sum of irreducible representations. Suppose V is reducible. Any subrepresentation W of V has an orthogonal complement $W^\perp$ (all vectors in $W^\perp$ are perpendicular to the ones in W) as another subrepresentation. Suppose $w \in W^\perp$, we have $\langle\!\langle v, w \rangle\!\rangle = 0$ for all $v \in W$. Then $\rho(B_p^i)w \in W^\perp$ because

$$\langle\!\langle v, \rho(B_p^i)w \rangle\!\rangle = \left\langle\!\left\langle \rho(B_p^{i^*})v, w \right\rangle\!\right\rangle = 0. \tag{B.16}$$

Hence, we decompose V into two subrepresentations W and $W^\perp$. (ρ, V) can be further decomposed until all subrepresentations are irreducible.

Third, δ_{ijk} gives a N-dimensional adjoint representation by

$$\rho_{jk}(B_p^i) = \langle B_p^j | B_p^i | B_p^k \rangle = \delta_{j^*ik}, \tag{B.17}$$

where $B_p^i | B_p^k \rangle = \sum_l \delta_{ikl^*} | B_p^l \rangle$ and $\left\langle B_p^j \middle| B_p^k \right\rangle = \delta_{j,k}$. By "adjoint" we mean each B_p^s forms a basis vector in this representation. Particularly, ρ_{j0} forms a basis of functions over $\{B_p^i\}$, because ρ_{j0} maps B_p^i to 1 if $i = j$ and 0 if $i \neq j$. Since the natural representation can be decomposed into a direct sum of irreducible representations, ρ_{j0} can be expressed as linear combination of $\rho_{\alpha\beta}^J$. This proves the completeness

$$\sum_J \sum_{\alpha,\beta=1}^{\dim(V^J)} \frac{1}{c_J} \rho_{\alpha\beta}^J(B_p^i)\overline{\rho_{\alpha\beta}^J(B_p^j)} = \delta_{i,j}. \tag{B.18}$$

Define

$$\left[X_j^J\right]_{\alpha\beta} := \frac{1}{\sqrt{c_J}}\rho_{\alpha\beta}^J(B_p^j). \tag{B.19}$$

Then irreducible representations $\{\rho^J, V_J\}$ determine the set of orthonormal projections

$$n^J := \sum_j \overline{\sum_{\alpha\beta} \left[X_j^J\right]_{\alpha\beta}} \left[X_0^J\right]_{\beta\alpha} B_p^j \tag{B.20}$$

Proof: It follows from Eq. (B.13) and (B.18).

Particularly, when $\delta_{ijk} = \delta_{jik}$, then $X_j^J := \frac{1}{\sqrt{c_J}}\rho^J(B_p^j)$ is the unique solution to Eqs. (6.1), (6.2), and (6.3).

APPENDIX C

LEVIN-WEN MODELS WITH GENERIC DATA

We made the multiplicity-free assumption that δ_{ijk} can be either 0 or 1 throughout the dissertation. For example, in the tensor product $i \otimes j \otimes k$ of any three irreducible representations of $SU(2)$, the trivial representation appears, at most, once. There can be more general situations where more than one copy of 0 appears in $i \otimes j \otimes k$, e.g., of $SU(3)$ representations. In general, we do not have the multiplicity-free assumption.

For completeness, we briefly present the definition of Levin-Wen models in this generic situation.

In general, an extra degree of freedom is put on each vertex. The input data to define the Levin-Wen model satisfy the following generalized conditions.

First, we fix a set of labels $I = 0, 1, ..., N-1$. There is star map $* : I \rightarrow I$ such that $j^{**} = j$. The fusion rule coefficient N_{ijk} are nonnegative integers, satisfying $N_{ijk} = N_{jki} = N_{k^*j^*i^*}$, and $N_{i^*i0} = 1$ for all i, j, k. Quantum dimensions d_j are required to satisfy $\sum_k d_k N_{ijk^*} = d_i d_j$.

Denote by $max(N)$ the maximum number of N_{ijk}, and set δ_{ijk}^α to be 1 if $\alpha \leq N_{ijk}$ and 0 otherwise, where $\alpha = 1, 2, ..., max(N)$.

The $6j$ symbols $G_{kln\mu\nu}^{ijm;\alpha\beta}$ carries 4 extra degrees of freedom, with the self-consistent conditions:

$$G_{kln;\mu\nu}^{ijm;\alpha\beta} = G_{nk^*l^*;\beta\mu}^{mij;\alpha\nu} = G_{ijn^*;\nu\mu}^{klm^*;\beta\alpha} = \alpha_m \alpha_n \overline{G_{l^*k^*n;\nu\mu}^{j^*i^*m^*;\alpha\beta}}$$

$$\sum_{n,\epsilon\xi\delta} d_n G_{kp^*n;\epsilon\xi}^{mlq;\alpha\beta} G_{mns^*;\sigma\eta}^{jip;\gamma\epsilon} G_{lkr^*;\nu\sigma}^{js^*n;\delta\xi} = \sum_\lambda G_{q^*kr^*;\nu\lambda}^{jip;\gamma\beta} G_{mls^*;\sigma\eta}^{riq^*;\lambda\alpha}$$

$$\sum_{n,\mu\nu} d_n G_{kp^*n;\mu\nu}^{mlq;\alpha\beta} G_{pk^*n;\nu\mu}^{l^*m^*i^*\eta\gamma} = \frac{\delta_{iq}}{d_i} \delta_{\alpha\eta} \delta_{\beta\gamma} \delta_{mlq}^\alpha \delta_{k^*ip}^\beta, \tag{C.1}$$

where $\alpha_m = \text{sgn}(d_m)$ and $\alpha_n = \text{sgn}(d_n)$ and should not be mixed with multiplicity label α in δ_{ijk}^α.

The general Levin-Wen model carries an extra degree of freedom $\alpha = 1, 2, ..., max(N)$ at each vertex. In the Hamiltonian, the operators $\hat{Q}_v$ and $\hat{B}_p^s$ also carry these extra d.o.f.,

$$\hat{Q}_v \left| \begin{array}{c} j_3 \\ j_1 \overbrace{}_{\alpha} j_2 \end{array} \right\rangle = \delta^{\alpha}_{j_1 j_2 j_3} \left| \begin{array}{c} j_3 \\ j_1 \overbrace{}_{\alpha} j_2 \end{array} \right\rangle \tag{C.2}$$

and

$$\left\langle \begin{array}{c} j_7 \ _{\alpha'} \ _{\eta'} \ j_{12} \\ j_8 \ j_1 \ j_6 \ j_5 \ _{\epsilon'} \\ _{\beta} \ j_2 \ j_4 \ j_{11} \\ j_9 \ _{\gamma} \ _{\delta} \ j_{10} \end{array} \right| \hat{B}_p^s \left| \begin{array}{c} j_7 \ _{\alpha} \ _{\eta} \ j_{12} \\ j_8 \ j_1 \ j_6 \ j_5 \ _{\epsilon} \\ _{\beta} \ j_2 \ j_4 \ j_{11} \\ j_9 \ _{\gamma} \ _{\delta} \ j_{10} \end{array} \right\rangle$$

$$= v_{j_1} v_{j_2} v_{j_3} v_{j_4} v_{j_5} v_{j_6} v_{j_1'} v_{j_2'} v_{j_3'} v_{j_4'} v_{j_5'} v_{j_6'} \sum_{\lambda_1 \lambda_2 \lambda_3 \lambda_4 \lambda_5 \lambda_6} G^{j_7 j_1^* j_6; \alpha \lambda_6}_{s^* j_6' j_1'^*; \alpha' \lambda_1} \times$$

$$G^{j_8 j_2^* j_1; \beta \lambda_1}_{s^* j_1' j_2'^*; \beta' \lambda_2} G^{j_9 j_3^* j_2; \gamma \lambda_2}_{s^* j_2' j_3'^*; \gamma' \lambda_3} G^{j_{10} j_4^* j_3; \delta \lambda_3}_{s^* j_3' j_4'^*; \delta' \lambda_4} G^{j_{11} j_5^* j_4; \epsilon \lambda_4}_{s^* j_4' j_5'^*; \epsilon' \lambda_5} G^{j_{12} j_6^* j_5; \eta \lambda_5}_{s^* j_5' j_6'^*; \eta' \lambda_6} \tag{C.3}$$

In general Levin-Wen model in (C.2) and (C.3), these three properties still hold, given the generalized transformations

$$\hat{T}_1 : \left| \begin{array}{c} j_1 \quad j_4 \\ _{\alpha} \overbrace{j_5}_{} _{\beta} \\ j_2 \quad j_3 \end{array} \right\rangle \rightarrow \sum_{j_5'} v_{j_5} v_{j_5'} G^{j_1 j_2 j_5; \alpha\beta}_{j_3 j_4 j_5'; \mu\nu} \left| \begin{array}{c} j_1 \ _{\mu} \ j_4 \\ j_5' \\ j_2 \ _{\nu} \ j_3 \end{array} \right\rangle$$

$$\hat{T}_2 : \left| \begin{array}{c} j_1 \ _{\mu} \ j_3 \\ j_2 \end{array} \right\rangle \rightarrow \sum_{j_4 j_5 j_6, \alpha\beta\gamma} \frac{v_{j_4} v_{j_5} v_{j_6}}{\sqrt{D}} G^{j_2 j_3 j_1; \mu\alpha}_{j_6^* j_4 j_5^*; \gamma\beta} \left| \begin{array}{c} j_1 \ _{\alpha} \ _{\beta} \ j_3 \\ j_4 \ _{j_6} \ j_5 \\ j_2 \ _{\gamma} \end{array} \right\rangle$$

$$\hat{T}_3 : \left| \begin{array}{c} j_1 \ _{\alpha} \ _{\beta} \ j_3 \\ j_4 \ _{j_6} \ j_5 \\ j_2 \ _{\gamma} \end{array} \right\rangle \rightarrow \frac{v_{j_4} v_{j_5} v_{j_6}}{\sqrt{D}} \sum_{\mu} G^{j_3^* j_2^* j_1^*; \mu\alpha}_{j_4^* j_6 j_5^*; \beta\gamma} \left| \begin{array}{c} j_1 \ _{\mu} \ j_3 \\ j_2 \end{array} \right\rangle \tag{C.4}$$

the GSD on a torus is

$$\mathrm{GSD}^{\mathrm{torus}} = D^{-1} \sum_{s j_1 j_2 j_3 j_1' j_2' j_3'} d_s d_{j_1} d_{j_2} d_{j_3} d_{j_1'} d_{j_2'} d_{j_3'} \sum_{\alpha\beta\gamma\delta\epsilon\zeta\alpha'\beta'\gamma'\delta'\epsilon'\zeta'}$$

$$\left(G^{j_1 j_2 j_3^*; \alpha\beta}_{s j_3'^* j_2'; \gamma\delta} G^{j_3'^* j_1 j_2'; \gamma\delta'}_{s j_2 j_1'; \epsilon\zeta} G^{j_2 j_3'^* j_1'; \epsilon\zeta'}_{s j_1 j_3^*; \alpha\beta'} \right) \left(G^{j_2^* j_3 j_1^*; \alpha'\zeta}_{s j_1'^* j_3'; \epsilon'\beta} G^{j_3' j_1^* j_2^*; \epsilon'\delta}_{s j_2'^* j_1^*; \gamma'\zeta'} G^{j_1^* j_2'^* j_3'; \gamma'\beta'}_{s j_3 j_2^*; \alpha'\delta'} \right) \tag{C.5}$$

REFERENCES

[1] K. Klitzing, G. Dorda, and M. Pepper. New Method for High-Accuracy Determination of the Fine-Structure Constant Based on Quantized Hall Resistance. *Physical Review Letters*, 45(6):494–497, August 1980.

[2] D. C. Tsui, H. L. Stormer, and A. C. Gossard. Two-Dimensional Magnetotransport in the Extreme Quantum Limit. *Physical Review Letters*, 48(22):1559–1562, May 1982.

[3] R. B. Laughlin. Anomalous Quantum Hall Effect: An Incompressible Quantum Fluid with Fractionally Charged Excitations. *Physical Review Letters*, 50(18):1395–1398, May 1983.

[4] V. Kalmeyer and R. Laughlin. Equivalence of the Resonating-Valence-Bond and Fractional Quantum Hall States. *Physical Review Letters*, 59(18):2095–2098, November 1987.

[5] X. Wen, Frank Wilczek, and A. Zee. Chiral Spin States and Superconductivity. *Physical Review B*, 39(16):11413–11423, June 1989.

[6] X. Wen. Mean-Field Theory of Spin-Liquid States with Finite Energy Gap and Topological Orders. *Physical Review B*, 44(6):2664–2672, August 1991.

[7] N. Read and Subir Sachdev. Large-N Expansion for Frustrated Quantum Antiferromagnets. *Physical Review Letters*, 66(13):1773–1776, April 1991.

[8] R. Moessner and S. L. Sondhi. Resonating Valence Bond Phase in the Triangular Lattice Quantum Dimer Model. *Physical Review Letters*, 86(9):1881–1884, February 2001.

[9] B. Andrei Bernevig and Shou-Cheng Zhang. Quantum Spin Hall Effect. *Physical Review Letters*, 96(10), March 2006.

[10] Markus König, Steffen Wiedmann, Christoph Brüne, Andreas Roth, Hartmut Buhmann, Laurens W Molenkamp, Xiao-Liang Qi, and Shou-Cheng Zhang. Quantum Spin Hall Insulator State in HgTe Quantum WWells. *Science (New York, N.Y.)*, 318(5851):766–70, November 2007.

[11] Liang Fu, C. Kane, and E. Mele. Topological Insulators in Three Dimensions. *Physical Review Letters*, 98(10), March 2007.

[12] Shuichi Murakami. Phase Transition Between the Quantum Spin Hall and Insulator Phases in 3D: Emergence of a Topological Gapless Phase. *New Journal of Physics*, 9(9):356–356, September 2007.

[13] D Hsieh, D Qian, L Wray, Y Xia, Y S Hor, R J Cava, and M Z Hasan. A Topological Dirac Insulator in a Quantum Spin Hall Phase. *Nature*, 452(7190):970–4, April 2008.

[14] A.Yu. Kitaev. Fault-Tolerant Quantum Computation by Anyons. *Annals of Physics*, 303(1):2–30, January 2003.

[15] Michael H. Freedman, Alexei Kitaev, Michael J. Larsen, and Zhenghan Wang. Topological Quantum Computation. *Bulletin of the American Mathematical Society*, 40(01):31–39, October 2002.

[16] Chetan Nayak, Ady Stern, Michael Freedman, and Sankar Das Sarma. Non-Abelian Anyons and Topological Quantum Computation. *Reviews of Modern Physics*, 80(3):1083–1159, September 2008.

[17] Zhenghan Wang. *Topological Quantum Computation*. American Mathematical Society, 1st edition, 2010.

[18] L. D. Landau. Theory of Phase Transformations. I. *Phys. Z. Sowjetunion*, 11:26, 1937.

[19] Y.-S. Wu. Personal communication.

[20] R. Tao and Yong-Shi Wu. Gauge Invariance and Fractional Quantum Hall Effect. *Physical Review B*, 30(2):1097–1098, July 1984.

[21] Qian Niu, D. Thouless, and Yong-Shi Wu. Quantized Hall Conductance as a tTpological Invariant. *Physical Review B*, 31(6):3372–3377, March 1985.

[22] X. Wen and Q. Niu. Ground-State Degeneracy Of The Fractional Quantum Hall States In The Presence Of A Random Potential And On High-Genus Riemann Surfaces. *Physical Review B*, 41(13):9377–9396, May 1990.

[23] F. Haldane and E. Rezayi. Finite-Size Studies of the Incompressible State of the Fractionally Quantized Hall Effect and its Excitations. *Physical Review Letters*, 54(3):237–240, January 1985.

[24] Yong-Shi Wu, Yasuhiro Hatsugai, and Mahito Kohmoto. Gauge Invariance of Fractionally Charged Quasiparticles and Hidden Topological Z_{n} Symmetry. *Physical Review Letters*, 66(5):659–662, February 1991.

[25] Yasuhiro Hatsugai, Mahito Kohmoto, and Yong-Shi Wu. Anyons on a Torus: Braid Group, Aharonov-Bohm Period, and Numerical Study. *Physical Review B*, 43(13):10761–10768, May 1991.

[26] Masatoshi Sato, Mahito Kohmoto, and Yong-Shi Wu. Braid Group, Gauge Invariance, and Topological Order. *Physical Review Letters*, 97(1):010601, July 2006.

[27] Frank Wilczek. Magnetic Flux, Angular Momentum, and Statistics. *Physical Review Letters*, 48(17):1144–1146, April 1982.

[28] Daniel Arovas, J. Schrieffer, and Frank Wilczek. Fractional Statistics and the Quantum Hall Effect. *Physical Review Letters*, 53(7):722–723, August 1984.

[29] Yong-Shi Wu. General Theory for Quantum Statistics in Two Dimensions. *Physical Review Letters*, 52(24):2103–2106, June 1984.

[30] Frank Wilczek, editor. *Fractional Statistics and Anyon Superconductivity*. World Scientific, 1990.

[31] N. Read and Dmitry Green. Paired States of Fermions in Two Dimensions with Breaking of Parity and Time-Reversal Symmetries and the Fractional Quantum Hall Effect. *Physical Review B*, 61(15):10267–10297, April 2000.

[32] Gregory Moore and Nicholas Read. Nonabelions in the Fractional Quantum Hall Effect. *Nuclear Physics B*, 360(2-3):362–396, August 1991.

[33] Martin Greiter, Xiao-Gang Wen, and Frank Wilczek. Paired Hall State at Half Filling. *Physical Review Letters*, 66(24):3205–3208, June 1991.

[34] B. Halperin. Quantized Hall Conductance, Current-Carrying Edge States, and the Existence of Extended States in a Two-Dimensional Disordered Potential. *Physical Review B*, 25(4):2185–2190, February 1982.

[35] X.G. Wen and A. Zee. Quantum Statistics and Superconductivity in Two Spatial Dimensions. *Nuclear Physics B - Proceedings Supplements*, 15:135–156, June 1990.

[36] Xiao-Gang Wen. Topological Orders and Edge Excitations in FQH States. *Advances in Physics*, 405:1–69, 1995.

[37] E Witten. Quantum Field Theory and the Jones Polynomial. *Commun. Math. Phys.*, 121:351, 1989.

[38] S. Zhang, T. Hansson, and S. Kivelson. Effective-Field-Theory Model for the Fractional Quantum Hall Effect. *Physical Review Letters*, 62(1):82–85, January 1989.

[39] N. Read and Subir Sachdev. Some Features of the Phase Diagram of the Square Lattice SU(N) Antiferromagnet. *Nuclear Physics B*, 316(3):609–640, 1989.

[40] B. Blok and X. Wen. Effective Theories of the Fractional Quantum Hall Effect: Hierarchy Construction. *Physical Review B*, 42(13):8145–8156, November 1990.

[41] J. Fröhlich and A. Zee. Large Scale Physics of the Quantum Hall Fluid. *Nuclear Physics B*, 364(3):517–540, October 1991.

[42] X. Wen and A. Zee. Classification of Abelian Quantum Hall States and Matrix Formulation of Topological Fluids. *Physical Review B*, 46(4):2290–2301, July 1992.

[43] Michael Levin and Xiao-Gang Wen. String-Net Condensation: A Physical Mechanism for Topological Phases. *Physical Review B*, 71(4):21, January 2005.

[44] Xiao-gang Wen. Quantum Order from String-Net Condensations and Origin of Light and Massless Fermions. *Physical Review B*, 68:065003, 2003.

[45] Xiao-Gang Wen. Artificial Light and Quantum Order in Systems of Screened Dipoles. *Physical Review B*, 68(11):115413, September 2003.

[46] Xie Chen, Zheng-Cheng Gu, and Xiao-Gang Wen. Local Unitary Transformation, Long-Range Quantum Entanglement, Wave Function Renormalization, and Topological Order. *Physical Review B*, 82(15):155138, October 2010.

[47] V. G. Turaev. *Quantum Invariants of Knots and 3-manifolds*. Walter de Gruyter, Berlin, 1994.

[48] Zoltán Kádár, Annalisa Marzuoli, and Mario Rasetti. Braiding and Entanglement in Spin Networks: A Combinatorial Approach to Topological Phases. *International Journal of Quantum Information*, 07(Supp):195, 2009.

[49] Michael Freedman, Chetan Nayak, Kirill Shtengel, Kevin Walker, and Zhenghan Wang. A Class of P,T-Invariant Topological Phases of Interacting Electrons. *Annals of Physics*, 310(2):428–492, April 2004.

[50] F. Burnell, Steven Simon, and J. Slingerland. Condensation of Achiral Simple Currents in Topological Lattice Models: Hamiltonian Study of Topological Symmetry Breaking. *Physical Review B*, 84(12):1–21, September 2011.

[51] Yu-Ting Hu and Yong-Shi Wu. Concrete Construction of Levin-Wen Models from Representations of Finite Groups. *In preparation.*

[52] Victor Ostrik. Module Categories, Weak Hopf Algebras and Modular Invariants. *Transformation Groups*, 8(2):177–206, June 2003.

[53] Jean-Robert Derome and W. T. Sharp. Racah Algebra for an Arbitrary Group. *Journal of Mathematical Physics*, 6(10):1584, October 1965.

[54] Oliver Buerschaper and Miguel Aguado. Mapping Kitaev̀s Quantum Double Lattice Models to Levin and Weǹs String-Net Models. *Physical Review B*, 80(15):1–8, October 2009.

[55] N. Reshetikhin and V. G. Turaev. Invariants of 3-Manifolds via Link Polynomials and Quantum Groups. *Inventiones Mathematicae*, 103(1):547–597, December 1991.

[56] Udo Pachner. Bistellare Äquivalenz kombinatorischer Mannigfaltigkeiten. *Arch. Math.*, 30:89–98, 1978.

[57] X. Wen and A. Zee. Topological Structures, Universality Classes, and Statistics Screening in the Anyon Superfluid. *Physical Review B*, 44(1):274–284, July 1991.

[58] Zheng-Cheng Gu, Michael Levin, Brian Swingle, and Xiao-Gang Wen. Tensor-Product Representations for String-Net Condensed States. *Physical Review B*, 79(8):085118, February 2009.

[59] R Dijkgraaf, V Pasquier, and P Roche. Quasi Hope Algebras, Group Cohomology and Orbifold Models. *Nuclear Physics B - Proceedings Supplements*, 18(2):60–72, January 1991.

[60] A N Kirillov and N Yu Reshetikhin. Representations of the Algebra $U_q(sl(2))$, q Orthogonal Polynomials and Invariants of Links. April 1988.

[61] G Masbaum and P Vogel. 3-Valent Graphs and the Kauffman Bracket. *Pacific J. Math*, 164(2), 1994.

[62] Edward Witten. 2 + 1 dimensional gravity as an exactly soluble system. *Nuclear Physics B*, 311(1):46–78, December 1988.

[63] X.-G. Wen and a. Zee. Topological Degeneracy of Quantum Hall Fluids. *Physical Review B*, 58(23):15717–15728, December 1998.

[64] Yu-Ting Hu and Yong-Shi Wu. Modular S and T Matrices and Correspondence between Ground States on a Torus and Quasiparticles in Levin-Wen Models. *In preparation.*

[65] Yu-Ting Hu and Yong-Shi Wu. Fractional Statistics in Fluxon Excitations of Levin-Wen Models. *In preparation.*

[66] Yong-Shi Wu. Statistical Distribution for Generalized Ideal Gas of Fractional-Statistics Particles. *Physical Review Letters*, 73(7):922–925, August 1994.

[67] F. Haldane. "Fractional Statistics" in Arbitrary Dimensions: A Generalization of the Pauli Principle. *Physical Review Letters*, 67(8):937–940, August 1991.

[68] Denis Bernard and Yong-Shi Wu. A Note on Statistical Interactions and the Thermodynamic Bethe Ansatz. Available at arXiv:cond-mat/9404025. April 1994.

[69] C. N. Yang. Thermodynamics of a One-Dimensional System of Bosons with Repulsive Delta-Function Interaction. *Journal of Mathematical Physics*, 10(7):1115, July 1969.

[70] Z.N.C. Ha. Fractional Statistics in One Dimension: View from an Exactly Solvable Model. *Nuclear Physics B*, 435(3):604–636, February 1995.

[71] Yasuhiro Hatsugai, Mahito Kohmoto, Tohru Koma, and Yong-Shi Wu. Mutual-Exclusion Statistics in Exactly Solvable Models in One and Higher Dimensions at Low Temperatures. *Physical Review B*, 54(8):5358–5367, August 1996.

[72] Song He, Xin-Cheng Xie, and Fu-Chun Zhang. Anyons, Boundary Constraint, and Hierarchy in Fractional Quantum Hall Effect. *Physical Review Letters*, 68(23):3460–3463, June 1992.

[73] Wu-Pei Su, Yong-Shi Wu, and Jian Yang. Mutual Exclusion Statistics between Quasiparticles in the Fractional Quantum Hall Effect. *Physical Review Letters*, 77(16):3423–3426, October 1996.

[74] Y. Wu, Y. Yu, Y. Hatsugai, and M. Kohmoto. Thermal Activation of Quasiparticles and Thermodynamics of Fractional Quantum Hall Liquids. *Physical Review B*, 57(16):9907–9919, April 1998.

[75] Charlotte Gils, Simon Trebst, Alexei Kitaev, Andreas W. W. Ludwig, Matthias Troyer, and Zhenghan Wang. Topology-Driven Quantum Phase Transitions in Time-Reversal-Invariant Anyonic Quantum Liquids. *Nature Physics*, 5(11):834–839, September 2009.

[76] J.K. Slingerland and F.A. Bais. Quantum Groups and Non-Abelian Braiding in Quantum Hall Systems. *Nuclear Physics B*, 612(3):229–290, October 2001.

[77] N. Read and E. Rezayi. Beyond Paired Quantum Hall States: Parafermions and Incompressible States in the First Excited Landau Level. *Physical Review B*, 59(12):8084–8092, March 1999.

[78] Igor Lesanovsky and Hosho Katsura. Interacting Fibonacci Anyons in a Rydberg Gas. *Physical Review A*, 86(4):041601, October 2012.

[79] Yuting Hu, Spencer D Stirling, and Yong-shi Wu. Emergent Exclusion Statistics of Fibonacci Anyons in 2D Topological Phases. Available at arXiv:1303.1586. March 2013.

[80] Yuting Hu, SD Stirling, and Yong-shi Wu. Ground-State Degeneracy in the Levin-Wen Model for Topological Phases. *Physical Review B*, 85(7):075107, 2012.

[81] Sathya Guruswamy and Kareljan Schoutens. Non-Abelian Exclusion Statistics. *Nuclear Physics B*, 556(3):530–544, September 1999.

[82] Yuting Hu, Yidun Wan, and Yong-Shi Wu. Twisted Quantum Double Model of Topological Phases in Two Dimensions. *Physical Review B*, 87(12):125114, March 2013.

[83] Edward Dijkgraaf, Robbert and Witten. Topological Gauge Theories and Group Cohomology. *Communications in Mathematical Physics*, 429:393–429, 1990.

[84] Salman Beigi, Peter W. Shor, and Daniel Whalen. The Quantum Double Model with Boundary: Condensations and Symmetries. *Communications in Mathematical Physics*, 306(3):663–694, June 2011.

[85] Alexei Kitaev and Liang Kong. Models for Gapped Boundaries and Domain Walls. *Communications in Mathematical Physics*, 313(2):351–373, June 2012.

[86] Michael Levin and Zheng-Cheng Gu. Braiding Statistics Approach to Symmetry-Protected Topological Phases. *Physical Review B*, 86(11):115109, September 2012.

[87] Christian Kassel. *Quantum Groups*, volume 155 of *Graduate Texts in Mathematics*. Springer, New York, NY, 1995.

[88] MW Propitius. *Topological Interactions in Broken Gauge Theories*. PhD thesis, University of Amsterdam, 1995.